PNAS
www.pnas.org

Supplementary Information for

Vertebrate adaptive radiation is assembled from an ancient and disjunct spatiotemporal landscape

Emilie J. Richards, Joseph A. McGirr, Jeremy R. Wang, Michelle E. St. John, Jelmer W. Poelstra, Maria J. Solano, Delaney C. O'Connell, Bruce J. Turner, Christopher H. Martin*

*Correspondence to: chmartin@berkeley.edu

This PDF file includes:

Supplementary text
Figures S1 to S17
Tables S1 to S19
SI References

Other supplementary materials for this manuscript include the following:

Datasets S1 to S9

38 # Table of Contents

39

1. Materials and Methods

1.1. Sampling.

Pupfishes were collected from across the complete Atlantic and Caribbean range of *Cyprinodon* from Massachusetts to Venezuela. For the three species in the SSI radiation, individual pupfish were collected from 15 isolated hypersaline lakes on SSI (Table S1; Data S1) and one estuary (Pigeon Creek) using hand and seine nets between 2011 and 2018. We sequenced 36 *Cyprinodon variegatus,* 47 *C. brontotheroides,* and 39 *C. desquamator* across these lakes, including six lakes in which one or two specialist species occur in sympatry with the generalist (Crescent Pond, Storr's Lake, Little Lake, Oyster Pond, Osprey Lake, Moon Rock Pond). We also sequenced outgroup high-coverage focal populations of generalist pupfish including 17 individuals from *C. laciniatus* from Lake Cunningham, New Providence Island, Bahamas; 18 *C. variegatus* from Lake George, Rum Cay, Bahamas; 12 *C. higuey* from Laguna Bavaro, Dominican Republic; 14 *C. variegatus* from Fort Fisher estuary, North Carolina, United States; and 14 *C. dearborni* from Isla Margarita, Venezuela. 37 individuals were also sequenced from other islands and localities spanning the range of *Cyprinodon* across the Caribbean and Atlantic coasts, including captive-bred individuals from the extinct species *Megupsilon aporus* and threatened species *Cualac tessellatus,* the most closely related outgroup genera to *Cyprinodon* ((*1*, *2*), Fig. 1A; Table S1; Data S1). Voucher specimens are catalogued in the Museum of Vertebrate Zoology Fishes collection under catalog numbers MVZ:Fish:467-626.

Fishes were euthanized in an overdose of buffered MS-222 (Finquel, Inc.) following approved protocols from the University of California, Davis Institutional Animal Care and Use Committee (#17455), the University of North Carolina at Chapel Hill Animal Care and Use

Committee (#18-061.0), and the University of California, Berkeley Animal Care and Use Committee (AUP-2015-01-7053) and preserved in 95-100% ethanol.

1.2 Genomic Library Prep.

DNA was extracted from muscle tissue using DNeasy Blood and Tissue kits (Qiagen, Inc.) and quantified on a Qubit 3.0 fluorometer (Thermofisher Scientific, Inc.). Genomic libraries were prepared using the automated Apollo 324 system (WaterGen Biosystems, Inc.) at the Vincent J. Coates Genomic Sequencing Center (QB3). Samples were fragmented using Covaris sonication, barcoded with Illumina indices, and quality checked using a Fragment Analyzer (Advanced Analytical Technologies, Inc.). Nine to ten samples were pooled per lane for 150PE sequencing on four lanes of an Illumina Hiseq4000 and an additional 96 individuals were sequenced on one 150PE lane of Illumina Novaseq with S4 chemistry. This included 42 individuals from a previous genomic study (*3*).

1.3 De novo genome assembly and annotation.

We constructed a hybrid de novo assembly from an inbred lab-raised individual of *C. brontotheroides* using three different sequencing technologies: Oxford Nanopore sequencing was performed at UNC's High Throughput Sequencing Facility, a 10X Genomics synthetic long-read library was prepared and sequenced by Hudson Alpha, and Chicago and HiC libraries were prepared and sequenced by Dovetail Genomics. Genomic DNA was extracted from an inbred F4 male *C. brontotheroides* individual, an offspring from three generations of full-sib mating in the lab, starting with an F0 pair collected from Crescent Pond, SSI (the type locality;(*4*)). 10X sequencing was performed on this individual according to 10X Genomics' recommended

protocol and sequenced on an Illumina HiSeq4000, resulting in 460 million 2x150 bp reads. DNA was extracted from this same molluscivore individual for Nanopore sequencing using a modified phenol:chloroform extraction protocol (*5*). Two libraries were sequenced on R9.4 flow cells on Nanopore's GridION desktop sequencer – one using the Rapid Sequencing Kit (RAD004) and one Ligation Kit (LSK109), producing 4.9 Gbp of sequences with a read length N50 of 4.7 Kbp.

10X Genomics sequences were first assembled using Supernova (v2.0.0, (*6*)) to produce a preliminary "pseudohap" assembly. Nanopore reads were corrected using FMLRC (*7*). The Supernova assembly was scaffolded with corrected nanopore reads using LINKS (*8*) with the recommended iterative approach (34 rounds). The Nanopore-scaffolded assembly was further scaffolded using HiC and Chicago sequences. We predicted Hi-C contacts using Juicer (v1.6.2; (*9*)), followed by scaffolding with 3D-DNA (v180922; (*10*)). We performed a final polishing with four rounds of Racon (v1.3.1; (*11*)) using the corrected Nanopore reads. The final assembly consisted of 1.16 Gbp in 15,698 scaffolds with an N50 of 32,013,756 bp (32 Mb).

To validate our assembly, we ran BUSCO (v3.0.1; (*12*)) to identify known single-copy conserved genes. We found 86.4% of BUSCOs in the Actinopterygii class assembled completely, and 83.4% into single copy orthologs. We annotated this assembly using the Maker pipeline (v3.01.02;(*13*)), providing alternate ESTs and protein evidence for ab-initio gene prediction from *C. variegatus* (*14*), which is closely related and expected to have very similar genic structure and codon usage. Predicted genes were assigned putative function by aligning (BLASTp) to the UniProt database (*15*).

1.4 Population genotyping.

Raw reads were mapped from 222 individuals to our de novo assembly of the *Cyprinodon brontotheroides* reference genome (v 1.0; total sequence length = 1,162,855,435 bp; number of scaffolds = 15,698, scaffold N50 = 32 Mb) with bwa-mem (v 0.7.12; (*16*)). Duplicate reads were identified using MarkDuplicates and BAM indices were created using BuildBamIndex in the Picard software package (http://picard.sourceforge.net; (v.2.0.1)). We followed the best practices guide recommended in the Genome Analysis Toolkit (v 3.5; (*17*)) to call and refine our single nucleotide polymorphism (SNP) variant dataset using the program HaplotypeCaller. We filtered SNPs based on the recommended hard filter criteria (i.e. QD < 2.0; FS < 60; MQRankSum < -12.5; ReadPosRankSum < -8; (*17, 18*)) because we lacked high-quality known alleles for these non-model species. Poorly mapped regions were removed using a mask file generated from the program SNPable (http://bit.ly/snpable; k-mer length = 50, and 'stringency' = 0.5). SNPs for SSI individuals were additionally filtered to remove those with a minor allele frequency below 0.05, genotype quality below 20, or containing more than 20% missing data across all individuals at the site using vcftools (v.0.1.15; (*19*)). This set of 9.3 million SNPs was then further filtered for alleles that had minor allele frequencies above 0.05 and less than 50% missing data across all Caribbean outgroup individuals with population level sampling. The resulting dataset that we used for all downstream analyses, unless otherwise noted, contained 5.5 million SNPs. The MAF threshold we used as a quality filter (excluding minor allele frequencies below 5%) will bias any search for rare alleles in this system. However, our main objective in this study was to characterize candidate adaptive alleles that have swept within specialist populations on SSI, alleles that would not be influenced by this MAF filter because they are not expected to be rare alleles within our specialist populations of interest. For some calculations that are heavily influenced by the presence/absence of minor alleles, such as *Dxy*, π, and allele frequency

distributions across Caribbean populations we used a version of the genetic dataset without the minor allele frequency filter and note when we have done so.

1.5 Population genetic analyses.

The filtered genomic dataset was first pruned to SNPs in linkage disequilibrium using the LD pruning function (--indep-pairwise 50 5 0.5) in plink (v1.9;(*20*)), leaving 2.6 million SNPs. To visualize population structure in our dataset, we ran a principal component analysis using the eigenvectors outputted by plink's pca function (--pca). The first two principal components were plotted in R (R Core Team 2018; v3.5.0). To visualize admixture among the species we estimated the proportion of shared ancestry among individuals in our dataset using ADMIXTURE (v.1.3.0;(*21*)). The number of populations (K) was chosen using ADMIXTURE's cross-validation method (--cv) across 1-20 values of K. K = 11 populations was then chosen using the broken-stick method, following (*22*). Ancestry proportions estimated by ADMIXTURE were plotted in R. Four individuals that appeared to exhibit recent hybrid ancestry between *C. variegatus* and *C. brontotheroides* and two individuals that appeared to exhibit recent hybrid ancestry between *C. variegatus* and *C. desquamator* were removed from downstream analyses. We also excluded 15 individuals that appeared as strong outliers in the PCA and ADMIXTURE analyses (3 *C. variegatus* from SSI, 1 *C. brontotheroides*, 3 *C. laciniatus*, 2 *C. higuey*, 3 *C. variegatus* from North Carolina, and 3 *C. dearborni* from Venezuela), resulting in 32 *Cyprinodon variegatus*, 44 *C. brontotheroides*, and 26 *C. desquamator* individuals from SSI, 16 individuals from *C. laciniatus* from Lake Cunningham, New Providence Island in the Bahamas, 17 *C. variegatus* from Lake George, Rum Cay, 10 *C. higuey* from Lake Bavaro, Dominican Republic, 12 *C. variegatus* from Fort Fisher estuary North Carolina, and 11 *C. dearborni* from

Isla Margarita, Venezuela (Fig 1E). None of the 37 single individuals from other locations were removed. The final dataset used in downstream analyses included 202 individuals.

For analyses of genetic variation within sliding windows, we used a window size of 50-kb based on the extent of linkage disequilibrium (LD) along a scaffold estimated by LD decay along the largest scaffold in our genome. We calculated LD decay from pairwise calculations of LD between all SNPs within 100-kb of each other along the largest scaffold using PLINK's LD function (--r^2). Linkage disequilibrium decayed to background rates after 50-kb at a threshold of $r^2 \geq 0.1$ (Fig. S6).

Within-population nucleotide diversity (π) was calculated in 50-kb windows across the genome for each of eight focal populations (>10 individuals resequenced) using the python script popGenWindows.py available from https://github.com/simonhmartin/genomics_general (*23*). Since this calculation can be heavily influenced by minor alleles, we calculated π without the 5% minor allele frequency filter. Instead, we filtered all minor alleles with a read depth less than 5 in order to remove any rare variants that may be the result of sequencing error rather than a true minor allele, resulting in 10.8 million variants. We then calculated *Dxy* and π in sliding windows. The number of nonvariant sites in each window was also factored into these calculations. To ensure equal sample sizes among populations, we downsampled individuals from each population to the number of individuals in the focal population with the lowest sampling (n = 10). We randomly selected 10 individuals from each population before calculating π in sliding windows. We repeated this 100 times and averaged π across the replicates (Fig. S1). Due to the large sample size of windows for each population (N=30,762), slight differences in mean genome-wide within-population genetic diversity resulted in statistically significant differences in genome-wide diversity among populations (ANOVA, P-value > 2.2×10^{-16}).

However, the effect sizes of the difference in these means were small in all comparisons except in the case of two comparisons. The SSI generalist population had a significantly greater genome-wide genetic diversity of an appreciable effect size compared to North Carolina (*Cohen's d*=0.87) and Venezuela generalist populations (*Cohen's d*=1.38). The significantly lower within-population genetic diversity in Venezuela than other generalist populations may be due to a recent population bottleneck that was not observed in any other populations (Fig. 1C and S1).

Finally, allowing for some admixture, we calculated highly differentiated SNPs between trophic specialists based on $F_{st} \geq 0.95$ (Fig. S2; Table S2-S4; Data S2-S3). F_{st} between the two specialist populations was calculated per variant site using –weir-pop-fist function in vcftools (v.0.1.15; (*19*)) on the 5.5 million variant dataset.

1.6 Mutation rate estimation

The spontaneous mutation rate for Caribbean pupfishes was estimated from moderate to high-coverage sequencing (15-69x) of parents and offspring from two independent pedigreed crosses of SSI species: one cross between a second generation inbred lab-reared generalist and third-generation inbred lab-reared molluscivore individual from Little Lake (*C. variegatus x C. brontotheroides*) and another between a second-generation lab-reared generalist and second-generation lab-reared scale-eater from Little Lake (*C. variegatus x C. desquamator*). Using the same pipeline for alignment to the *C. brontotheroides* reference genome and variant calling as above, we obtained 9 million SNPs across 7 individuals from these two crosses after using GATK's recommend hard filter criteria (i.e. QD < 2.0; FS < 60; MQRankSum < -12.5;

ReadPosRankSum < -8). Following the mutation rate estimation protocol outlined in (*24*), we independently called alleles for these same individuals again using samtools mpileup (v1.9) with the command line arguments *bcftools mpileup -Ou | bcftools call -m -Ob -f GQ,GP*. For both sets of alleles (GATK and samtools), poorly mapped regions were then removed using a mask file generated from the program SNPable (http://bit.ly/snpable; k-mer length =50, and 'stringency'=0.5). We further excluded sequences in which indels were called in any sample, as well as 3 bp of sequence around the indel.

After variant calling, we searched for new mutations in the offspring by identifying sites where an offspring was heterozygous for an allele not found in either of the parents. We first looked for alleles which were heterozygous in the offspring and alternately homozygous in the parents (i.e. known heterozygous sites). Ten measures of variant quality scores for these known heterozygous sites in the offspring were then used to filter sites for new mutations in the offspring following similar pipelines and filters from several previous studies (*24–26*). This included filtering by 1) genotype quality, 2) mapping quality, 3) base quality rank sum, 4) mapping quality rank sum, 5) quality by depth, 6) site depth, 7) allele depth, 8) read position rank sum, 9) strands odds ratios, and 10) fisher strand scores. Sites were filtered to those greater than or equal to the mean score for known heterozygous sites in the offspring for filters 1 and 2 and scores within 2 standard deviations of the mean score for filters 3-10. For example, only new mutation sites that had a depth within 2 standard deviations of the mean depth of the known heterozygous sites in the offspring were kept (all specific values used for thresholds reported in Table S9). Additionally, new mutations in the offspring were determined from sites in which parents were homozygous for the reference allele and the offspring were heterozygous with quality scores within the range of known heterozygous sites (Table S9) and an allele balance

score between 0.3 and 0.7. This set of alleles was then filtered for those independently called in both GATK and samtools following (*24*).

Using the GATK function *callable loci*, we then determined the 'accessible genome': the total number of base pairs from the genome in which mutations could be confidently called for each cross. This number was estimated using the same variant quality filters as for the mutation estimate, excluding those filters that were only applicable to the new mutations and heterozygous sites (i.e. filters assessing quality of alternative allele calls). Genomic regions were excluded if 1) read map depth for a variant was not within two standard deviations of the average read map depth (varies by sample; Table S9), 2) mapping quality scores were less than 50, or 3) base quality scores were less than 30.

Since the de novo mutations observed could have originated on either chromosome, the point estimate of the per site mutation rate is the number of new mutations observed divided by two times the size of the accessible genome, following (*25*). The mutation rates were then averaged across individual offspring for each cross (Table S9) to obtain a mean mutation rate estimate of 1.56×10^{-8} mutations per site per generation. This is faster than mutation rate estimates for other teleosts (*26–28*); however, short-lived smaller species with higher metabolism rates like pupfishes are expected to exhibit faster mutation rates (*29*). We estimated generation times in the field to be approximately one year based on laboratory and field (*30*) longevity studies.

1.7 Demographic Inferences

Various demographic histories can shift the distribution of low- and high-frequency derived alleles to falsely resemble signatures of hard selective sweeps. In order to account for demography in downstream analyses, we used the MSMC (v. 1.0.1; *24*) to infer historical effective population size (N_e) changes in our seven focal populations. We ran MSMC on unphased GATK-called genotypes separately for a high-coverage individual in each of seven focal populations (excluding generalist *C. higuey* due to poor sequencing quality of our single high-coverage individual; 17-28x mean coverage across individuals; Fig 1D; Table S10). As recommended in the MSMC documentation, we masked sites with less than half or more than double the mean coverage for that individual or with a genotype quality below 20. We also excluded sites with less than 10 reads as recommended by Nadachowska-Brzyska et al. (*32*). To scale the output of MSMC to real time and effective population sizes, we used a one-year generation time (*29*) and the estimated spontaneous mutation rate of 1.56×10^{-8} per generation per base pair for Caribbean pupfishes (see previous section).

1.8 Introgression in SSI specialists

We characterized differential introgression between specialists in the SSI radiation on both a genome-wide and local level. We visualized the directionality of hybridization and introgression on a genome-wide level using *TreeMix* (v 1.13; (*33*)). *TreeMix* estimates a maximum likelihood phylogeny of the focal populations and then fits a user specified number of migration edges to the tree by comparing genetic covariances of allele frequencies among populations. We ran *TreeMix* with *C. dearborni* as the root node with 0 through 20 migration edges. The most likely number of migration events was chosen using the broken-stick approach (Fig. S7).

We investigated how signatures of hybridization at the genome-wide level contributed variation potentially important to the divergence between species using the f_d statistic, which is designed to look for signatures of introgression across sliding genomic windows (*23*). The f_d statistic, a modified version of the *D*-statistic, looks at allele frequencies fitting two allelic patterns referred to as ABBA and BABA based on the tree (((P1,P2),P3),O), where O is an outgroup species in which no gene flow is thought to occur with the other populations (*23*). We used 2 individuals of *C. artifrons* from Cancun, Mexico as our outgroup population for this test, which forms the deepest divergence event with *C. variegatus* within the *Cyprinodon* clade (*1*), and focused on introgression between SSI specialists and outgroup Caribbean generalist populations. Based on the tree (((P1,P2),P3), *C. artifrons*), the f_d statistic was calculated for the combinations of populations in which the focal population (P2) was either the scale-eater or the molluscivore, the other specialist population was the sister group (P1), and P3 was one of the Caribbean outgroup populations (Table S11 and S12). f_d statistics were calculated from 50-kb sliding windows with a minimum of 100 variant sites and no missing data in a population using the ABBABABA.py script (available on https://github.com/simonhmartin/genomics_general;(*23*)). To compare these patterns of introgression into the specialist to patterns of introgression into focal generalist populations on other islands, we also calculated f_d statistics for focal generalist populations (whenever we had sister groups to fit the relationships necessary for the test (Table S12B and S12D)). Significance of f_d values in sliding windows across the genome was evaluated using simulations with no migration using ms-move (*34*). We used estimates of changes in effective population size for each population from our MSMC analyses. We set the divergence time between the two specialists to 10,000 years based on the age of the hypersaline lakes on SSI. The threshold for

significant introgression regions was determined by simulating f_d statistics across the genome under a coalescent model with no gene flow, consisting of 150,000 50-kb windows each containing the mean number of alleles observed in our dataset. Empirical windows were considered candidates for introgression if the f_d statistic was above the maximum simulated f_d value (Table S11). We merged consecutive 50-kb f_d outlier windows to estimate the sizes of introgressed regions and approximate the age of introgression events (Fig. 3E-F).

1.9 Search for candidate adaptive alleles in SSI specialists

1.9.1 Selective sweep detection.

We searched for hard selective sweeps in the trophic specialist populations using two different approaches. The first method is based on the site frequency spectrum (SFS) calculated with SweeD (v.3.3.4;(*35*)). This method calculates the composite likelihood ratio (CLR) of a sweep. We incorporated our empirical estimate of the decrease in population size for each focal population estimated from MSMC analyses in 50-kb windows across scaffolds that were at least 100-kb in length (99 scaffolds; 85.6% of the genome). We also calculated CLRs across 100,000 scaffolds consisting of neutrally evolving sequences simulated with ms-move (*34*), controlling for the impact of the inferred population size decreases over time for each population from MSMC runs mentioned above (Fig. 1D; Table S7). The CLR ratios for the simulated datasets were then used to assess outlier CLR ratios from the empirical dataset. We considered regions with CLR ratios above the 95th percentile value of CLR from the neutral simulated dataset as candidate hard selective sweep regions (scale-eater: CLR > 5.28; molluscivore: CLR > 4.47; Table S7). We also inferred candidate hard selective sweep regions for the five focal Caribbean

generalist populations (sample size ≥ 10) following the same method outlined above for the specialists (Table S10).

To complement our SweeD selection analyses, we also used an LD-based approach for detecting hard selective sweeps implemented in OmegaPlus (*36*). OmegaPlus implements the ω-statistic introduced in (*37*) that looks for strong patterns of elevated LD in regions that are associated with selective sweeps. We estimated ω-statistic values in similar 50-kb windows across the scaffolds and across the same simulated datasets used in the SweeD analysis to assess outlier selective sweep regions in the specialist genomes. There was strong overlap in the candidate adaptive alleles between OmegaPlus and SweeD for 93% of candidate adaptive alleles in the scale-eater and 99% of candidate adaptive alleles in the molluscivore (Table S2). OmegaPlus detected many more outlier regions than SweeD (Table S2). LD-based estimates are ideally suited for use with haplotype data rather than genotype data and might be more susceptible to high false positive rates in cases where the demographic model is overly simplistic (*38*). To be conservative, we only analyzed candidate adaptive alleles detected by both methods.

We chose to focus on detecting hard selective sweeps for our candidate adaptive variants because a) their stronger pattern is easier to discern from neutral processes with our moderate population-level sampling and coverage, and b) theoretical and experimental work suggest that soft sweeps of multiple copies of an allele are unlikely for groups with smaller population sizes (*39*). However, we acknowledge that we may have missed some candidate adaptive variation in the specialists in the form of partial or soft selective sweeps.

1.9.2 Selection of candidate adaptive allele for both specialists

To identify candidate adaptive alleles underlying trophic specialists species divergence on SSI, we looked for strongly divergent SNPs between the two specialist species in regions of the genome that showed evidence of hard selective sweeps. We considered divergent SNPs to be those that were nearly fixed ($F_{st} \geq 0.95$) between the specialists to accommodate the small amounts of admixture that can occur between these nascent species (Fig. S2; Table S3-S4; Data S2-S3). For the rest of this study, we considered the 3,258 and 1,477 alleles that were nearly fixed between the species on San Salvador ($F_{st} \geq 0.95$) and located in a candidate selective sweep (empirical CLR > demographic simulations CLR; empirical ω > demographic simulations; Table S2) as the adaptive alleles for the scale-eater and molluscivore, respectively (Table S3-S4; Data S2-S3).

1.9.3 Categorization of the spatial distribution of adaptive alleles.

We then surveyed all pupfish individuals sampled from outside these populations for this set of adaptive alleles. Alleles were separated into three categories of genetic variation: de novo (the specialist allele was found only on SSI), introgressed (the specialist allele fell in a candidate introgression region determined in the Introgression section) or standing genetic variation (the specialist allele was also found in at least one generalist population sampled outside of SSI). Introgressed variation was further parsed by geographic region of the outgroup source generalist population: North Carolina (NC), New Providence Island (NP), or Dominican Republic (DR).

Given that the majority of the adaptive alleles for both specialists (98 and 100% the scale-eater and molluscivores, respectively) exist as standing genetic variation across the Caribbean (Fig. 2A), we looked for how many of these adaptive alleles in the specialists also showed evidence of hard selective sweeps in focal generalist populations outside of SSI. Only

2% of the scale-eater adaptive alleles and 6% of the molluscivore adaptive alleles occurred in regions that similarly exhibited signatures of a hard selective sweep in generalist populations outside of SSI (Fig. S3).

1.10 Introgression in outgroup generalist populations

We were interested in whether San Salvador Island specialist genomes exhibited more introgression in regions undergoing hard selective sweeps than other generalist populations. In the absence of a clear null expectation for the number of introgressed regions, we calculated the number of these adaptive introgression regions for the specialists that were also outlier f_d regions in other combinations of populations across the Caribbean (Table S11), to determine if those adaptive introgression regions observed in the specialists had also introgressed in other populations. Since several outgroup generalist populations had multiple values for the number of adaptive introgression regions (due to several different combinations of sister lineages (P1) available for testing against: Table S11), only the mean number of adaptive introgression regions per generalist population was shown for ease of visualization (Table S11; Fig. 3E-F). North Carolina and Venezuela were excluded as focal populations for these introgression tests because we lacked suitable outgroup taxa for them. Since these counts were not normally distributed, we used the non-parametric Mann-Whitney U test to determine if the mean number of adaptive introgression regions in each specialist was greater than the mean in the rest of the Caribbean (Table S12A v. S12B and Table S12C v. S12D) and calculated 95% confidence intervals around these means using the boot.ci function in the R package boot (v1.3; Fig. 3C). Since neither of the SSI specialists appear to have experienced adaptive introgression from the Venezuela *C.*

dearborni population, it was excluded as a potential donor population for the focal generalist populations on other islands as well in these comparative analyses.

1.12 Functional characterization of adaptive alleles through GO analysis

We performed gene ontology (GO) enrichment analyses for genes near candidate adaptive alleles using ShinyGo (v.0.51;(*40*)). For genes with focal GO terms (e.g. feeding behavior, muscle, mouth, eye and craniofacial development) relevant to stages of diversification in this system (i.e. habitat preference, trophic morphology, and pigmentation; Fig. 2C; Fig. 4; Table S5), we also checked other annotation databases and studies for verification of putative function, including Phenoscape Knowledgebase (https://kb.phenoscape.org/#/home), NCBI's PubMed (https://www.ncbi.nlm.nih.gov/pubmed), and the Gene Ontology database using AMIGO2 (*41*). All genes had consistent annotations across databases, except *galr2*. *Galr2* was annotated for feeding behavior in the Biological Processes database (Ensemble 92), but recent studies indicate that it does not play a role in feeding behavior (*42*, *43*). Thus, we removed its annotation as a candidate gene for feeding behavior, but kept it as a candidate for trophic morphology (Table S5-S6).

1.13 Functional characterization of adaptive alleles through genome-wide association mapping

1.13.1 Morphometrics and caudal fin pigmentation

We measured two key morphological traits associated with the major axes of phenotypic diversification in the SSI radiation, lower jaw length and nasal protrusion distance. Ethanol-preserved specimens from SSI were measured from external landmarks on the skull using digital calipers. Measurements were repeated on both lateral sides and averaged for each specimen. Lower jaw length was measured from the quadrate-articular jaw joint to the tip of the most anterior tooth on the dentary (Data S6). Nasal protrusion distance was measured by placing a tangent line from the dorsal surface of the neurocranium to the tip of the premaxilla and measuring the perpendicular distance that the nasal region protrudes from this tangent (Fig. S8A; Data S6). Each specimen was also measured for standard length using digital calipers to remove the effects of variation in body size on the craniofacial trait measurements among individuals and species. We log-transformed morphological measurements and regressed them against log-transformed standard length (Fig. S9; Data S6) and used the residuals for association mapping analyses.

The major axis of divergence in reproductive coloration and patterning between trophic specialists on SSI is the overall lightness or darkness of breeding males. Scale-eaters reach a nearly jet black coloration in the wild while guarding a breeding territory whereas molluscivore males remain paler throughout their body and fins (Fig 4). This pair of sympatric specialists exceeds the lightness contrast in male reproductive breeding coloration observed across all other *Cyprinodon* pupfishes. Females of each species show the same general pattern of lightness/darkness. We detected no difference in the total number of melanocytes on the caudal, anal, or pectoral fins among the SSI species. Instead, we found that scale-eater individuals were significantly darker overall on their caudal fins (two-tailed *t*-test, t=5.25, df=45.5, *P* -value= 3.8 x 10^{-6}; Fig. 4B; Data S6), perhaps due to larger melanocyte areas relative to molluscivores. We

found similar patterns for anal and pectoral fins and used only caudal fin lightness values for genome-wide association mapping. A Meiji EMZ-8TR stereomicroscope with standardized external illumination and an OMAX 18 Mp digital microscope camera was used to take lateral photographs of the caudal fin of each individual against the same white reference background in each image (Fig. 4B;Data S6). Adobe Photoshop (Creative Cloud) was used to select a rectangular area from inside the caudal fin, not including the caudal peduncle region or terminal marginal band, and measure the mean overall lightness of this region relative to a control region selected from the illuminated white background (following (*44*)). Standardized caudal fin pigmentation was then calculated as the proportion of the caudal fin lightness value relative to the control background lightness value for downstream analyses.

1.13.2 Genome-wide association mapping analyses

We employed a Bayesian sparse linear mixed model (BSLMM) implemented in the GEMMA software package (v. 0.94.1; (*45*)) to identify genomic regions associated with variation in lower oral jaw length, caudal fin pigmentation, and nasal protrusion distance across the three species on SSI. We only included individuals from SSI given extensive Caribbean-wide population structure (Fig 1C). We specifically performed genome-wide association mapping with GEMMA because of its demonstrated effectiveness in accounting for relatedness among samples and in controlling for population stratification by internally calculating a genetic relatedness matrix and incorporating it as a covariate in the BSLMM. The BSLMM uses Markov Chain Monte Carlo (MCMC) sampling to estimate the proportion of phenotypic variation explained by all SNPs included in the analysis (proportion of phenotypic variance explained [PVE]; Fig. S10A-C), only SNPs of large effect (proportion of genetic variance explained by sparse effects [PGE]; Fig.

S10D-F), and the number of large-effect SNPs needed to explain PGE (nSNPs; Fig. S10G-I). GEMMA also estimates a posterior inclusion probability (PIP) for each SNP. We used PIP, the proportion of steps in MCMC chain in which a SNP is estimated to have a non-zero effect on phenotypic variation, to assess the significance of regions associated with jaw size variation. We performed 10 independent MCMC runs of the BSLMM with 100 million steps and a burn-in of 50 million steps for three traits (lower oral jaw size (n = 78), caudal fin pigmentation (n = 61), and nasal protrusion distance (n = 65)). We chose to only include SSI individuals in these analyses given extensive Caribbean-wide population structure that could confound significant associations (Fig. 1C). We summed PIP parameter estimates across 20-kb windows to avoid dispersion of the posterior probability density across SNPs in linkage disequilibrium due to physical linkage following (*46*). All 10 independent runs were consistent in reporting the strongest associations for the same 20-kb windows. We identified regions strongly associated with our traits of interests by a PIP score in the 99th percentile across all regions (Data S7-9). Our PIP estimates for strongly associated windows suggest that jaw length may be controlled predominantly by a few loci of moderate effect (see bimodal PGE distribution, Fig. S10H). This is consistent with a previous QTL mapping study in an F2 intercross between SSI trophic specialists which detected one significant QTL with moderate effects on oral jaw size explaining up to 15% of the variation and three to four additional potential quantitative trait loci (QTL) with similar moderate effects (*47*).

1.14 Functional characterization of adaptive alleles through differential gene expression and QTL analysis from previous studies

1.14.1 Differential gene expression

Additionally, we looked for overlap between genes associated with our set of adaptive alleles and genes differentially expressed between the two specialists in whole embryos at two early developmental stages (2 and 8 days post-fertilization (dpf)) reported in previous studies (*48*, *49*). Tables with significantly differentially expressed genes at 2 and 8 dpf from these studies are provided in Data S4 and S5.

1.14.2 QTL analysis for jaw size

We also investigated our set of adaptive alleles for effects on craniofacial morphology by overlapping scaffolds with a previously published linkage map and QTL analysis of an F2 intercross between specialist species (*47*). We overlapped markers from this study that spanned the 95% Bayesian credible interval for a significant QTL for lower jaw length (LG15; taken from Fig S2 in (*47*)). The fasta sequences for these two markers bookending the QTL region on a single scaffold were then blasted against the *Cyprinodon brontotheriodes* genome using the blastn function in BLAST+ (*50*) and we selected the result with the highest percent identity and lowest e-value (Table S8). We then looked at all the genic regions within the interval between these two markers to investigate overlap between the QTL region and the alleles in this current study. The top hits for overlap between the sequences of two markers that spanned the LG15 QTL region and the *Cyprinodon brontotheroides* reference genome showed that this QTL corresponds to an 18 Mb region on scaffold c_bro_v1_0_ scaf8 (Table S8). However, this large region contained only a few adaptive alleles associated with the genes *map2k6* (3 alleles), *galr2* (2 alleles), and *grid2ip* (4 alleles).

1.15 Timing of divergence for adaptive alleles

If adaptive diversification in this radiation of pupfishes occurred in temporal stages as proposed in other systems (e.g. 'behavior-first evolution'; (*51–53*)), we predicted that there would be an ordering of divergence times among sweeps containing genes annotated for traits related to different trait axes in this system (Table S6-S7). In order to determine if there have been stages of adaptation in this adaptive radiation of pupfishes, we first estimated divergence times between molluscivores and scale-eaters for each adaptive allele. Many methods for estimating divergence times and allele ages rely on the pattern of variation in the haplotype background surrounding the allele of interest. Heuristic approaches, particularly those that use point estimates of the number of derived mutations within a chosen distance of the site are accessible, quick ways to approximate divergence times among regions and allele ages without extensive haplotype data (*54*, *55*). We estimated sequence divergence in regions surrounding alleles using D_{xy}, an absolute measure of genetic divergence. We calculated D_{xy} in 50-kb windows between the genomes for the SSI specialists (scale-eater vs. snail-eater) using the python script popGenWindows.py available from https://github.com/simonhmartin/genomics_general (*23*).

To get a heuristic estimate of divergence time between specialists at these adaptive alleles, we used this D_{xy} count of the number of alleles that have accumulated between specialists and the approximation that the observed genetic differences between two lineages should be equal to 2μt: t, the time since their divergence and μ, the mutation rate (*56*). Using the per generation mutation rate estimated above (1.56×10^{-8}), we calculated the time since divergence for adaptive alleles and compared that time to the estimated 6-19 kya age of the radiation (based on estimates of the last period of drying of hypersaline lake basins on SSI (*57*, *58*) and the last glacial maximum (*59*)).

To look for stages of diversification along different trait axes using these divergence time estimates, we matched adaptive alleles to potential phenotypes in two ways: 1) from our GO enrichment analyses for genes relevant to the major axes of adaptive radiation in this system (e.g. craniofacial morphology and behavior), and 2) regions strongly associated with either lower jaw size, nasal protrusion distance, or caudal fin pigmentation in the GWAS for SSI pupfish species. We found 31 regions containing adaptive alleles in or near genes with relevant GO terms and 24 regions containing adaptive alleles significantly associated with traits in the GWAS (Fig 4).

Six significantly enriched GO terms from the GO enrichment analysis of all the adaptive alleles reflect major axes of trait diversification in the radiation: divergent behavior or feeding behavior (GO terms: behavior and feeding behavior) and divergent craniofacial morphology (GO terms: eye, muscle tissue, skeletal and mouth development). There is strong morphological divergence in oral jaw size, eye orbit diameter, and adductor muscle mass among the SSI species. We therefore focused our comparison of divergence time estimates on alleles associated with genes annotated for these traits and 6 GO terms in downstream analyses of stages of adaptation across different trait axes. Melanin pigmentation is another divergent trait in this system, but it was not a significantly enriched GO term in our analyses. We include descriptions of alleles potentially relevant to pigmentation in the main text.

We then plotted the divergence time estimates for all adaptive alleles based on their spatial origins (de novo on SSI, introgression, or standing genetic variation). We also plotted all neutral regions that contained a fixed or nearly fixed allele, but no signature of a hard selective sweep (Fig 4, S11 and S12). We pruned alleles by randomly selecting one from the group of alleles that fell within the same 50-kb window so that each plotted point was independent. Some windows had multiple alleles with different spatial distributions (e.g. de novo vs. standing

genetic variation), so we made an alternative plot for alternative spatial distributions of alleles that occurred within a single 50-kb window (the smaller vs larger spatial distribution; Fig. 4 and Fig. S12). This applied to several adaptive alleles that were characterized as either introgressed or standing genetic variation in two regions containing genes with relevant adaptive annotations (*galr2* and *kcnk2*). In Figure 4 we plotted these alleles in the introgression and de novo columns. In Figure S12 we plotted these alleles in the standing genetic variation column.

We also explored the impact that the choice of pairwise species used in D_{xy} calculations had on the estimates of divergence times and relative ordering of those times among adaptive alleles. We measured D_{xy} between each of the specialists and *C. artifrons*, the outgroup used in the f_d statistic to estimate divergence times. The ordering of divergence times among genes and across phenotypic axes in this new calculation was similar to the ordering found for divergence times estimated with D_{xy} between the specialists (Fig 4, Fig S12). This indicates that the older divergence times among some regions is probably not due to 3 in mutation rate between the specialists on SSI that isn't observed in other outgroup generalist populations.

1.16 Timing of selective sweeps on adaptive alleles

1.16.1 Estimating posterior distribution of sweep ages for adaptive alleles

We also looked for evidence that adaptation occurred in stages by estimating the ages of selective sweeps of adaptive alleles. We used a coalescent-based approach implemented in the R package starTMRCA (v0.6.1; (*60*)) to get sweep age estimates for adaptive alleles. Estimating sweep ages for all 1,477 molluscivore adaptive alleles and 3,258 scale-eater adaptive alleles was computationally infeasible using this Bayesian approach, so we chose to estimate sweep ages for two subsets of these adaptive alleles (Table S17-18). For the first subset, we estimated sweep

ages for all alleles in or near (within 20-kb of) genes annotated for significantly enriched GO terms from our GO enrichment analysis that were relevant to behavior and trophic morphology. This subset included all 12 genes assigned to the behavior GO term, all 10 genes assigned to eye development GO term, all 12 genes assigned to the muscle tissue development GO terms, and all 4 genes assigned to the mouth development GO term (Table S5-S7). Several genes were annotated for multiple GO terms, so we ended up estimating sweep ages for a set of adaptive alleles associated with 25 different genes with relevant GO terms for the scale-eater and 6 for the molluscivore. For the second subset of adaptive alleles, we estimated sweep ages for all de novo and introgressed alleles regardless of annotation. This left a large pool of adaptive alleles distributed as standing genetic variation (illustrated in Fig. 4) that we could not estimate selective sweeps for. Therefore in a third subset of alleles, we selected all alleles with equivalently old and young divergence age estimates to our adaptive alleles from the first subset (those annotated for focal GO terms). In these alleles, we investigated what the genes they were in or near are annotated for to determine if they had any relevance to behavior or trophic morphology we may have missed. If the regions surrounding the adaptive alleles were unannotated, we aligned the 100-kb region surrounding the allele to the references genomes of *C. variegatus*, zebrafish and medaka available on Ensembl 96 (*61*) using the same protocol in Section 1.14.2 to look for potentially relevant gene annotations we may have missed in annotating the *C. bronotheriodes* reference genome in this study.

For each candidate adaptive allele from the two subsets mentioned above, a 1-Mb window surrounding the variant was extracted into a separate vcf for both specialist populations and the SSI generalists. We removed 2 generalist and 1 molluscivore individuals from this analysis that had with more than 10% missing data because starTMRCA requires complete

593 genotype data. For all remaining individuals, we then used the LD KKNI command in Tassel5
594 (*62*) to infer missing sites based on LD if possible. After this imputation step, we then removed
595 the small number of sites with any missing data across individuals within each population.

596 We then input this dataset with no missing allele information into starTMRCA. We used
597 the mutation rate estimate of 1.56×10^{-8} substitutions per base pair estimated in this study and a
598 recombination rate of 3.11×10^{-8} (from genome-wide recombination rate estimate for
599 stickleback; (*63*)) in order to estimate the age of selective sweeps for adaptive alleles. For the
600 cases in which we had more than one adaptive allele in a selective sweep region, the variant with
601 the highest F_{st} was chosen as the location of the beneficial allele for the sweep age estimate. We
602 thus estimated sweep ages for 86 sets of adaptive alleles across scale-eater and molluscivores.
603 We calculated posterior distributions of sweep age estimates using three independent runs of
604 10,000 steps. All runs were checked for convergence of age estimates between and within runs.

605 We then ran permutation tests to determine how likely the ordering of selective sweep ages by
606 trait axes (i.e. feeding behavior, trophic morphology) was to occur by chance alone. To do this
607 we randomly reassigned the ordering of the ages we estimated across the 22 sets of adaptive
608 alleles 10,000 times without replacement. Then we estimated the probability of seeing the
609 observed number of times the oldest sweep ages were all associated with a particular trait axes
610 by counting the number of random permutations which matched or exceeded the observe pattern.
611 For example, 5 out of these 22 adaptive allele sets were associated with feeding behavior. We
612 then counted how many random permutations had an ordering in which the first three (the
613 observed pattern), four, or five oldest sweeps were associated with feeding behavior to calculate
614 an empirical *P*-value.

615

616 *1.16.2 The robustness of sweep age estimates across genealogical assumptions*

617 Additionally, we explored how robust these sweep age estimates were to the assumption made
618 by starTMRCA that the sweep left a star-shaped genealogy pattern. This pattern is expected for
619 sweeps that arose from a single copy of an allele in which many alleles in one generation
620 coalesce back to a single ancestor in the previous generation. We wanted to explore how robust
621 our age estimates were particularly because we are comparing alleles with very different spatial
622 distributions (de novo, introgressed, and standing). If the underlying allelic genealogy does not
623 follow the star-shaped pattern of coalescence expected by selective sweeps from a single allele
624 copy and instead swept from multiple copies in a soft sweep, using different subsets of
625 individuals from a population or species could result in vastly different sweep age estimates (*60*)
626 and indicate that they do not fit the star-shaped pattern assumed by starTMRCA .

627 Therefore, we re-estimated our sweep ages solely using the Osprey lake populations of
628 scale-eaters and molluscivores and compared these age estimates to those from the entire
629 population of scale-eaters on SSI. The age estimates for Osprey Lake were very similar to the
630 entire SSI population and the relative ordering of age estimates across adaptive alleles was nearly
631 identical (Fig. S14). This indicates that the sweep ages estimates, particularly their relative
632 ordering, were robust to differences in spatial distribution and potential differences in
633 genealogical patterns among alleles.

634

635 *1.16.3 The robustness of sweep age estimates across different methods*

We also explored the robustness of selective sweep ages estimated by starTMRCA by additionally estimating sweep ages using an independent R package called McSwan (v1.1.1;; https://github.com/sunyatin/McSwan; (*64*)). McSwan detects hard selective sweeps by comparing local site frequency spectra (SFS) simulated under neutral and selective demographic models, which it uses to assign selective sweeps to regions of the genome and predict the age of selection events (*64*). By using information from the SFS, McSwan is advantageous for estimating selective sweep ages in non-model organisms because it does not require high quality haplotype data to detect sweeps and predict their ages. However, this flexibility comes at the cost of not jointly estimating the selection coefficient of a particular sweep, so it assumes the strength of selection is equal across all sweeps (*64*). With a mutation rate estimate, neutral demographic model (effective population size changes and divergence events), and variant file, McSwan generates simulated and observed SFSs and a prior of sweep ages, whose upper bound is determined by the divergence time estimate specified in the demographic model (in our case: 10,000 years). McSwan uses these simulated selective and neutral SFSs to scan the input variant file for selective sweep regions and produce a posterior distribution of sweep ages for each sweep region it detects.

To simulate the SFSs required by McSwan to estimate sweep ages, we used our estimated mutation rate (1.56×10^{-8}), the same demographic models of changes in effective population sizes used in our SweeD runs for the generalists and scale-eater populations (Table S10), and a divergence time estimate between SSI generalist and scale-eater of 10,000 years. We first simulated neutral and selection SFSs that were each comprised of 2,000 simulations (default recommendation) across sequences 50-kb in length. To look for selective sweeps in the specialists, we then generated empirical SFSs from scans across the 500-kb region surrounding

each of the 22 sets of adaptive alleles highlighted in Figure 4. To precisely determine the boundaries of hard selective sweeps, McSwan iterates its genomic scans over adjacent windows of various lengths and offsets and compares the empirical SFS to the simulated SFS under selection to assign regions as selective sweeps. We set up the iterative scans across these 500-kb regions in sliding windows that ranged from 1000 bp to 200-kb in length and a minimum of 50 alleles required per window. Each sliding scan of the 500-kb region used 100 overlapping steps (default setting). We then looked for overlap between the regions detected as hard selective sweeps by McSwan with adaptive allelles previously detected with SweeD and F_{st} (Table S2-S3).

For these 11 regions, we filtered the distribution of sweep ages for estimates that had a stability value (a parameter that represents the strength of support for a selective sweep model over a neutral model) in the 95th percentile. To get a likely range of selective sweep age estimates for each region, we calculated the 95% high posterior density (HPD) region with the R package HDIntervals (v0.2; https://cran.r-project.org/web/packages/HDInterval/index.html) from their respective posterior distributions. We repeated this process for the 6 sets of adaptive alleles found in the molluscivore, only three of which were also detected as being under a selective sweep in McSwan. The 95% HPD of these age estimates for the scale-eater and molluscivore populations are presented in Figure 4C, S15 and Table S19 and the full posteriors are shown in Figure S16 and S17. We then assessed the probability of observing the same ordering of sweep ages across alleles from different trait axes (i.e. feeding behavior and trophic morphology) using the same permutation approach described in Section 1.13.1.

2. Supplementary Results and Discussion

2.1 Spatiotemporal stages of adaption based on timing of divergence among adaptive alleles

2.2.1 Evidence of stages of adaptation across different axes of trait diversification from divergence time estimates

Based on relevant GO terms, we found that several adaptive alleles in or near genes annotated for feeding behavior exhibited the oldest divergence times (Fig 4A and S12) while adaptive alleles in or near genes annotated for craniofacial morphology and pigmentation showed younger divergence times (Fig 4A and S12). Similarly, we found younger divergence times among regions with genes annotated for traits related to trophic morphology based on GWAS annotations (Fig 4B).

When we compare divergence estimates from across all adaptive alleles and not just those with relevant GO annotations, there are three sets of alleles with similarly old divergence time estimates to our oldest feeding behavior candidates (*prlh* and *cfap20*; Fig 4A) in the scale-eater and six sets of alleles with similarly old divergence time estimates to our oldest eye morphology candidate in the molluscivores (*zhx2*; Fig 4B). We investigated the genomic regions surrounding these adaptive alleles for any annotations relevant to behavior or craniofacial morphology that we may have missed from the GO enrichment analysis. If the regions were unannotated in our *C. brontotheroides* genome, we blasted the regions to the *C. variegatus* and model organism medaka and zebrafish references genomes on Ensembl (96;(*61*)) to check for additional gene annotations.

From this additional search, we found three sets of adaptive alleles with similar divergence times to the oldest feeding behavior alleles (*prlh* and *cfap20;* Fig 4A) but the single

gene (*gpr20)* these alleles were near did not appear to have any relevant annotations for behavior or craniofacial morphology and the additional two unannotated regions were also unannotated in the other reference genomes (*Cyprinodon variegatus*, medaka, and zebrafish). Similarly in molluscivores, two sets of adaptive alleles (*shisa2* and *gga1*) with older divergence estimates (Fig 4B) were not near any genes annotated for feeding behavior or craniofacial traits and the four unannotated regions were unannotated in other reference genomes as well. We also searched all adaptive alleles comparable in age to the youngest adaptive alleles from our stages of adaptation analysis (*twist1* and *slc16a1*). The genes associated with these two sets of alleles (*tstd1* and *slc35e1*) with younger ages than the *twist1* allele similarly did not have relevant annotations for feeding behavior or craniofacial morphology.

2.1.3 The ordering of divergence times among adaptive alleles not driven by variation in mutation rate among regions of the genome

Differences in mutation rate across the genome could confound our estimates of divergence times. For example, regions with the oldest divergence time estimates might only appear old because they are located in regions with higher mutation rates than other regions in the genome. To explore this possibility, we found that the scaffolds containing feeding behavior genes do not appear to have higher counts of de novo mutations in our controlled laboratory crosses (Fig S13A-C) nor more called variants than other scaffolds in the larger genomic dataset of wild individuals from across the Caribbean. Thus, we did not find any evidence of elevated mutation rates on the three scaffolds containing the oldest divergence times for feeding behavior genes (Fig S13D).

2.2 Spatiotemporal stages of adaption based on timing of selection on adaptive alleles

2.2.1 Evidence of stages of adaptation across different axes of trait diversification from starTMRCA

Although we ran starTMRCA on all scale-eater and molluscivores adaptive alleles that were in or near all genes annotated for behavior or craniofacial morphology from our GO enrichment analysis, we were unable to get estimates for twelve sets of adaptive alleles due to poor convergence within 10,000 steps across the 3 independent runs in starTMRCA. These alleles were discarded from sweep age comparisons. The lack of power to estimate sweep ages with certainty for these alleles may be due to weaker selection on these adaptive alleles or greater variability in the strength of selection across populations in different lakes.

Therefore, our downstream analyses included sweep age estimates from 26 of the 31 sets of sweep age estimates from alleles associated with genes that have behavior or craniofacial morphology GO term annotations (22 of 25 for scale-eater, and 4 of 6 in molluscivores; Fig 4E-F). For the molluscivore, we are missing sweep age estimates for the adaptive alleles near the gene *atp8a2* (annotated for eye development and feeding behavior) and *tiparp* (annotated for craniofacial morphology). For the scale-eater, we are missing sweep ages for adaptive alleles in or near two genes annotated for eye development (*gnat2, zhx2*) and one annotated for muscle tissue development (*med1*). However, we did have sweep age estimates for all adaptive alleles in or near genes relevant to behavior and mouth morphology for the scale-eater. We therefore believe that the ‘behavior-first’ stage of adaptation we see is fairly robust in comparison to a second stage of adaptive divergence in trophic morphology.

We observed a notably 'behavior-first' stage of adaptive diversification, largely driven by the fact that the three oldest selective sweeps occurred in adaptive alleles in or near genes annotated for feeding behavior among the scale-eater alleles. We further investigated the probability that this 'behavior first' pattern could occur by chance using a permutation test. The probability that the first three or more of the oldest selective sweeps would all be associated with feeding behavior by chance alone is small (permutation test, *P*-value =0.01).

2.2.2 Evidence of stages of adaptation across different axes of trait diversification from McSwan

For the scale-eater population, only 8 of the 25 sets of alleles detected as hard selective sweeps using SweeD were also detected as hard selective sweeps using McSwan and given age estimates. In Tournebize et al. (*64*), they noted low power to detect selective sweeps when selection was relatively weak ($s \leq 0.05$) and recent (Supplemental information Section 2 of (*64*)). In one case, the alleles surrounding the adjacent genes *cenpf* and *kcnk2* were detected within the same large selective sweep in McSwan and thus have the same age estimates (Fig. S15B). However, the twelve additional adaptive alleles undetected by McSwan may be under weaker selection or more recent. Due to the very recent timing of selection in this system and the much larger set of sweep age estimates obtained from starTMRCA, we present only the starTMRCA sweep ages in the main text.

We also found a similar 'behavior-first' stage of adaptive diversification with this smaller subset of sweep age estimates from McSwan. The two oldest sweeps in the scale-eater

were both associated with feeding behavior (*prlh* and *cfap20*). The probability of observing this pattern by chance alone is small (permutation test; *P*-value = 0.033).

2.2.3 Spatiotemporal stages of adaptive introgression from different source populations

We estimated selective sweep ages across all de novo and introgressed variants in the scale-eater and molluscivores regardless of gene annotations as well. We find evidence that introgressed adaptive alleles swept before any de novo adaptive alleles (Fig S5) and selection on introgressed variation occurred throughout the process of radiation. Introgressed alleles sweeping before de novo alleles further supports a role for hybridization being necessary for radiation in this system.

We also assessed whether there were significant differences in the timing of selection across de novo and introgressed alleles coming from different source populations using ANOVA. We found that alleles originating in North Carolina swept significantly earlier than introgressed alleles from New Providence Island and the Dominican Republic (*P*-value =0.03 and *P*-value=0.02 respectively; Fig 4G-H). Sweeps of adaptive alleles introgressed from North Carolina also trended older than sweeps of de novo adaptive alleles, although this was not a significant difference (*P*-value=0.06). Sweeps of de novo adaptive alleles occurred concurrently with sweeps of introgressed alleles from New Providence Island and the Dominican Republic (*P*-value=0.61).

References

1. A. A. Echelle, E. W. Carson, A. F. Echelle, D. Bussche, T. E. Dowling, Historical Biogeography of the New-World Pupfish Genus Cyprinodon (Teleostei: Cyprinodontidae). *Copeia*. **2005**, 320–339 (2005).
2. A. Valdés González, L. Martínez Estévez, M. E. Ángeles Villeda, G. Ceballos, The

extinction of the Catarina pupfish Megupsilon aporus and the implications for the conservation of freshwater fish in Mexico. *Oryx*. **54**, 154–160 (2020).
3. E. J. Richards, C. H. Martin, Adaptive introgression from distant Caribbean islands contributed to the diversification of a microendemic adaptive radiation of trophic specialist pupfishes. *PLoS Genet.* **13**, 1–35 (2017).
4. C. H. Martin, P. C. Wainwright, A remarkable species flock of Cyprinodon pupfishes endemic to San Salvador Island, Bahamas. *Bull. Peabody Museum Nat. Hist.* **54**, 231–241 (2013).
5. M. R. Green, J. Sambrook, Isolation of high-molecular-weight DNA using organic solvents. *Cold Spring Harb. Protoc.* **2017**, 356–359 (2017).
6. N. I. Weisenfeld, V. Kumar, P. Shah, D. M. Church, D. B. Jaffe, Corrigendum: Direct determination of diploid genome sequences. *Genome Res.* **28**, 757–767 (2018).
7. J. R. Wang, J. Holt, L. McMillan, C. D. Jones, FMLRC: Hybrid long read error correction using an FM-index. *BMC Bioinformatics*. **19**, 1–11 (2018).
8. R. L. Warren, C. Yang, B. P. Vandervalk, B. Behsaz, A. Lagman, S. J. M. Jones, I. Birol, LINKS: Scalable, alignment-free scaffolding of draft genomes with long reads. *Gigascience*. **4** (2015), doi:10.1186/s13742-015-0076-3.
9. N. C. Durand, M. S. Shamim, I. Machol, S. S. P. Rao, M. H. Huntley, E. S. Lander, E. L. Aiden, Juicer Provides a One-Click System for Analyzing Loop-Resolution Hi-C Experiments. *Cell Syst.* **3**, 95–98 (2016).
10. O. Dudchenko, S. S. Batra, A. D. Omer, S. K. Nyquist, M. Hoeger, N. C. Durand, M. S. Shamim, I. Machol, E. S. Lander, A. P. Aiden, E. L. Aiden, *Science (80-.).*, in press, doi:10.1126/science.aal3327.
11. R. Vaser, I. Sovic, N. Nagarajan, Š. Mile, Fast and accurate de novo genome assembly from long uncorrected reads. *Genome Res.*, 1–10 (2017).
12. F. A. Simão, R. M. Waterhouse, P. Ioannidis, E. V Kriventseva, E. M. Zdobnov, BUSCO: assessing genome assembly and annotation completeness with single-copy orthologs. *Bioinformatics*. **31**, 3210–3212 (2015).
13. B. L. Cantarel, I. Korf, S. M. C. Robb, G. Parra, E. Ross, B. Moore, C. Holt, A. S. Alvarado, M. Yandell, MAKER: An easy-to-use annotation pipeline designed for emerging model organism genomes. *Genome Res.* **18**, 188–196 (2008).
14. E. S. Lencer, W. C. Warren, R. Harrison, A. R. McCune, The Cyprinodon variegatus genome reveals gene expression changes underlying differences in skull morphology among closely related species. *BMC Genomics*. **18**, 424 (2017).
15. A. Bateman, UniProt: A worldwide hub of protein knowledge. *Nucleic Acids Res.* **47**, D506–D515 (2019).
16. H. Li, R. Durbin, Inference of human population history from individual whole-genome sequences. *Nature*. **475**, 493–496 (2011).
17. M. A. DePristo, E. Banks, R. Poplin, K. V Garimella, J. R. Maguire, C. Hartl, A. A. Philippakis, G. del Angel, M. A. Rivas, M. Hanna, A. McKenna, T. J. Fennell, A. M. Kernytsky, A. Y. Sivachenko, K. Cibulskis, S. B. Gabriel, D. Altshuler, M. J. Daly, A framework for variation discovery and genotyping using next-generation DNA sequencing data. *Nat. Genet.* **43**, 491–8 (2011).
18. C. D. Marsden, Y. Lee, K. Kreppel, A. Weakley, A. Cornel, H. M. Ferguson, E. Eskin, G. C. Lanzaro, Diversity, differentiation, and linkage disequilibrium: prospects for association mapping in the malaria vector Anopheles arabiensis. *G3 (Bethesda).* **4**, 121–31

(2014).
19. P. Danecek, A. Auton, G. Abecasis, C. A. Albers, E. Banks, M. A. DePristo, R. E. Handsaker, G. Lunter, G. T. Marth, S. T. Sherry, G. McVean, R. Durbin, 1000 Genomes Project Analysis Group, The variant call format and VCFtools. *Bioinformatics*. **27**, 2156–2158 (2011).
20. S. Purcell, B. Neale, K. Todd-Brown, L. Thomas, M. A. R. Ferreira, D. Bender, J. Maller, P. Sklar, P. I. W. de Bakker, M. J. Daly, P. C. Sham, PLINK: A Tool Set for Whole-Genome Association and Population-Based Linkage Analyses. *Am. J. Hum. Genet.* **81**, 559–575 (2007).
21. D. H. Alexander, J. Novembre, K. Lange, Fast model-based estimation of ancestry in unrelated individuals. *Genome Res.* **19**, 1655–1664 (2009).
22. G. Evanno, S. Regnaut, J. Goudet, Detecting the number of clusters of individuals using the software STRUCTURE: A simulation study. *Mol. Ecol.* **14**, 2611–2620 (2005).
23. S. H. Martin, J. W. Davey, C. D. Jiggins, Evaluating the use of ABBA-BABA statistics to locate introgressed loci. *Mol. Biol. Evol.* **32**, 244–257 (2015).
24. C. Feng, M. Pettersson, S. Lamichhaney, C. J. Rubin, N. Rafati, M. Casini, A. Folkvord, L. Andersson, Moderate nucleotide diversity in the Atlantic herring is associated with a low mutation rate. *Elife*. **6**, 1–14 (2017).
25. F. L. Wu, M. Przeworski, P. Moorjani, M. Przeworski, A. I. Strand, L. A. Cox, L. A. Cox, C. Ober, J. D. Wall, A. I. Strand, P. Moorjani, *A comparison of humans and baboons suggests germline mutation rates do not track cell divisions* (2020; http://dx.doi.org/10.1371/journal.pbio.3000838), vol. 18.
26. M. Malinsky, H. Svardal, A. M. Tyers, E. A. Miska, M. J. Genner, G. F. Turner, R. Durbin, Whole-genome sequences of Malawi cichlids reveal multiple radiations interconnected by gene flow. *Nat. Ecol. Evol.* **2**, 1940–1955 (2018).
27. A. F. Kautt, G. Machado-Schiaffino, A. Meyer, Multispecies Outcomes of Sympatric Speciation after Admixture with the Source Population in Two Radiations of Nicaraguan Crater Lake Cichlids. *PLoS Genet.* **12**, 1–33 (2016).
28. B. Guo, F. J. J. Chain, E. Bornberg-Bauer, E. H. Leder, J. Merilä, Genomic divergence between nine- and three-spined sticklebacks. *BMC Genomics*. **14**, 756 (2013).
29. C. H. Martin, J. E. Crawford, B. J. Turner, L. H. Simons, Diabolical survival in Death Valley: recent pupfish colonization, gene flow and genetic assimilation in the smallest species range on earth. *Proc. R. Soc. B Biol. Sci.* **283**, 20152334 (2016).
30. C. H. Martin, K. Gould, C. Bocklage, Surprising spatiotemporal stability and frequency-independence across multiple fitness peaks driving adaptive radiation in the wild (2019).
31. S. Schiffels, R. Durbin, Inferring human population size and separation history from multiple genome sequences. *Nat. Genet.* **46**, 919 (2014).
32. K. Nadachowska-Brzyska, R. Burri, L. Smeds, H. Ellegren, PSMC analysis of effective population sizes in molecular ecology and its application to black-and-white Ficedula flycatchers. *Mol. Ecol.* **25**, 1058–1072 (2016).
33. J. K. Pickrell, J. K. Pritchard, Inference of Population Splits and Mixtures from Genome-Wide Allele Frequency Data. *PLoS Genet.* **8**, e1002967 (2012).
34. D. Garrigan, A. Geneva, msmove: A modified version of Hudson's coalescent simulator ms allowing for finer control and tracking of migrant genealogies (2014), , doi:10.6084/m9.figshare.1060474.
35. P. Pavlidis, D. Živković, A. Stamatakis, N. Alachiotis, SweeD: Likelihood-based

detection of selective sweeps in thousands of genomes. *Mol. Biol. Evol.* **30**, 2224–2234 (2013).
36. N. Alachiotis, A. Stamatakis, P. Pavlidis, OmegaPlus: a scalable tool for rapid detection of selective sweeps in whole-genome datasets. *Bioinformatics*. **28**, 2274–2275 (2012).
37. Y. Kim, R. Neilsen, Linkage disequilibrium as a signature of selective sweeps. *Genetics*. **167**, 1513–1524 (2004).
38. P. Pavlidis, N. Alachiotis, A survey of methods and tools to detect recent and strong positive selection. *J. Biol. Res.* **24**, 7 (2017).
39. J. D. Jensen, On the unfounded enthusiasm for soft selective sweeps. *Nat. Commun.* **5**, 5281 (2014).
40. S. X. Ge, D. Jung, ShinyGO: a graphical enrichment tool for animals and plants. *bioRxiv*, 2 (2018).
41. E. Balsa-Canto, D. Henriques, A. Gabor, J. R. Banga, AMIGO2, a toolbox for dynamic modeling, optimization and control in systems biology. *Bioinformatics*. **32**, 1–2 (2016).
42. M. E. Anderson, J. Runesson, I. Saar, Ü. Langel, J. K. Robinson, Galanin, through GalR1 but not GalR2 receptors, decreases motivation at times of high appetitive behavior. *Behav. Brain Res.* **239**, 90–93 (2013).
43. S. Wang, L. Ghibaudi, T. Hashemi, C. He, C. Strader, M. Bayne, H. Davis, J. J. Hwa, The GalR2 galanin receptor mediates galanin-induced jejunal contraction, but not feeding behavior, in the rat: Differentiation of central and peripheral effects of receptor subtype activation. *FEBS Lett.* **434**, 277–282 (1998).
44. C. H. Martin, S. Johnsen, A field test of the Hamilton-Zuk hypothesis in the Trinidadian guppy (Poecilia reticulata). *Behav. Ecol. Sociobiol.* **61**, 1897–1909 (2007).
45. X. Zhou, P. Carbonetto, M. Stephens, Polygenic modeling with bayesian sparse linear mixed models. *PLoS Genet.* **9**, e1003264 (2013).
46. J. A. McGirr, C. H. Martin, Novel candidate genes underlying extreme trophic specialization in Caribbean pupfishes. *Mol. Biol. Evol.* **34**, 873–888 (2016).
47. C. H. Martin, P. A. Erickson, C. T. Miller, The genetic architecture of novel trophic specialists: higher effect sizes are associated with exceptional oral jaw diversification in a pupfish adaptive radiation. *Mol. Ecol.* **26**, 624–638 (2017).
48. J. A. Mcgirr, C. H. Martin, Parallel evolution of gene expression between trophic specialists despite divergent genotypes and morphologies. *Evol. Lett.* **2**, 62–75 (2018).
49. J. A. McGirr, C. H. Martin, Ecological divergence in sympatry causes gene misexpression in hybrids. *Mol. Ecol.* **29**, 2707–2721 (2020).
50. C. Camacho, G. Coulouris, V. Avagyan, N. Ma, J. Papadopoulos, K. Bealer, T. L. Madden, BLAST+: Architecture and applications. *BMC Bioinformatics*. **10**, 1–9 (2009).
51. E. Mayr, *Animal species and evolution* (Belknap, Cambridge, MA, 1963).
52. R. B. Huey, P. E. Hertz, B. Sinervo, Behavioral drive versus behavioral inertia in evolution: A null model approach. *Am. Nat.* **161**, 357–366 (2003).
53. J. B. Losos, T. W. Schoener, D. A. Spiller, Predator-induced behaviour shifts and natural selection in field-experimental lizard populations. *Nature*. **432**, 505–508 (2004).
54. R. R. Hudson, The Variance of Coalescent Time Estimates from DNA Sequences. *J. Mol. Evol.* **64**, 702–705 (2007).
55. G. Coop, K. Bullaughey, F. Luca, M. Przeworski, The Timing of Selection at the Human FOXP2 Gene. *Mol. Biol. Evol.* **25**, 1257–1259 (2008).
56. N. Masatoshi, Genetic distance between populations. *Am. Nat.* **106**, 283–292 (1972).

57. F. M. Hagey, J. . Mylroie, Pleistocene lake and lagoon deposits, San Salvador Island, Bahamas. *Geol. Soc. Am.* **30**, 77–90 (1995).
58. B. J. Turner, D. D. Duvernell, T. M. Bunt, M. G. Barton, Reproductive isolation among endemic pupfishes (Cyprinodon) on San Salvador Island, Bahamas: Microsatellite evidence. *Biol. J. Linn. Soc.* **95**, 566–582 (2008).
59. P. U. Clark, A. S. Dyke, J. D. Shakun, A. E. Carlson, J. Clark, B. Wohlfarth, J. X. Mitrovica, S. W. Hostetler, A. M. McCabe, The Last Glacial Maximum. *Science (80-.).* **325**, 710–714 (2009).
60. J. Smith, G. Coop, M. Stephens, J. Novembre, Estimating Time to the Common Ancestor for a Beneficial Allele. *Mol. Biol. Evol.* **35**, 1003–1017 (2018).
61. A. D. Yates, P. Achuthan, W. Akanni, J. Allen, J. Allen, J. Alvarez-Jarreta, M. R. Amode, I. M. Armean, A. G. Azov, R. Bennett, J. Bhai, K. Billis, S. Boddu, J. C. Marugán, C. Cummins, C. Davidson, K. Dodiya, R. Fatima, A. Gall, C. G. Giron, L. Gil, T. Grego, L. Haggerty, E. Haskell, T. Hourlier, O. G. Izuogu, S. H. Janacek, T. Juettemann, M. Kay, I. Lavidas, T. Le, D. Lemos, J. G. Martinez, T. Maurel, M. McDowall, A. McMahon, S. Mohanan, B. Moore, M. Nuhn, D. N. Oheh, A. Parker, A. Parton, M. Patricio, M. P. Sakthivel, A. I. Abdul Salam, B. M. Schmitt, H. Schuilenburg, D. Sheppard, M. Sycheva, M. Szuba, K. Taylor, A. Thormann, G. Threadgold, A. Vullo, B. Walts, A. Winterbottom, A. Zadissa, M. Chakiachvili, B. Flint, A. Frankish, S. E. Hunt, G. Iisley, M. Kostadima, N. Langridge, J. E. Loveland, F. J. Martin, J. Morales, J. M. Mudge, M. Muffato, E. Perry, M. Ruffier, S. J. Trevanion, F. Cunningham, K. L. Howe, D. R. Zerbino, P. Flicek, Ensembl 2020. *Nucleic Acids Res.* **48**, D682–D688 (2020).
62. P. J. Bradbury, Z. Zhang, D. E. Kroon, T. M. Casstevens, Y. Ramdoss, E. S. Buckler, TASSEL: Software for association mapping of complex traits in diverse samples. *Bioinformatics*. **23**, 2633–2635 (2007).
63. M. Roesti, D. Moser, D. Berner, Recombination in the threespine stickleback genome - Patterns and consequences. *Mol. Ecol.* **22**, 3014–3027 (2013).
64. R. Tournebize, V. Poncet, M. Jakobsson, Y. Vigouroux, S. Manel, McSwan: A joint site frequency spectrum method to detect and date selective sweeps across multiple population genomes. *Mol. Ecol. Resour.* **19**, 283–295 (2019).
65. M. M. Stevenson, Karyomorphology of Several Species of Cyprinodon. *Copeia*, 494–498 (1981).
66. Y. Ofran, B. Rost, ISIS: Interaction sites identified from sequence. *Bioinformatics*. **23**, 13–16 (2007).
67. E. V. Davydov, D. L. Goode, M. Sirota, G. M. Cooper, A. Sidow, S. Batzoglou, Identifying a high fraction of the human genome to be under selective constraint using GERP++. *PLoS Comput. Biol.* **6** (2010), doi:10.1371/journal.pcbi.1001025.
68. M. Nei, W. H. Li, *Proc. Natl. Acad. Sci.*, in press, doi:10.1073/pnas.76.10.5269.
69. A. C. McDonald, J. A. Schuijers, A. L. Gundlach, B. L. Grills, Galanin treatment offsets the inhibition of bone formation and downregulates the increase in mouse calvarial expression of TNFα and GalR2 mRNA induced by chronic daily injections of an injurious vehicle. *Bone*. **40**, 895–903 (2007).
70. T. M. Maia, D. Gogendeau, C. Pennetier, C. Janke, R. Basto, Bug22 influences cilium morphology and the posttranslational modification of ciliary microtubules. *Biol. Open*. **3**, 138–151 (2014).
71. M. Taye, J. Kim, S. H. Yoon, W. Lee, O. Hanotte, T. Dessie, S. Kemp, O. A. Mwai, K.

Caetano-Anolles, S. Cho, S. J. Oh, H. K. Lee, H. Kim, Whole genome scan reveals the genetic signature of African Ankole cattle breed and potential for higher quality beef. *BMC Genet.* **18**, 1–14 (2017).
72. A. Suwa, M. Yoshino, C. Yamazaki, M. Naitou, R. Fujikawa, RMI1 deficiency in mice protects from diet and genetic-induced obesity. **277**, 677–686 (2010).
73. L. Qiao, M. Du, X. Liang, Y. Hao, X. He, F. Si, T. Mei, B. Chen, Tyrosine Hydroxylase is crucial for maintaining pupal tanning and immunity in Anopheles sinensis. *Sci. Rep.* **6**, 1–11 (2016).
74. L. K. Marles, E. M. Peters, D. J. Tobin, N. A. Hibberts, K. U. Schallreuter, Tyrosine hydroxylase isoenzyme I is present in human melanosomes: a possible novel function in pigmentation. *Exp. Dermatol.* **12**, 61–70 (2003).
75. T. S. Hnasko, M. S. Szczypka, W. A. Alaynick, M. J. During, R. D. Palmiter, A role for dopamine in feeding responses produced by orexigenic agents. **1023**, 309–318 (2004).
76. K. LaMonica, H. Ding, K. B. Artinger, prdm1a functions upstream of itga5 in zebrafish craniofacial development. *Genesis*. **53**, 270–277 (2015).
77. J. G. Crump, M. E. Swartz, C. B. Kimmel, An Integrin-Dependent Role of Pouch Endoderm in Hyoid Cartilage Development. **2** (2004), doi:10.1371/journal.pbio.0020244.
78. S. Brewer, W. Feng, J. Huang, S. Sullivan, T. Williams, Wnt1-Cre-mediated deletion of AP-2α causes multiple neural crest-related defects. *Dev. Biol.* **267**, 135–152 (2004).
79. R. M. Green, W. Feng, T. Phang, J. L. Fish, H. Li, R. A. Spritz, R. S. Marcucio, J. Hooper, H. Jamniczky, B. Hallgrímsson, T. Williams, Tfap2a-dependent changes in mouse facial morphology result in clefting that can be ameliorated by a reduction in Fgf8 gene dosage. *DMM Dis. Model. Mech.* **8**, 31–43 (2015).
80. H. E. Seberg, E. Van Otterloo, S. K. Loftus, H. Liu, G. Bonde, R. Sompallae, D. E. Gildea, J. F. Santana, J. R. Manak, J. Pavan, T. Williams, R. A. Cornell, *TFAP2 paralogs regulate melanocyte differentiation in parallel with MITF* (2017).
81. Y. Horiuchi, M. Ishikawa, N. Kaito, Y. Iijima, Y. Tanabe, H. Ishiguro, T. Arinami, Experimental Evidence for the Involvement of PDLIM5 in Mood Disorders in Hetero Knockout Mice. *PLoS One*. **8**, 1–10 (2013).
82. J. Lee, B.-K. Lee, J. M. Gross, Bcl6a function is required during optic cup formation to prevent p53-dependent apoptosis and colobomata. *Hum. Mol. Genet.* **22**, 3568–3582 (2013).
83. C. S. Teng, M. C. Ting, D. T. Farmer, M. Brockop, R. E. Maxson, J. G. Crump, Altered bone growth dynamics prefigure craniosynostosis in a zebrafish model of Saethre-Chotzen syndrome. *Elife*. **7**, 1–23 (2018).
84. A. Das, J. G. Crump, Bmps and Id2a act upstream of twist1 to restrict ectomesenchyme potential of the cranial neural crest. *PLoS Genet.* **8** (2012), doi:10.1371/journal.pgen.1002710.
85. Y. Takayanagi, H. Matsumoto, M. Nakata, T. Mera, S. Fukusumi, S. Hinuma, Y. Ueta, T. Yada, G. Leng, T. Onaka, Endogenous prolactin-releasing peptide regulates food intake in rodents. *J. Clin. Invest.* **118**, 4014–4024 (2008).
86. X. Zhao, T. Brade, T. J. Cunningham, G. Duester, Retinoic acid controls expression of tissue remodeling genes Hmgn1 and Fgf18 at the digit–interdigit junction. *Dev. Dyn.* **239**, 665–671 (2010).
87. K. Laue, M. Jänicke, N. Plaster, C. Sonntag, M. Hammerschmidt, Restriction of retinoic acid activity by Cyp26b1 is required for proper timing and patterning of osteogenesis

during zebrafish development. **3787**, 3775–3787 (2008).
88. K. M. Spoorendonk, J. Peterson-maduro, J. Renn, T. Trowe, S. Kranenbarg, C. Winkler, S. Schulte-merker, Retinoic acid and Cyp26b1 are critical regulators of osteogenesis in the axial skeleton. **3774**, 3765–3774 (2008).
89. C. Mccormick, Y. Leduc, D. Martindale, K. Mattison, L. E. Esford, A. P. Dyer, F. Tufaro, The putative tumour suppressor EXT1 alters the expression of cell-surface heparan sulfate. **19**, 158–161 (1998).
90. K. R. Fitch, K. A. McGowan, C. D. Van Raamsdonk, H. Fuchs, D. Lee, A. Puech, Y. Hérault, D. W. Threadgill, M. H. De Angelis, G. S. Barsh, Genetics of dark skin in mice. *Genes Dev.* **17**, 214–228 (2003).
91. M. D. Shirley, H. Tang, C. J. Gallione, J. D. Baugher, L. P. Frelin, B. Cohen, P. E. North, D. A. Marchuk, A. M. Comi, J. Pevsner, Sturge–Weber Syndrome and Port-Wine Stains Caused by Somatic Mutation in GNAQ. *N. Engl. J. Med.* **368**, 1971–1979 (2013).
92. H. J. McMillan, A. Telegrafi, A. Singleton, M. T. Cho, D. Lelli, F. C. Lynn, J. Griffin, A. Asamoah, T. Rinne, C. E. Erasmus, D. A. Koolen, C. A. Haaxma, B. Keren, D. Doummar, C. Mignot, I. Thompson, L. Velsher, M. Dehghani, M. Y. Vahidi Mehrjardi, R. Maroofian, M. Tchan, C. Simons, J. Christodoulou, E. Martín-Hernández, M. J. Guillen Sacoto, L. B. Henderson, H. McLaughlin, L. L. Molday, R. S. Molday, G. Yoon, Recessive mutations in ATP8A2 cause severe hypotonia, cognitive impairment, hyperkinetic movement disorders and progressive optic atrophy. *Orphanet J. Rare Dis.* **13**, 1–10 (2018).

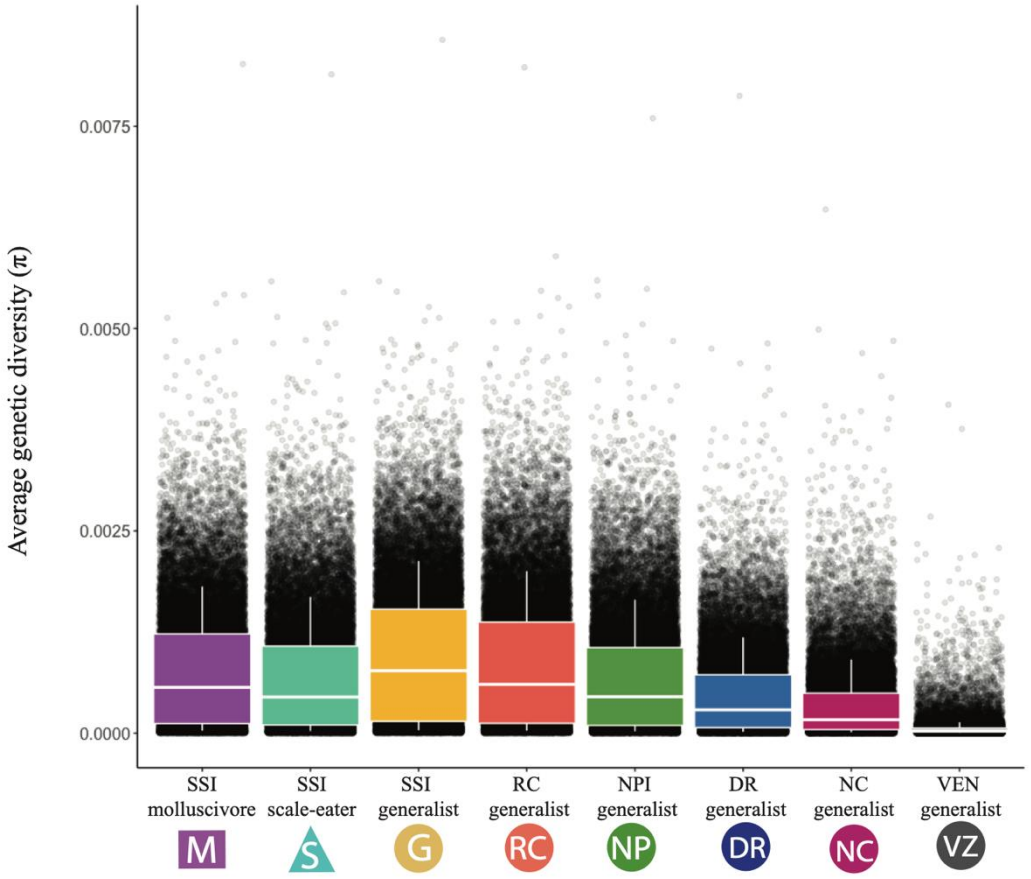

Fig. S1. Similar genome-wide level genetic diversity across Caribbean pupfish populations. Within population (π) nucleotide diversity in 50-kb sliding windows across the genomes of the SSI (SSI) species and generalist species on Rum Cay (RC), New Providence Island (NPI), Dominican Republic (DR), North Carolina (NC) and Venezuela (VZ). π values are averaged across 100 random samples of 10 individuals from each population in order to down-sample from populations with larger sample sizes and compare π across populations.

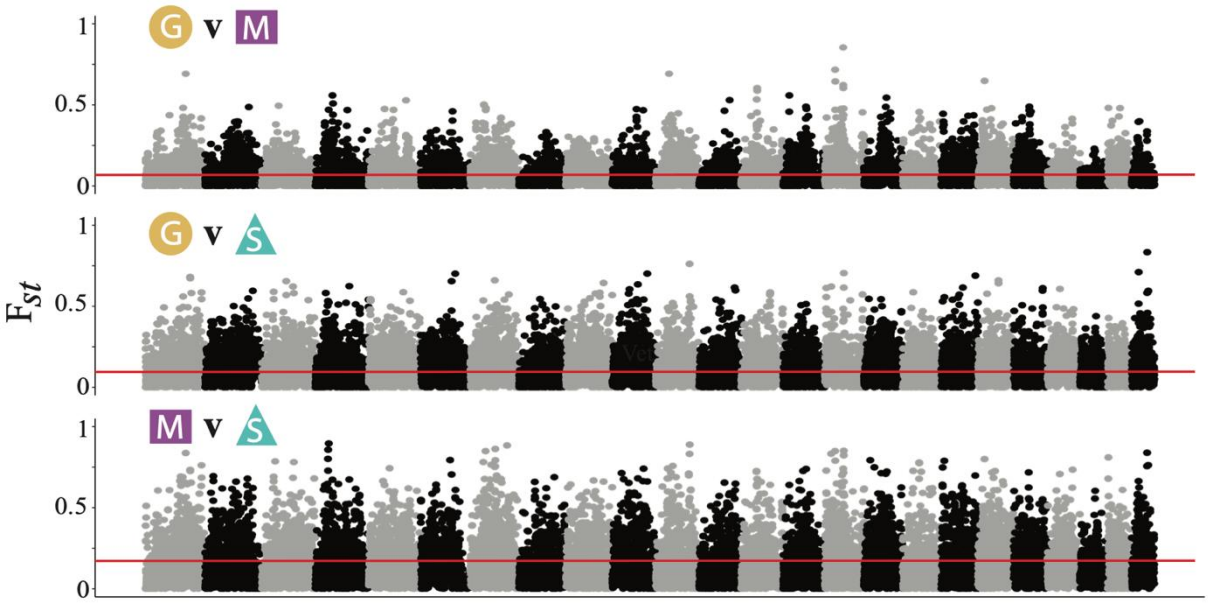

Fig. S2. Genetic divergence among SSI species. Manhattan plot of F_{st} in 50-kb windows across the genome for the three SSI species on the largest 24 scaffolds in the molluscivore (*C. brontotheroides*) genome corresponding to the 24 chromosomes in *Cyprinodon* (*65*). Solid red line represents the average F_{st} values for each comparison (generalist vs. molluscivore; 0.07; generalist vs. scale-eater: 0.11; molluscivore vs. scale-eater: 0.15).

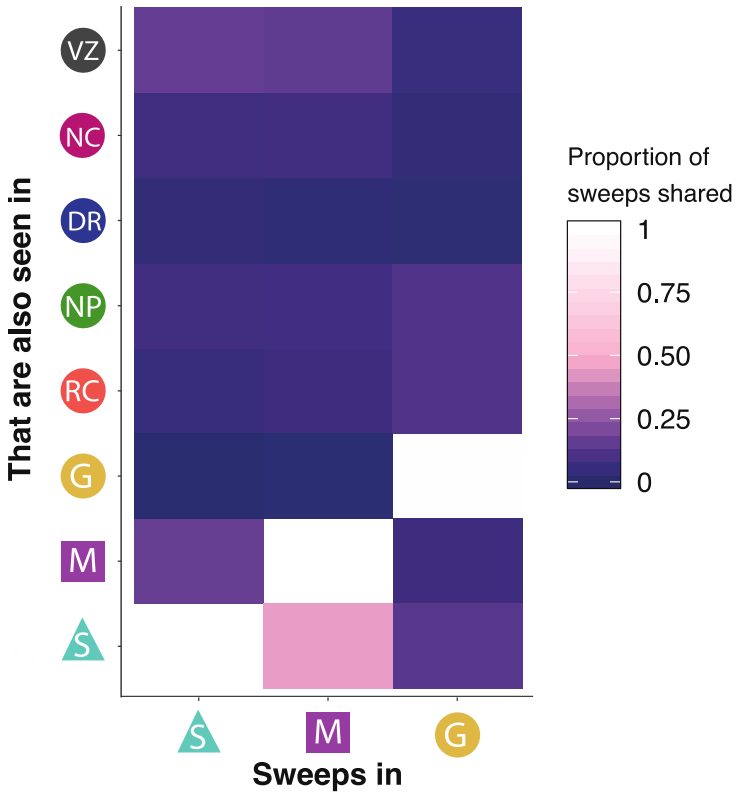

Fig. S3. Selective sweeps in SSI population shared with other Caribbean populations. The proportion of hard selective sweeps in the SSI species that are also found sweeping in other Caribbean populations. Regions under hard selective sweep were identified as those with a SweeD CLR estimate greater than those calculated from demographic simulations of a similar sized population evolving neutrally (e.g. SweeD CLR > 5.28 for scale-eaters and SweeD CLR > 4.43 for molluscivores, see Table S8 for threshold values for all populations). Note that 42% of hard selective sweeps in the molluscivore population also showed signs of a sweep in the scale-eater population.

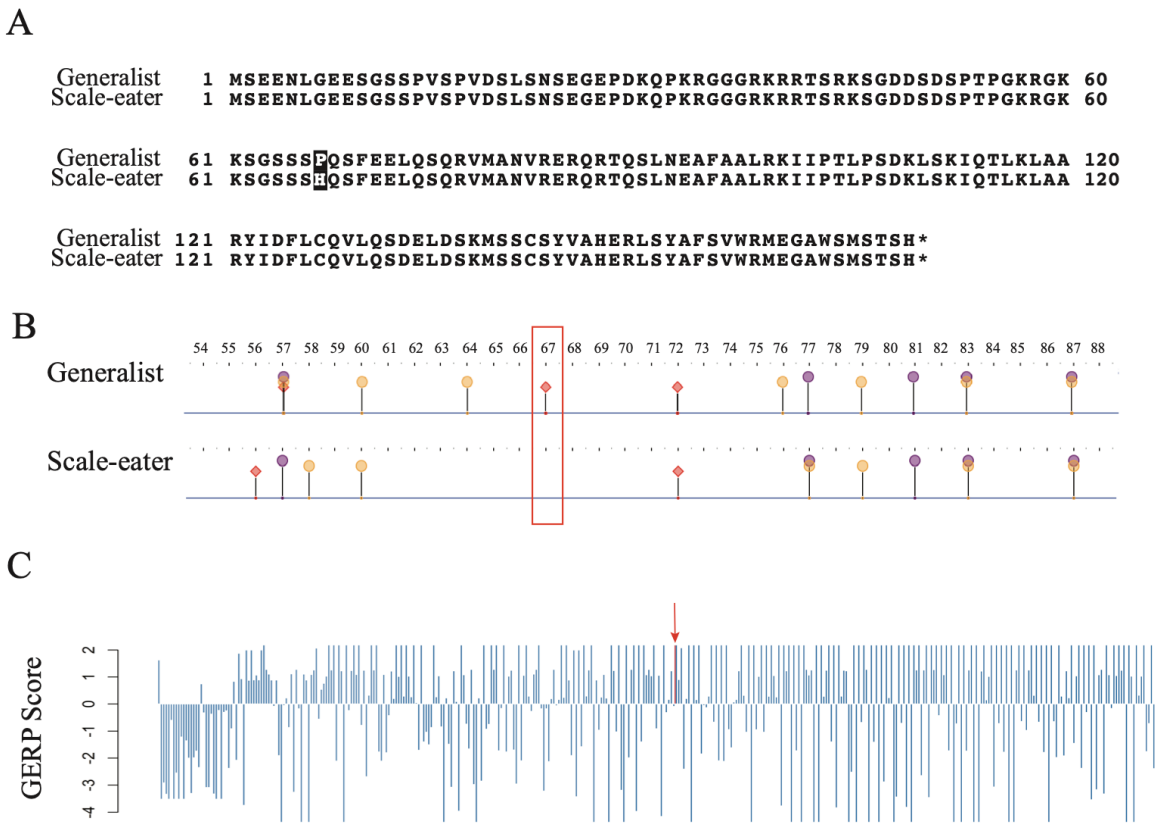

Fig. S4. Sequence conservation among fishes around candidate gene *twist1*.

A) Amino acid sequence of *twist1* protein for SSI generalists and scale-eaters. The non-synonymous substitution that is nearly fixed between the two species changes the amino acid from a proline to histidine (highlighted in black). B) This amino acid substitution alters a protein binding site (highlighted in red box) predicted and visualized with Predict Protein Open (https://open.predictprotein.org) using the machine-learning prediction method PPsites2 (*66*). C) GERP scores for the 500 base pair region surrounding the non-synonymous coding substitution in *twist1* (red arrow) found only on SSI. Conservation scores were obtained from aligning scale-eater genomes to the 60 fish EPO low coverage genome alignment on Ensembl (release 98). A conservation score above 2 is considered highly conserved (*67*).

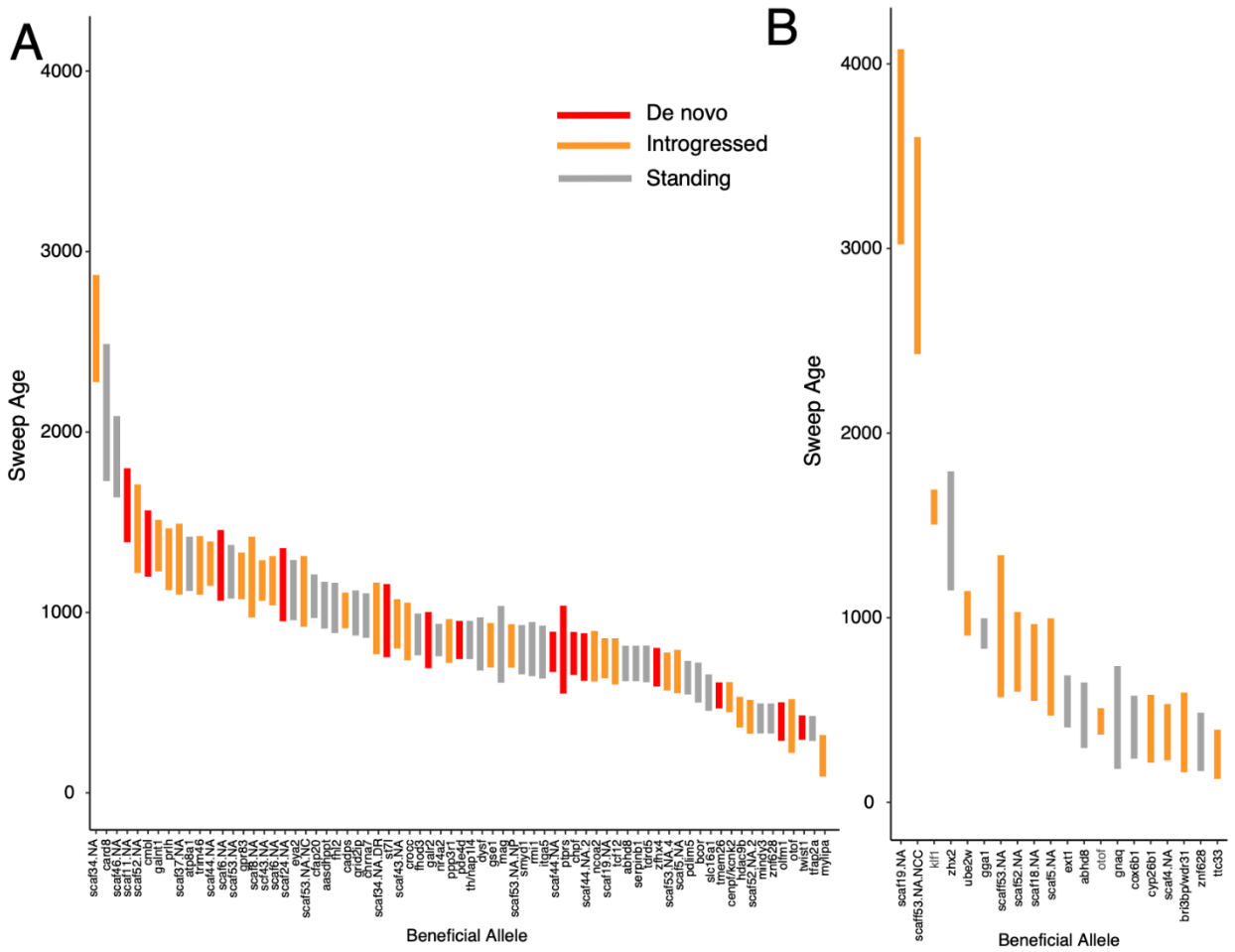

Fig. S5. Selective sweep ages across spatial source of genetic variation.

95% HPD interval of the posterior distribution for selective sweep ages estimates calculated from starTMRCA for all introgressed and de novo of the specialists adaptive alleles, as well as all adaptive alleles in or near (within 20-kb) of genes annotated for behavior and craniofacial GO terms in our GO enrichment analysis (Fig 4). Selective sweep ages in the scale-eaters (A) and molluscivores (B) are colored by spatial distribution of the adaptive genetic variation (standing, introgressed or de novo alleles). Adaptive alleles are labeled by the gene region they are associated with. Alleles that are in unannotated regions are labeled by the scaffold they are found on. The exact position of the variant on that scaffold is listed in Table S16).

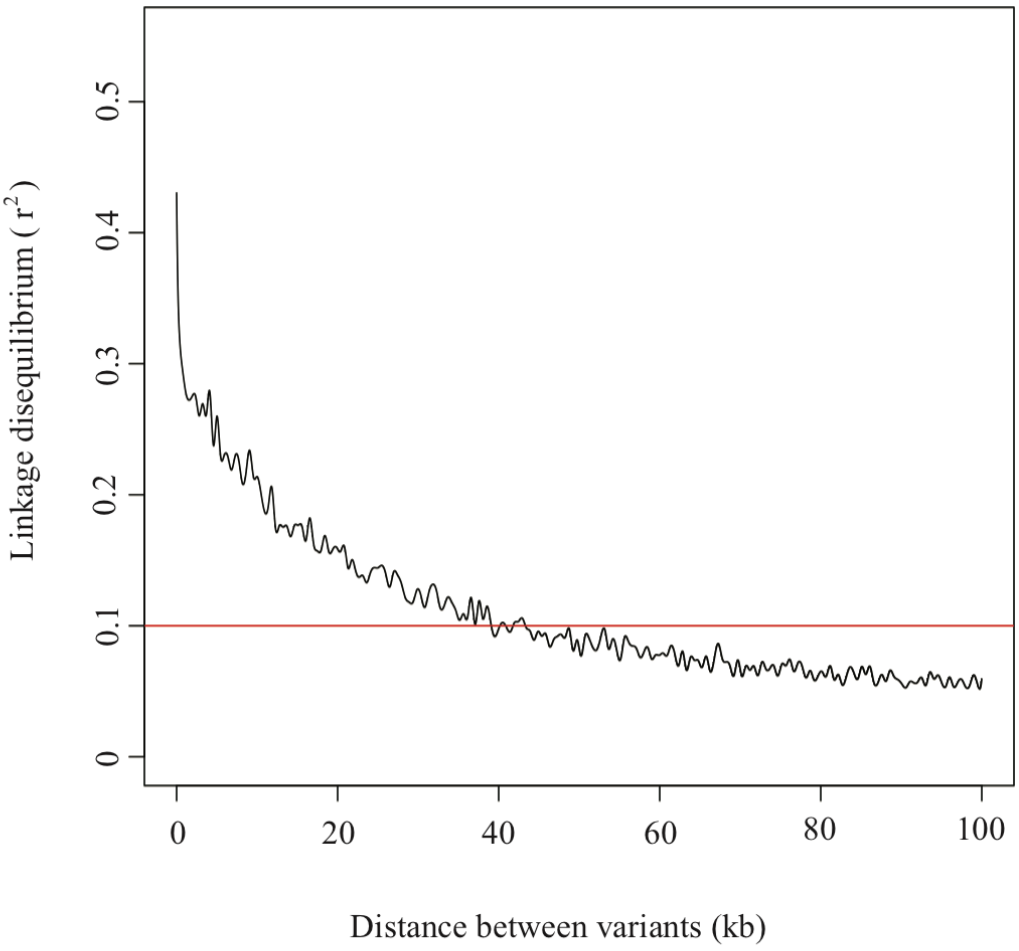

Fig. S6. Linkage disequilibrium decay along the genome. LD decay over pairwise combinations of alleles within 100 kb of each other on the longest scaffold in the genome (49,059,223 bp), with r^2=0.1 marked for reference. From this pattern of decay, we chose a window size of 50-kb for sliding windows analyses used in this study.

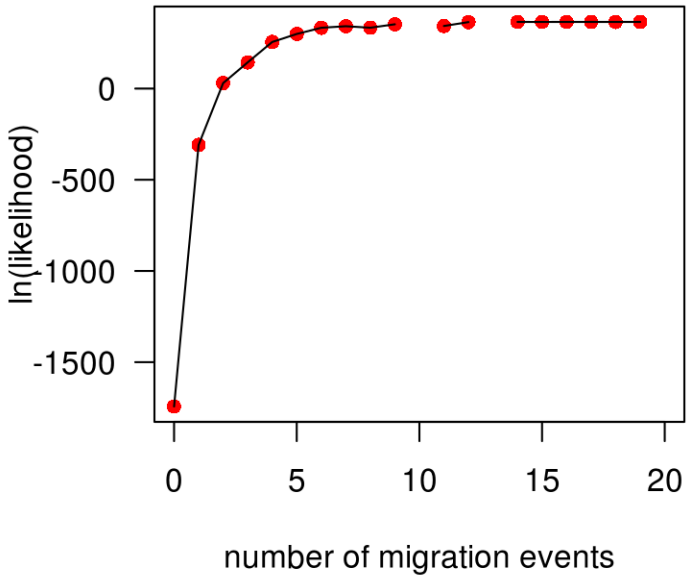

Fig. S7. The likelihood of migration events on the TREEMIX population graph of admixture events across Caribbean populations. The log likelihood of different population graphs with 0-20 migration events model on them using TREEMIX (*33*) and an LD-pruned set of 2.3 million SNPs across the SSI species, the 5 focal outgroup generalist populations (>8 individuals) and *C.artifrons*. The rate of change in the likelihood began to decline after three migration events, so three migration arrows were included in the population graph in Fig. 4B.

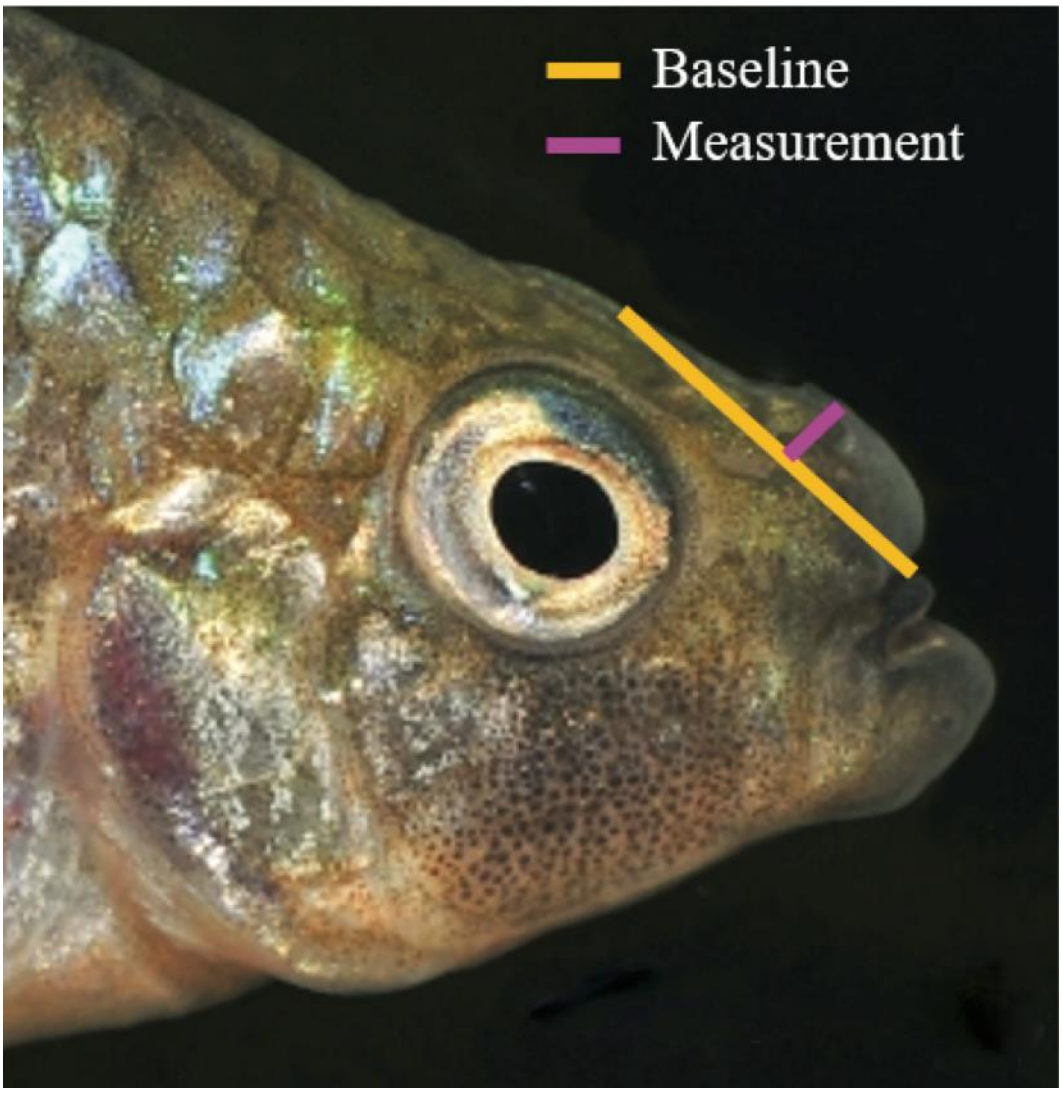

Fig S8. Example image of nasal protrusion distance measurement for GWAS. The purple line represents the nasal protrusion distance on a *C. brontotheroides* specimen. The yellow line represents a baseline tangent line from the dorsal surface of the neurocranium to the tip of the premaxilla used for reference. Photo by Tony Terceira.

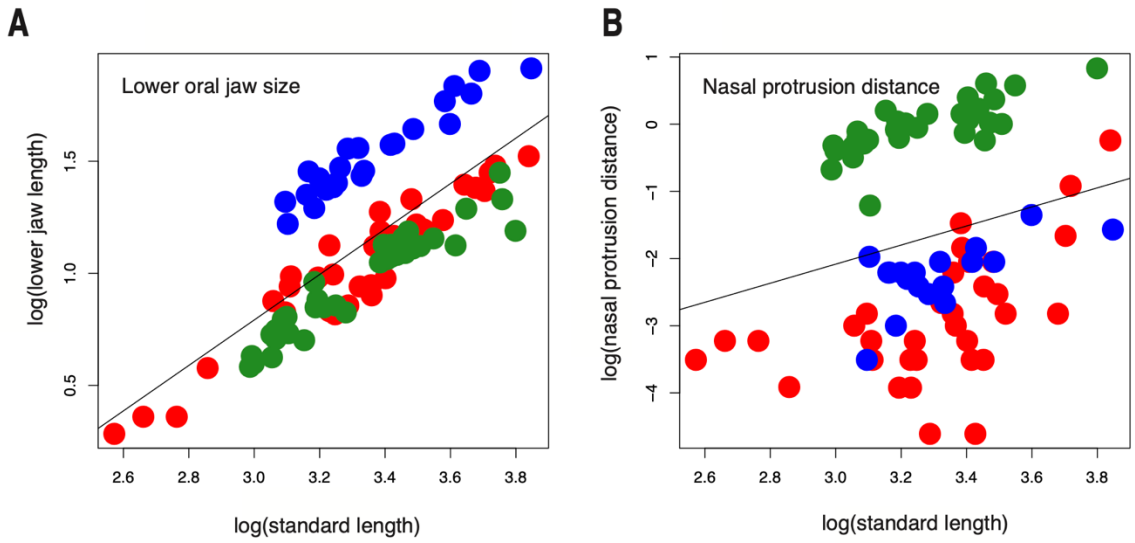

Fig. S9. Standardized craniofacial trait measurements in SSI species. Log-transformed A) lower oral jaw length (mm) and B) nasal protrusion distance (mm) standardized by log-transformed standard length (mm) for SSI generalist (red), molluscivore (green), and scale-eater (blue).

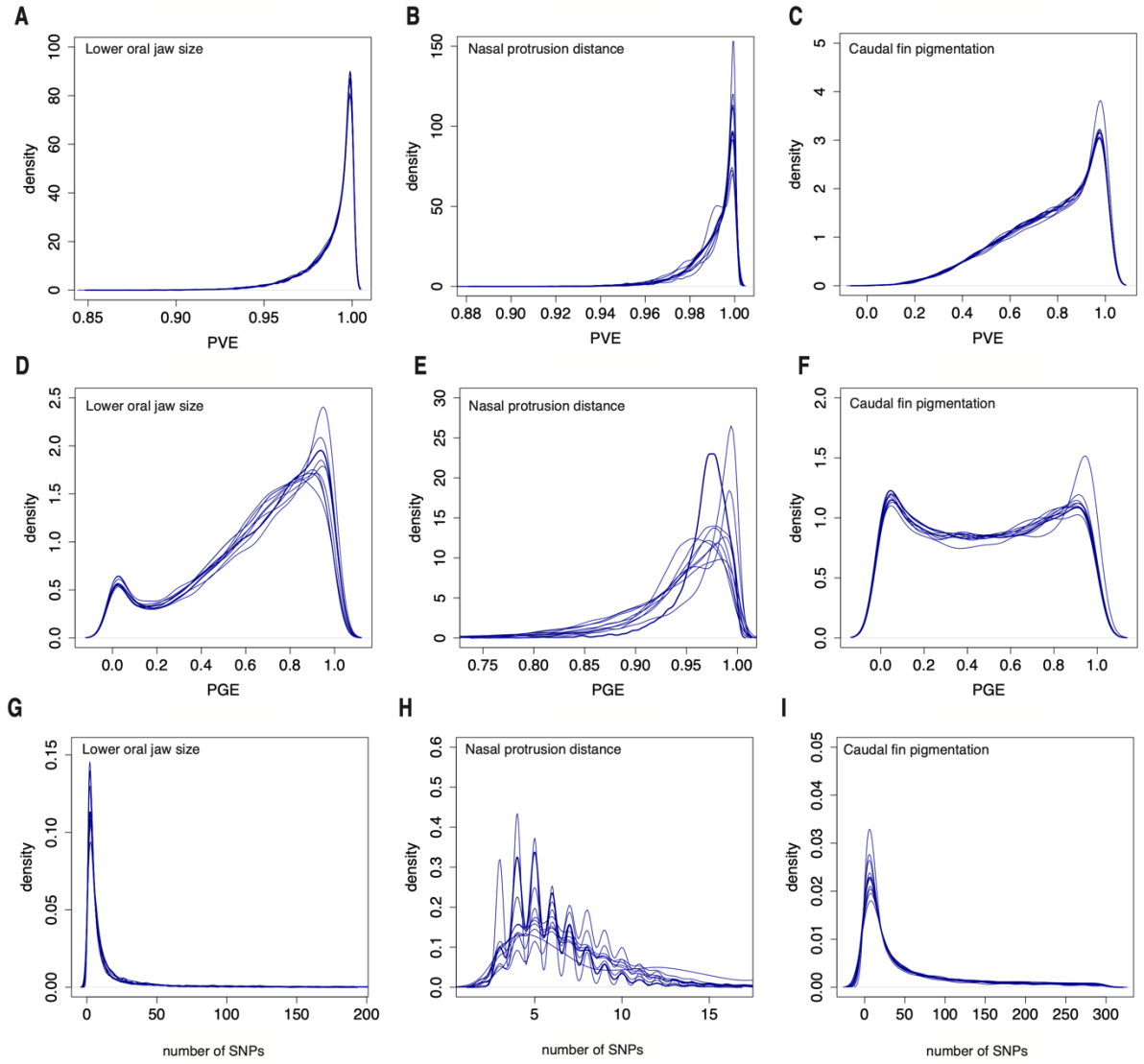

Fig. S10. Posterior density distributions for hyper-parameters describing the proportion of variance in phenotypes for the three focal traits. The variance in lower jaw size, nasal protrusion distance, and caudal fin pigmentation explained by A-C) every SNP (proportion of phenotype variance explained [PVE]), D-F) SNPs of large effect (proportion of genetic variance explained by sparse effects [PGE]), and G-H) the number of large effect SNPS required to explain PGE. Individual lines represent 10 independent MCMC runs of GEMMA's Bayesian sparse linear mixed model.

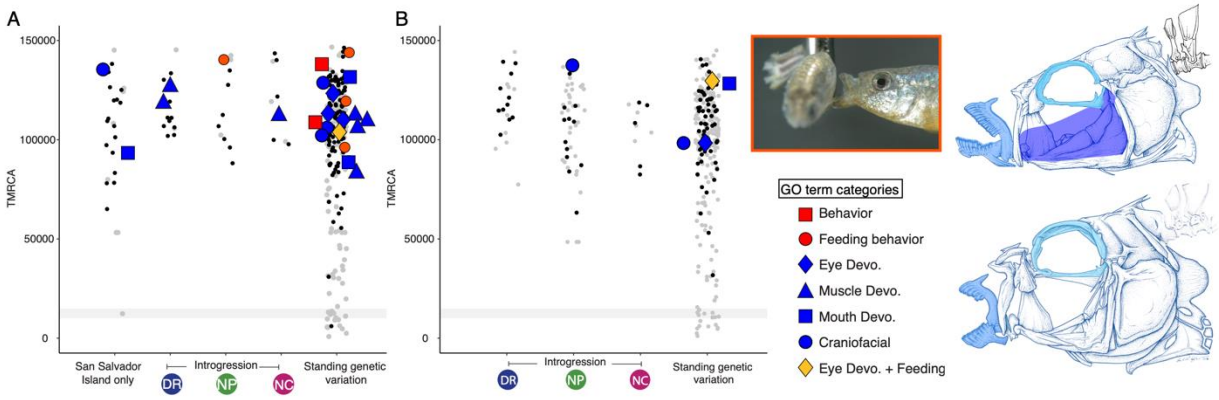

Fig. S11. The spatiotemporal landscape of adaptive radiation based on divergence time from an outgroup generalist population. Time to most recent common ancestor (TMRCA) of adaptive alleles based on D_{xy} in their 50-kb window. TMRCA estimates based on genetic divergence (D_{xy}) between outgroup *C. artifrons* and A) scale-eaters or B) molluscivores. Each column separates adaptive alleles by their spatial distribution: de novo (SSI only), adaptive introgression from one of three outgroup populations (DR: Dominican Republic, NP: New Providence, NC: North Carolina), and standing genetic variation. Gray bars highlight the approximate origins of the microendemic radiation on SSI at approximately 6-19 kya (based on range of geological age estimates for filling of hypersaline lakes on SSI (*57*, *58*) since the last glacial maximum (*59*)). All adaptive alleles associated with genes for behavior (red) or craniofacial morphology (blue) are illustrated by a colored point. Black points show adaptive alleles for non-focal GO terms or unannotated; gray points show all nearly fixed alleles between specialists ($F_{st} \geq 0.95$) with no signal of a hard selective sweep.

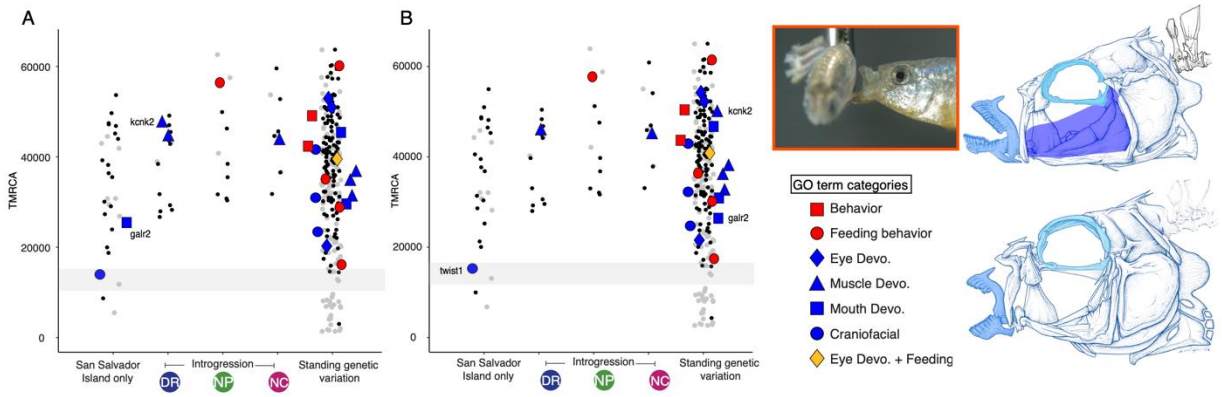

Fig. S12. The alternative spatiotemporal landscape of adaptive radiation in scale-eaters. Divergence time plot in which the two labelled alleles that were plotted in the introgression and de novo column (A) are plotted as their alternative spatial distribution in standing variation column (B). Time to most recent common ancestor (TMRCA) of adaptive alleles based on D_{xy} in their 50-kb window based on the larger spatial distrubtion of adaptive alleles. TMRCA estimates based on genetic divergence (D_{xy}) between the two specialists across alternative distributions for scale-eater adaptive alleles. Points labeled with gene names indicate the two alleles in which there are two or more adaptive alleles in the same linkage block that have different spatial distributions: A) alleles with smaller spatial scales (de novo or introgressed) and B) and alleles with larger spatial scales (standing genetic variation). Each column separates adaptive alleles by their spatial distribution: de novo (SSI only), adaptive introgression from one of three outgroup populations (DR: Dominican Republic, NP: New Providence, NC: North Carolina), and standing genetic variation. Gray bars highlight the approximate origins of the microendemic radiation on SSI at approximately 6-19 kya (based on range of geological age estimates for filling of hypersaline lakes on SSI (*57*, *58*) since the last glacial maximum (*59*)). All adaptive alleles associated with genes for behavior (red) or craniofacial morphology (blue) are illustrated by a colored point. Black points show adaptive alleles for non-focal GO terms or

unannotated; gray points show all nearly fixed alleles between specialists ($F_{st} \geq 0.95$) with no signal of a hard selective sweep.

Time to most recent common ancestor (TMRCA) of the region surrounding candidate adaptive alleles (LD-pruned so that each point is independent) based on relative genetic divergence metric *Dxy* (*68*) which captures only the amount divergence that has accumulated since the two populations diverged for A) scale-eaters and B) molluscivores. Each column separates adaptive alleles by their spatial distribution: de novo (SSI only), adaptive introgression from one of three outgroup populations (DR: Dominican Republic, NP: New Providence, NC: North Carolina), and standing genetic variation. Gray bars highlight the approximate origins of the microendemic radiation on SSI: from the last glacial maximum (approximately 6-19 kya; ranging from to the youngest age estimate for filling of hypersaline lakes on SSI (*59*)) to the last glacial maximum before which lakes on SSI were completely dry (*58*)).Alleles are colored by evidence of hard selective sweeps: black for fixed or nearly fixed ($F_{st} \geq 0.95$) adaptive alleles annotated for non-focal GO terms or unannotated; gray for fixed or nearly fixed alleles between specialists with no signal of hard selective sweep; and triangles represent alleles additionally associated with pigmentation. All alleles annotated for the GO categories of behavior (red shades) and craniofacial morphology (blue shades) are included. Genes highlighted in the text are labeled by their associated variant. Yellow shade indicates genes annotated for feeding behavior and eye development. Triangle shape indicates gens also annotated for pigmentation.

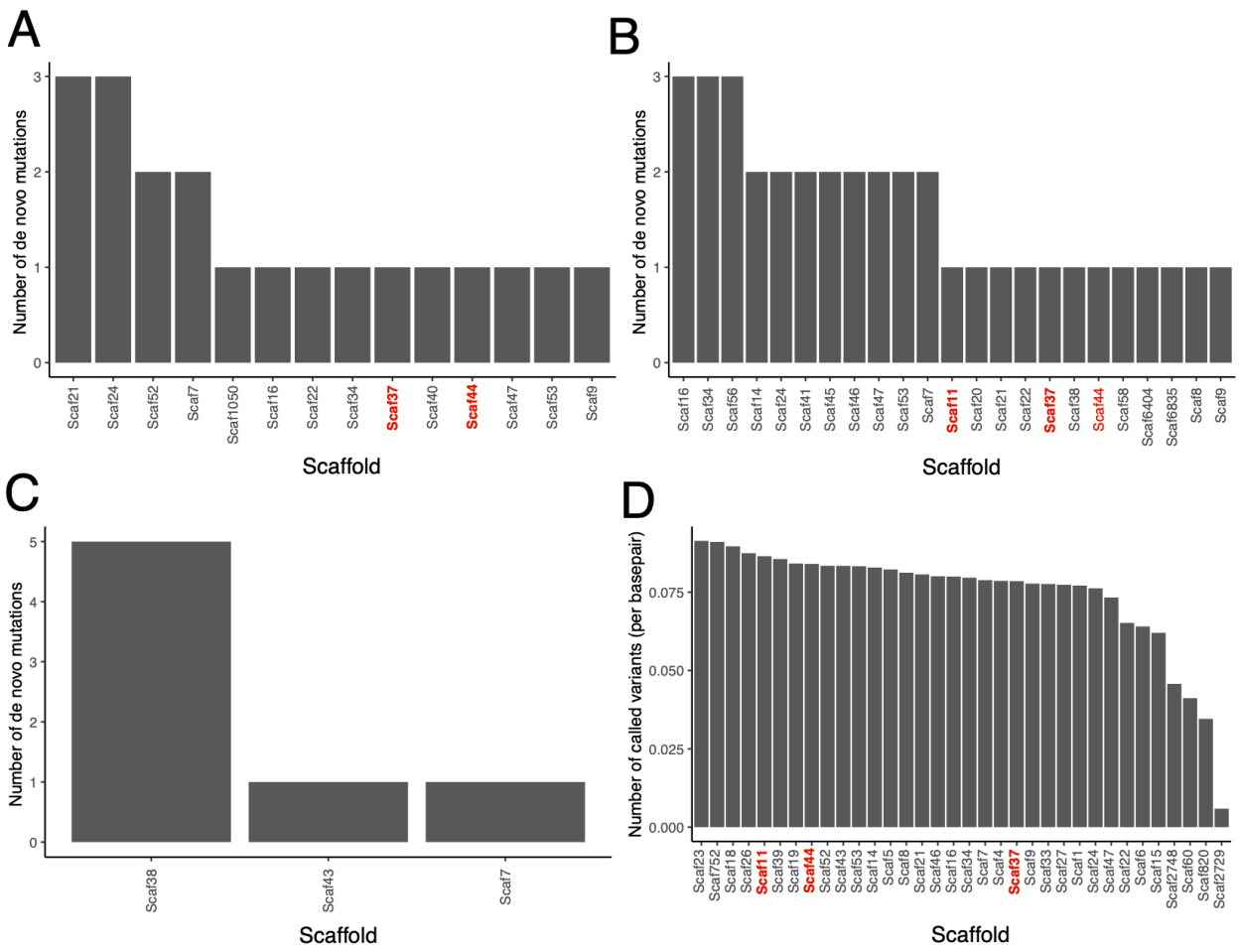

Fig. S13. Raw counts of alleles found across scaffolds. The count of de novo mutations in genome of A-B) two hybrids from molluscivores x generalist cross and C) single hybrid from scale-eater x generalist sequenced to high coverage (15-69x) that were used to estimate average mutations rate for pupfish. D) The relative number of alleles per scaffold (absolute count divided by number of base pairs in the scaffold) that candidate adaptive alleles were found on. Scaffolds highlighted in red are three scaffolds that contain the feeding behavior genes with the oldest divergence time and selective sweep age estimates.

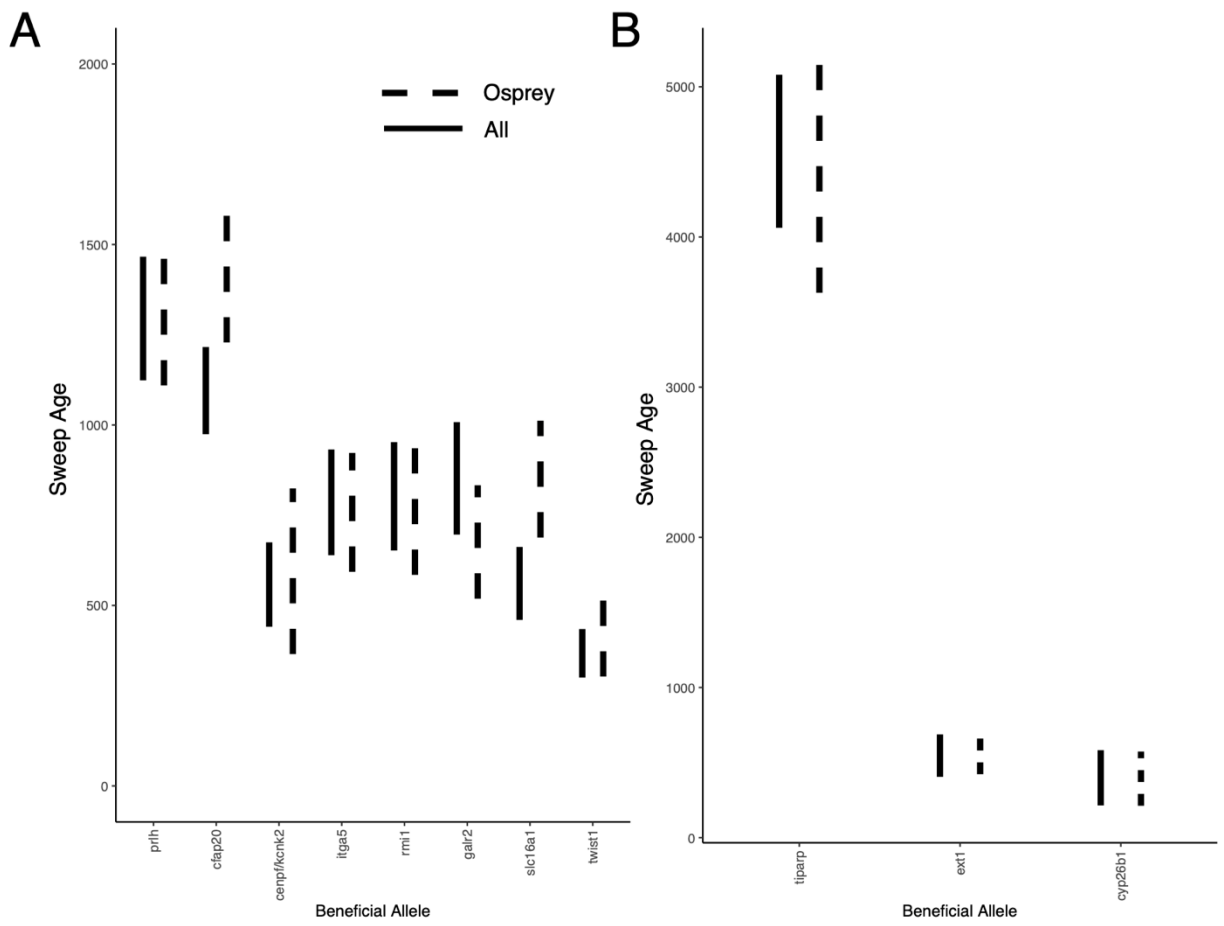

Fig. S14. Allele age estimates from single population of specialists compared to estimates from all individuals. A) 95% HPD interval from the posterior distribution of allele age estimates calculated with starTMRCA on all scale-eater individuals (*N*=26) compared to just individuals from the Osprey Lake population (*N*=11). B) 95% HPD interval from the posterior distribution of allele age estimates calculated with starTMRCA on all molluscivore individuals (*N*=43) compared to just individuals from the Osprey Lake population (*N*=10).

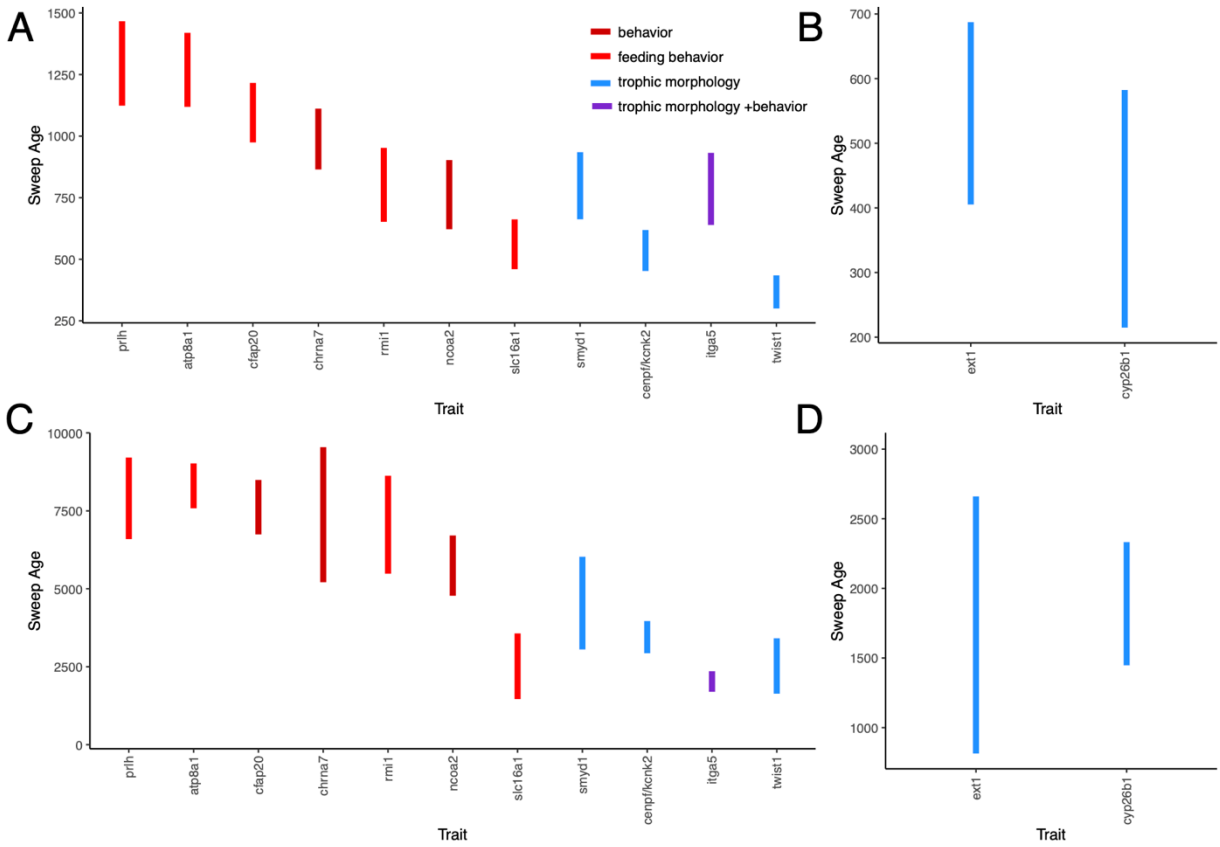

Fig. S15. Overlapping hard selective sweep age estimates from starTMRCA and McSwan. 95% HPD interval for selective sweep ages for overlapping set of adaptive alleles across starTMRCA for scale-eaters (A) and molluscivores (B) compared to the 95% HPD interval estimate from McSwan for scale-eaters (C) and molluscivores (D). Selective sweep ages are colored by GO annotations relevant to two major stages of adaptation: behavior (behavior and feeding behavior), trophic morphology (craniofacial, muscle development) and both.

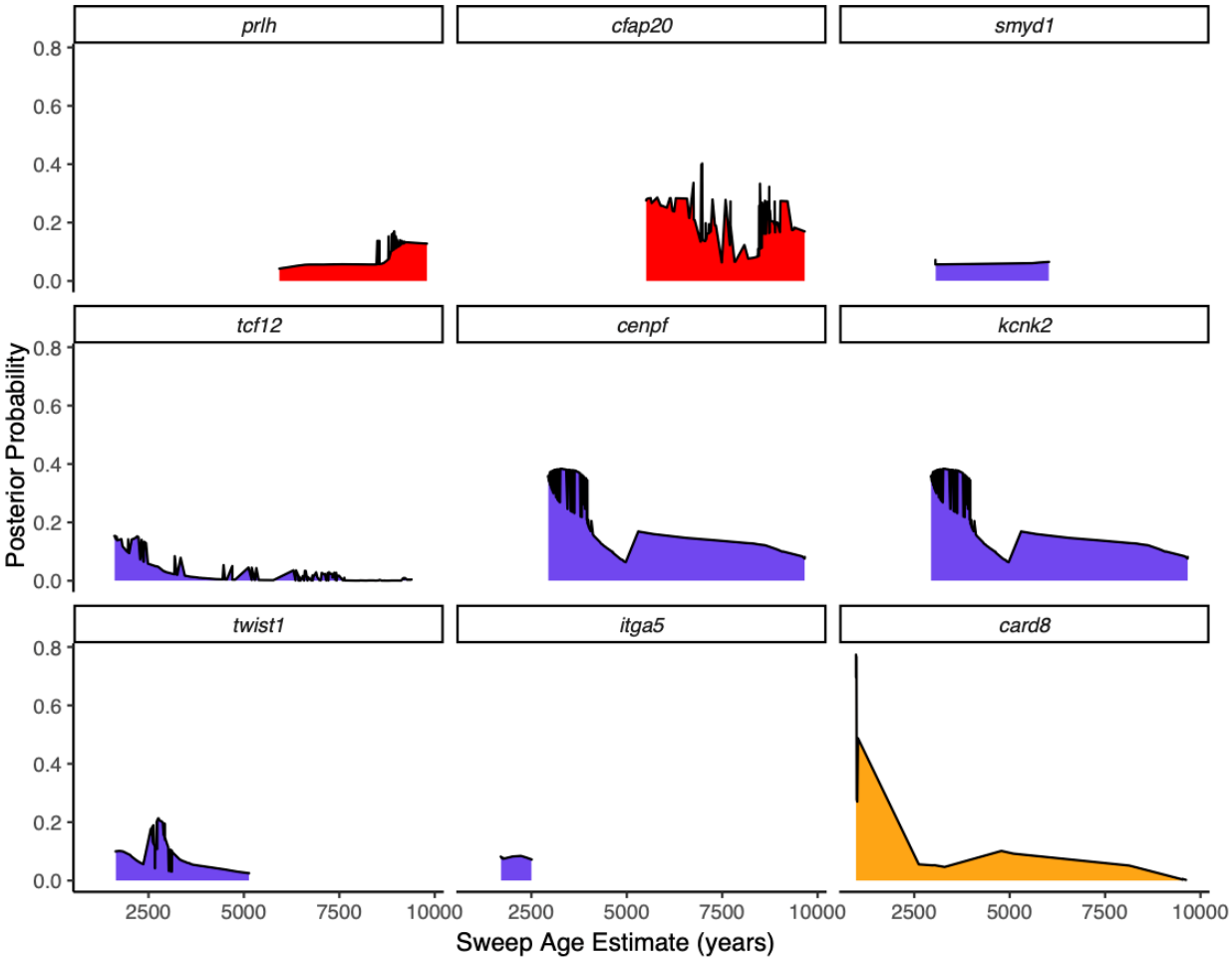

Fig. S16. Full posterior distributions for scale-eater sweeps. The posterior distributions of sweep ages estimated from focal adaptive alleles (Table S13) calculated from McSwan. These nine regions contained fixed or nearly fixed variants ($F_{st} \geq 0.95$) between specialists that were estimated to be hard selective sweeps using both SweeD and McSwan. Sweep ages are colored based on GO and GWAS annotations relevant to the stages proposed in the stages of adaptation: feeding behavior (red), trophic morphology (craniofacial and muscle: blue-violet), and sexual communication (pigmentation: orange).

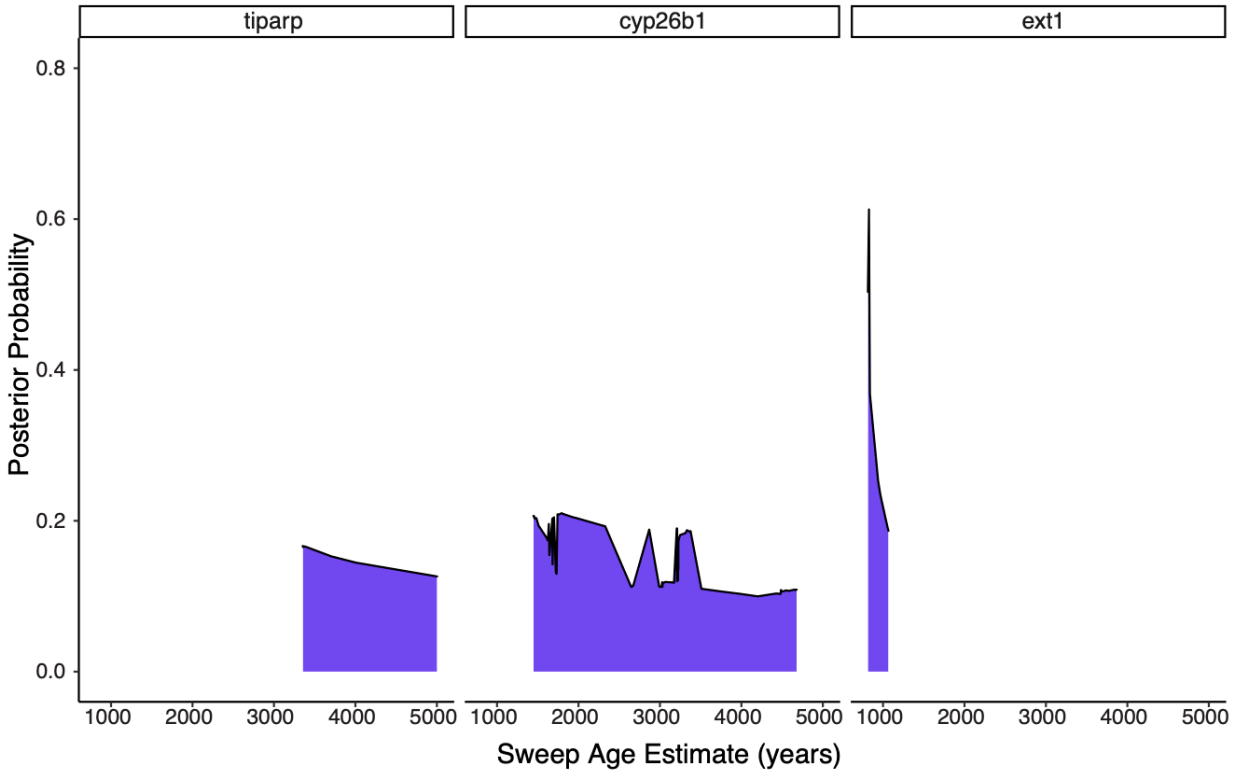

Fig. S17. Full posterior distributions for molluscivore sweeps. The posterior distributions of sweep ages estimated for focal adaptive alleles (Table S13) calculated from McSwan. These three regions contained fixed or nearly fixed variants ($F_{st} \geq 0.95$) between specialists that were estimated to be hard selective sweeps using both SweeD and McSwan. Sweep ages are colored based on GO and GWAS annotations relevant to the stages proposed in the stages of adaptive radiation hypothesis: trophic morphology (craniofacial and muscle: blue-violet).

Table S1. Summary of Caribbean pupfish sampling. The sampling localities of individuals resequenced from San Salvador Island radiation (SSI), other *Cyprinodon* across the Caribbean, Mexico, and United States, and two outgroups. Full details including sample codes, collectors, and GPS coordinates are included in Data S1 table.

Group	Species	Lake/Site	Island/Nation	Sample size
SSI generalist	*Cyprinodon variegatus*	Clear Pond	SSI, Bahamas	1
SSI generalist	*Cyprinodon variegatus*	Crescent Pond	SSI, Bahamas	4
SSI generalist	*Cyprinodon variegatus*	Granny Lake	SSI, Bahamas	1
SSI generalist	*Cyprinodon variegatus*	Great Lake	SSI, Bahamas	2
SSI generalist	*Cyprinodon variegatus*	Little Lake	SSI, Bahamas	1
SSI generalist	*Cyprinodon variegatus*	Stout's Pond	SSI, Bahamas	2
SSI generalist	*Cyprinodon variegatus*	Mermaid Pond	SSI, Bahamas	1
SSI generalist	*Cyprinodon variegatus*	Moon Rock Pond	SSI, Bahamas	1
SSI generalist	*Cyprinodon variegatus*	North Little Lake	SSI, Bahamas	1
SSI generalist	*Cyprinodon variegatus*	Osprey Lake	SSI, Bahamas	12
SSI generalist	*Cyprinodon variegatus*	Oyster Lake	SSI, Bahamas	2
SSI generalist	*Cyprinodon variegatus*	Oyster Lake	SSI, Bahamas	1
SSI generalist	*Cyprinodon variegatus*	Pain Pond	SSI, Bahamas	1
SSI generalist	*Cyprinodon variegatus*	Reckley Hill Pond	SSI, Bahamas	1
SSI generalist	*Cyprinodon variegatus*	Six Pack Pond	SSI, Bahamas	1
SSI generalist	*Cyprinodon variegatus*	Wild Dilly Pond	SSI, Bahamas	1
SSI molluscivore	*Cyprinodon brontotheroides*	Crescent Pond	SSI, Bahamas	12
SSI molluscivore	*Cyprinodon brontotheroides*	Little Lake	SSI, Bahamas	5
SSI molluscivore	*Cyprinodon brontotheroides*	Moon Rock Pond	SSI, Bahamas	6
SSI molluscivore	*Cyprinodon brontotheroides*	Osprey Lake	SSI, Bahamas	12
SSI molluscivore	*Cyprinodon brontotheroides*	Oyster Pond	SSI, Bahamas	8
SSI scale-eater	*Cyprinodon desquamator*	Crescent Pond	SSI, Bahamas	10

SSI scale-eater	*Cyprinodon desquamator*	Little Lake	SSI, Bahamas	5
SSI scale-eater	*Cyprinodon desquamator*	Osprey Lake	SSI, Bahamas	10
SSI scale-eater	*Cyprinodon desquamator*	Oyster Lake	SSI, Bahamas	1
Dominican Republic	*Cyprinodon higuey*	Laguna Bavaro	Dominican Republic	10
New Providence Island	*Cyprinodon laciniatus*	Lake Cunningham	New Providence Island, Bahamas	16
Rum Cay	*Cyprinodon variegatus*	Lake George - main lake	Rum Cay, Bahamas	17
North Carolina	*Cyprinodon variegatus*	Fort Fisher estuary	NC, USA	11
Venezuela	*Cyprinodon dearborni*	Isla Margarita	Venezuela	11
Caribbean outgroup generalist	*Cyprinodon artifrons*	Cancun	Mexico	2
Caribbean outgroup generalist	*Cyprinodon variegatus*	North Salt Pond	Acklins Island, Bahamas	1
Caribbean outgroup generalist	*Cyprinodon dearborni*	--	Bonaire	1
Caribbean outgroup generalist	*Cyprinodon variegatus*	--	Caicos Island	1
Caribbean outgroup generalist	*Cyprinodon variegatus*	Great Lake	Cat Island, Bahamas	1
Caribbean outgroup generalist	*Cyprinodon dearborni*	--	Curacao	2
North American outgroup generalist	*Cyprinodon albivelis*	Rio Yaqui basin	Mexico	1
North American outgroup generalist	*Cyprinodon eremus*	Quitobaquito Spring	AZ, USA	1
North American outgroup generalist	*Cyprinodon eximius*	Rio Conchos basin	Mexico	1
North American outgroup generalist	*Cyprinodon fontinalis*	Ojo de Carbonera Spring	Mexico	1
North American outgroup generalist	*Cyprinodon longidorsalis*	Charco Palma	Mexico	1
North American outgroup generalist	*Cyprinodon macularius*	Coachella	CA, USA	1
North American outgroup generalist	*Cyprinodon macrolepis*	Ojo de Hacienda Delores	Mexico	1
North American outgroup generalist	*Cyprinodon radiosus*	Owens Valley	CA, USA	1
Caribbean outgroup generalist	*Cyprinodon veronicae*	Ojo de Agua Charco Azul	Mexico	1
North American outgroup generalist	*Cyprinodon variegatus*	Salt pond near Dean's blue hole	Long Island, Bahamas	1
Caribbean outgroup generalist	*Cyprinodon variegatus*	Unnamed lake ‘near Rokers Point’	Exumas, Bahamas	2
Caribbean outgroup generalist	*Cyprinodon variegatus*	Unnamed lake ‘Ephemeral’	Exumas, Bahamas	1
Caribbean outgroup generalist	*Cyprinodon bondi*	Etang Saumautre	Dominican Republic	1

Caribbean outgroup generalist	*Cyprinodon variegatus*	Unnamed lake	Mayaguana	1
Caribbean outgroup generalist	*Cyprinodon variegatus*	Sarasota estuary	Florida, United States	1
Caribbean outgroup generalist	*Cyprinodon variegatus*	Lake Kilarney	New Providence Island, Bahamas	1
Caribbean outgroup generalist	*Cyprinodon variegatus*	Great Lake in the south	Long Island, Bahamas	1
Caribbean outgroup generalist	*Cyprinodon ovinus*	Falmouth River	Massachusetts, USA	1
Caribbean outgroup generalist	*Cyprinodon variegatus*	New Bight	Cat Island, Bahamas	1
Caribbean outgroup generalist	*Cyprinodon variegatus*	Pirate's Well Lake	Mayaguana, Bahamas	1
Caribbean outgroup generalist	*Cyprinodon variegatus*	Salt Pond	Exumas, Bahamas	1
Caribbean outgroup generalist	*Cyprinodon variegatus*	Scully Lake	Mayaguana, Bahamas	1
Lake Chichancab pupfish radiation outgroup	*Cyprinodon maya*	Laguna Chichancanab	Quintana Roo, Mexico	1
Lake Chichancab pupfish radiation outgroup	*Cyprinodon simus*	Laguna Chichancanab	Quintana Roo, Mexico	1
Cualac outgroup	*Cualac tessellatus*	Media Luna	Mexico	1
Megupsilon outgroup	*Megupsilon aporus*	El Potosi	Mexico	1

Table S2. The number of selective sweeps found in specialist genomes. The number of selective sweeps detected in total across the specialist genomes using and SFS-based approach SweeD and LD-based approach OmegaPlus. Hard selective sweeps were determined based on demographic simulation-based thresholds (SweeD CLR > 5.28; OmegaPlus ω > 3.31 for scale-eaters and SweeD CLR > 4.47; OmegaPlus ω > 4.23 for molluscivores). The alleles that overlapped with nearly fixed (F_{st} ≥0.95) SNP(s) between the specialists with hard selective sweeps detecting jointly in both sweep programs were then used the total number of candidate adaptive alleles in this study.

	Molluscivore		Scale-eater	
	SweeD	OmegaPlus	SweeD	OmegaPlus
Number of selective sweeps detected	8269	12060	14729	18387
Number of windows tested	52744	49822	52696	51561
Number of alleles that overlap with sweep	1490	3917	3463	3766
Number of alleles with uniquely detected selective sweep	13	2427	230	303
Number of alleles with jointly detected selective sweep	1477		3233	

Table S3. Candidate adaptive alleles for the San Salvador Island (SSI) scale-eater.

Location of the genic regions that contained signatures of a strong selective sweep in the scale-eater (above demographic simulation based thresholds SweeD CLR > 5.28;OmegaPlus ω > 3.31) and at least one divergent variant between the specialists ($F_{st} \geq 0.95$). Full list of alleles, including unannotated candidate regions provided in Data S2. Adaptive alleles highlighted in Figure 4 are listed in bold.

Gene	Scaffold	Gene Start	Gene End	Number of Alleles
coq7	c_bro_v1_0_scaf1	28974409	28979038	3
gpr83	c_bro_v1_0_scaf1	38351481	38355816	2
klf1	c_bro_v1_0_scaf1	29239984	29242454	13
notum2	c_bro_v1_0_scaf1	28950946	28957848	1
rbm20	c_bro_v1_0_scaf1	15024176	15044016	1
rps15a	c_bro_v1_0_scaf1	28942599	28947456	2
ube2k	c_bro_v1_0_scaf1	41168936	41171561	2
atp8a2	c_bro_v1_0_scaf11	13000335	13035561	92
cd226	c_bro_v1_0_scaf11	10936603	10941232	7
cdk8	c_bro_v1_0_scaf11	13057400	13067971	1
cmbl	c_bro_v1_0_scaf11	9934853	9938096	11
crispld1	c_bro_v1_0_scaf11	11066268	11081938	7
dok6	c_bro_v1_0_scaf11	10963193	10972277	50
fbxl7	c_bro_v1_0_scaf11	21351783	21356510	6
hnf4g	c_bro_v1_0_scaf11	8350195	8354295	1
med1	c_bro_v1_0_scaf11	21393330	21400087	26
mtrr	c_bro_v1_0_scaf11	9943625	9954042	2
ncoa2	c_bro_v1_0_scaf11	11949666	11977882	4
prlh	**c_bro_v1_0_scaf11**	**9494231**	**9495565**	**18**
rnf6	c_bro_v1_0_scaf11	13047328	13052736	4
shisa2	c_bro_v1_0_scaf11	12945178	12953040	38
slc51a	c_bro_v1_0_scaf11	9862250	9873650	29
spice1	c_bro_v1_0_scaf11	12934206	12942196	2
zfhx4	c_bro_v1_0_scaf11	8078834	8095610	1
zbed1	c_bro_v1_0_scaf14	23383635	23383982	9
abhd8	c_bro_v1_0_scaf16	13452740	13457468	24
b3gnt3	c_bro_v1_0_scaf16	10003286	10004410	15

bmb	c_bro_v1_0_scaf16	10649637	10654441	38
brinp3	c_bro_v1_0_scaf16	11738302	11756508	33
crocc	c_bro_v1_0_scaf16	32985892	33009791	1
dda1	c_bro_v1_0_scaf16	13466708	13470377	2
eef1d	c_bro_v1_0_scaf16	10028318	10042958	30
ptprs	c_bro_v1_0_scaf16	8205473	8246024	56
pycr3	c_bro_v1_0_scaf16	10045452	10047013	8
rfc4	c_bro_v1_0_scaf16	35817866	35832867	38
serpinb1	c_bro_v1_0_scaf16	10634868	10638000	14
tdrd5	c_bro_v1_0_scaf16	12808042	12822317	47
tjp3	c_bro_v1_0_scaf16	35777675	35795399	21
tsta3	c_bro_v1_0_scaf16	10641946	10647463	23
zfp2	c_bro_v1_0_scaf16	35859060	35860865	8
zfp26	c_bro_v1_0_scaf16	35907423	35909825	2
znf271	c_bro_v1_0_scaf16	35840463	35842592	7
znf45	c_bro_v1_0_scaf16	35879283	35880581	7
anks1a	c_bro_v1_0_scaf18	18164811	18167681	1
gnat2	c_bro_v1_0_scaf18	13731762	13735798	2
itga5	c_bro_v1_0_scaf18	28908235	28944244	2
mybph	c_bro_v1_0_scaf18	26461834	26474649	15
nfasc	c_bro_v1_0_scaf18	17031686	17047770	1
sarg	c_bro_v1_0_scaf18	18185730	18187828	2
slc16a1	c_bro_v1_0_scaf18	29586755	29599009	1
nap1l4	c_bro_v1_0_scaf19	7836170	7842620	1
smap	c_bro_v1_0_scaf19	2027249	2028419	2
th	**c_bro_v1_0_scaf19**	**7787018**	**7794685**	**1**
trim44	c_bro_v1_0_scaf19	6431393	6435783	13
aasdhppt	c_bro_v1_0_scaf21	26911467	26919394	1
b3gat1	c_bro_v1_0_scaf21	29988110	29992848	1
cntn5	c_bro_v1_0_scaf21	10012673	10063457	1
col26a1	c_bro_v1_0_scaf21	20284619	20287102	12
emid1	c_bro_v1_0_scaf21	20254093	20266161	2
ifi44	c_bro_v1_0_scaf21	32843968	32848322	9
irf8	c_bro_v1_0_scaf21	41216201	41218789	1
mrm3	c_bro_v1_0_scaf21	15198156	15201994	1
nipsnap2	c_bro_v1_0_scaf21	24482700	24491999	33
nxn	c_bro_v1_0_scaf21	15204991	15221395	8
pde4d	c_bro_v1_0_scaf21	32298408	32320844	1
slc35e1	c_bro_v1_0_scaf21	31978195	31986378	1
tiparp	c_bro_v1_0_scaf21	33709833	33728566	1

trarg1	c_bro_v1_0_scaf21	25190856	25191383	1
atad2	c_bro_v1_0_scaf22	7942666	7961336	3
cyp26b1	c_bro_v1_0_scaf24	20457960	20473004	8
dysf	c_bro_v1_0_scaf24	20196578	20211497	1
ext1	c_bro_v1_0_scaf26	271389	272345	8
ext1b	c_bro_v1_0_scaf26	241224	252635	1
ppp1r3a	c_bro_v1_0_scaf26	8473965	8479904	4
soga3	c_bro_v1_0_scaf26	428526	434421	23
washc5	c_bro_v1_0_scaf26	301047	314009	1
zdhhc14	c_bro_v1_0_scaf2748	17727	21969	1
bri3bp	c_bro_v1_0_scaf33	12638129	12642531	28
gnaq	c_bro_v1_0_scaf33	12884125	12889121	9
pip5k1b	c_bro_v1_0_scaf33	2845282	2870905	6
wdr31	c_bro_v1_0_scaf33	12650071	12652945	20
cadps	c_bro_v1_0_scaf34	25394387	25411387	3
eya2	c_bro_v1_0_scaf34	32387513	32410375	2
srgap3	c_bro_v1_0_scaf34	26044753	26082456	2
st7l	c_bro_v1_0_scaf34	31252675	31262720	1
tfap2a	**c_bro_v1_0_scaf34**	**32260190**	**32264933**	**6**
znf362	c_bro_v1_0_scaf34	27775403	27792854	1
arhgap29	c_bro_v1_0_scaf37	30354970	30373446	1
atp5if1a	c_bro_v1_0_scaf37	3215186	3217688	1
cfap20	**c_bro_v1_0_scaf37**	**5089635**	**5093234**	**24**
chrna7	c_bro_v1_0_scaf37	3585852	3605137	8
dgat1	c_bro_v1_0_scaf37	5067735	5086382	37
dlx6a	c_bro_v1_0_scaf37	12742190	12744024	1
gpr20	c_bro_v1_0_scaf37	5101678	5107779	6
kcnn3	c_bro_v1_0_scaf37	3554189	3565883	4
mylipa	c_bro_v1_0_scaf37	8279827	8292615	1
slc45a4	c_bro_v1_0_scaf37	5115894	5125512	11
tbc1d20	c_bro_v1_0_scaf37	5047715	5065680	25
trim46	c_bro_v1_0_scaf37	3671825	3693120	1
trps1	c_bro_v1_0_scaf37	5649512	5665892	2
rmi1	c_bro_v1_0_scaf39	4258986	4266819	1
smyd1	c_bro_v1_0_scaf39	1675166	1684412	7
ubox5	c_bro_v1_0_scaf39	1621625	1630916	7
c1d	c_bro_v1_0_scaf43	30356623	30357420	6
dst	c_bro_v1_0_scaf43	16259900	16336750	2
ppp3r1	c_bro_v1_0_scaf43	30309740	30313100	4
sertad2	c_bro_v1_0_scaf43	10397273	10398532	4

sptlc3	c_bro_v1_0_scaf43	12316311	12350292	3
tmem26	c_bro_v1_0_scaf43	26556107	26570766	5
znf451	c_bro_v1_0_scaf43	16192481	16198948	15
atp8a1	c_bro_v1_0_scaf44	14934291	14999736	19
cenpf,kcnk2	**c_bro_v1_0_scaf44**	**12548021**	**12569724**	**16**
gpm6a	c_bro_v1_0_scaf44	24566260	24570802	9
kcnk2	**c_bro_v1_0_scaf44**	**12526223**	**12538276**	**23**
tsc22d3	c_bro_v1_0_scaf44	11339700	11340952	3
tstd1	c_bro_v1_0_scaf44	12012710	12013203	1
card8	**c_bro_v1_0_scaf46**	**1328324**	**1329460**	**10**
ccdc178	c_bro_v1_0_scaf46	15536795	15561009	1
xrn1	c_bro_v1_0_scaf46	25988805	26007498	39
dnm1	c_bro_v1_0_scaf47	21986865	22007761	1
map1b	c_bro_v1_0_scaf47	16222149	16245672	9
pdlim5	c_bro_v1_0_scaf47	24141068	24152322	1
ptger4	c_bro_v1_0_scaf47	16158956	16164333	4
aldh1a2	c_bro_v1_0_scaf5	27683247	27700000	1
esrp2	c_bro_v1_0_scaf5	34229725	34252121	1
gse1	c_bro_v1_0_scaf5	28378694	28397287	1
tcf12	**c_bro_v1_0_scaf5**	**27885956**	**27895543**	**15**
bcor	c_bro_v1_0_scaf52	5564938	5578475	2
chpf	c_bro_v1_0_scaf52	21895691	21907353	1
nr4a2	c_bro_v1_0_scaf52	13846770	13849514	4
st6gal2	c_bro_v1_0_scaf52	6730438	6731400	2
vgll3	c_bro_v1_0_scaf52	23953279	23956671	1
cox6b1	c_bro_v1_0_scaf53	24790612	24793003	8
cyp21a2	c_bro_v1_0_scaf53	18529622	18536111	2
eva1b	c_bro_v1_0_scaf53	29794772	29795353	2
fhod3	c_bro_v1_0_scaf53	18622119	18644926	2
galnt1	c_bro_v1_0_scaf53	20852048	20872629	17
glipr2	c_bro_v1_0_scaf53	20433230	20435503	3
hdac9b	c_bro_v1_0_scaf53	19008287	19034268	1
mag	c_bro_v1_0_scaf53	17408478	17413240	2
map7d1	c_bro_v1_0_scaf53	29904810	29922183	25
mindy3	c_bro_v1_0_scaf53	20097197	20106215	8
nacad	c_bro_v1_0_scaf53	20437309	20451974	2
pxn1	c_bro_v1_0_scaf53	20366555	20367417	1
rasip1	c_bro_v1_0_scaf53	24769523	24786366	13
slc2a3	c_bro_v1_0_scaf53	24809669	24817209	15
steap4	c_bro_v1_0_scaf53	20313856	20325260	26

tbrg4	c_bro_v1_0_scaf53	20454806	20462512	2
them4	c_bro_v1_0_scaf53	21823050	21830844	5
tnc	c_bro_v1_0_scaf53	18536783	18542213	1
twist1	**c_bro_v1_0_scaf53**	**18968733**	**18969242**	**1**
zhx2	c_bro_v1_0_scaf53	11078442	11084544	6
znf628	c_bro_v1_0_scaf53	24721275	24732863	6
trim25	**c_bro_v1_0_scaf60**	**1610217**	**1614325**	**2**
znf214	c_bro_v1_0_scaf60	1787099	1793538	1
foxo3	c_bro_v1_0_scaf7	12823341	12824321	3
myct1	c_bro_v1_0_scaf7	13100090	13100656	1
otof	c_bro_v1_0_scaf7	12616933	12629352	3
otof	c_bro_v1_0_scaf7	12642391	12658039	5
smek1	c_bro_v1_0_scaf7	12319537	12332574	1
43530	c_bro_v1_0_scaf752	1258	12292	29
nat1	c_bro_v1_0_scaf752	13172	14020	7
zdhhc20	c_bro_v1_0_scaf752	16935	24566	7
galr2	**c_bro_v1_0_scaf8**	**19974117**	**19979248**	**2**
grid2ip	c_bro_v1_0_scaf8	21581872	21603752	4
map2k6	c_bro_v1_0_scaf8	19746299	19760895	3
dcun1d2	c_bro_v1_0_scaf9	28311034	28313774	7
fhl2	c_bro_v1_0_scaf9	25288775	25292382	1
fut9	c_bro_v1_0_scaf9	25262573	25263652	16

Table S4. Adaptive alleles for the San Salvador Island (SSI) molluscivore.

Location of the genic regions that contained signatures of a strong selective sweep in the molluscivore (SweeD CLR ≥ 4.47; OmegaPlus ω > 4.23) and at least one divergent variant between the specialists (F_{st} ≥ 0.95). Full list of alleles, including one unannotated candidate regions provided in Data S3. Adaptive alleles highlighted in Figure S5 are listed in bold.

Gene	Scaffold	Gene Start	Gene Stop	Number of Alleles
alox15b	c_bro_v1_0_scaf1	34682742	34695090	1
coq7	c_bro_v1_0_scaf1	28974409	28979038	3
gga1	c_bro_v1_0_scaf1	29195804	29209213	5
gpr83	c_bro_v1_0_scaf1	38351481	38355816	2
klf1	c_bro_v1_0_scaf1	29239984	29242454	13
notum2	c_bro_v1_0_scaf1	28950946	28957848	1
rbm20	c_bro_v1_0_scaf1	15024176	15044016	1
rps15a	c_bro_v1_0_scaf1	28942599	28947456	2
atp8a2	c_bro_v1_0_scaf11	13000335	13035561	92
cd226	c_bro_v1_0_scaf11	10936603	10941232	6
ncoa2	c_bro_v1_0_scaf11	11949666	11977882	7
shisa2	c_bro_v1_0_scaf11	12945178	12953040	18
spice1	c_bro_v1_0_scaf11	12934206	12942196	4
ube2w	c_bro_v1_0_scaf11	11253461	11259709	48
abhd8	c_bro_v1_0_scaf16	13452740	13457468	17
b3gnt3	c_bro_v1_0_scaf16	10003286	10004410	15
b3gnt3	c_bro_v1_0_scaf16	10019232	10020410	1
eef1d	c_bro_v1_0_scaf16	10028318	10042958	64
ptprs	c_bro_v1_0_scaf16	8205473	8246024	20
pycr3	c_bro_v1_0_scaf16	10045452	10047013	8
rfc4	c_bro_v1_0_scaf16	35817866	35832867	31
anks1a	c_bro_v1_0_scaf18	18164811	18167681	1
mybph	c_bro_v1_0_scaf18	26461834	26474649	7
nfasc	c_bro_v1_0_scaf18	17031686	17047770	1
sarg	c_bro_v1_0_scaf18	18185730	18187828	2
trim44	c_bro_v1_0_scaf19	6431393	6435783	14
b3gat1	c_bro_v1_0_scaf21	29988110	29992848	1
cntn5	c_bro_v1_0_scaf21	10012673	10063457	1

tiparp	**c_bro_v1_0_scaf21**	**33709833**	**33728566**	**1**
trarg1	c_bro_v1_0_scaf21	25190856	25191383	1
atad2	c_bro_v1_0_scaf22	7942666	7961336	3
cyp26b1	**c_bro_v1_0_scaf24**	**20457960**	**20473004**	**8**
ext1	c_bro_v1_0_scaf26	271389	272345	8
ext1b	c_bro_v1_0_scaf26	241224	252635	1
sox9	c_bro_v1_0_scaf27	22135691	22136918	2
bri3bp	c_bro_v1_0_scaf33	12638129	12642531	26
gnaq	c_bro_v1_0_scaf33	12884125	12889121	9
wdr31	c_bro_v1_0_scaf33	12650071	12652945	20
cadps	c_bro_v1_0_scaf34	25394387	25411387	2
znf362	c_bro_v1_0_scaf34	27775403	27792854	1
dlx6a	c_bro_v1_0_scaf37	12742190	12744024	1
mylipa	c_bro_v1_0_scaf37	8279827	8292615	1
trps1	c_bro_v1_0_scaf37	5649512	5665892	2
vps9d1	c_bro_v1_0_scaf4	15227575	15257418	1
slc29a3	c_bro_v1_0_scaf43	13679707	13685975	2
ttc33	c_bro_v1_0_scaf47	16128909	16148227	7
esrp2	c_bro_v1_0_scaf5	34229725	34252121	1
fn1	c_bro_v1_0_scaf52	19355212	19387175	1
st6gal2	c_bro_v1_0_scaf52	6730438	6731400	2
vgll3	c_bro_v1_0_scaf52	23953279	23956671	1
cox6b1	c_bro_v1_0_scaf53	24790612	24793003	8
map7d1	c_bro_v1_0_scaf53	29904810	29922183	25
rasip1	c_bro_v1_0_scaf53	24769523	24786366	13
slc2a3	c_bro_v1_0_scaf53	24809669	24817209	15
zhx2	c_bro_v1_0_scaf53	11078442	11084544	5
znf628	c_bro_v1_0_scaf53	24721275	24732863	5
foxo3	c_bro_v1_0_scaf7	12823341	12824321	3
otof	c_bro_v1_0_scaf7	12616933	12629352	11
otof	c_bro_v1_0_scaf7	12642391	12658039	5
smek1	HiC_scaffold_7	12319537	12332574	1

Table S5. Full list of functional terms associated with genes in adaptive alleles for the scale-eaters that were significantly enriched (FDR < 0.05) in a GO analysis.

Focal functional terms related to key axes of diversification in this system: habitat preference (scale-eating/snail-eating niches), trophic morphology, and/or pigmentation.

Functional Category	Enrichment FDR	Genes in list	Total genes	Genes
Neuron differentiation	0.00608452	25	1400	*map1b,atp8a2,tcf12,gpm6a,nr4a2,brinp3,tnc,ptprs,mag,foxo3,med1,rnf6,aldh1a2,gnat2,pdlim5,trim46,nfasc,washc5,zhx2,th,ext1,galr2,anks1a,chrna7,dok6*
Camera-type eye morphogenesis	0.00608452	7	114	*tbc1d20,atp8a2,gnat2,zhx2,th,tfap2a,twist1*
Generation of neurons	0.00608452	26	1553	*map1b,atp8a2,tcf12,gpm6a,nr4a2,brinp3,tnc,ptprs,mag,foxo3,twist1,med1,rnf6,aldh1a2,gnat2,pdlim5,trim46,nfasc,washc5,zhx2,th,ext1,galr2,anks1a,chrna7,dok6*
Muscle tissue development	0.00608452	12	400	*cyp26b1,eya2,kcnk2,smyd1,fhl2,cenpf,twist1,med1,aldh1a2,fhod3,pdlim5,tiparp*
Regulation of biological quality	0.00608452	50	4146	*kcnk2,klf1,dnm1,foxo3,atp8a1,abhd8,atp8a2,gnaq,ptger4,chrna7,gpr20,pde4d,xrn1,cyp26b1,cfap20,ube2k,rasip1,trim44,crocc,eya2,prlh,ptprs,mag,map2k6,otof,med1,rnf6,steap4,aldh1a2,map1b,gnat2,fhod3,dysf,slc16a1,tsc22d3,pdlim5,cadps,tiparp,nxn,rmi1,th,galr2,dgat1,grid2ip,tbc1d20,tbrg4,them4,trim46,rfc4,cyp21a2*
Cell development	0.00708671	32	2196	*map1b,atp8a2,tcf12,gpm6a,brinp3,tnc,ptprs,mag,fhl2,foxo3,twist1,med1,tbc1d20,rnf6,aldh1a2,gnat2,fhod3,dysf,nr4a2,tdrd5,pdlim5,trim46,nfasc,washc5,zhx2,th,ext1,galr2,anks1a,pde4d,chrna7,dok6*
Neural retina development	0.00819009	5	64	*atp8a2,gnat2,gpm6a,zhx2,tfap2a*
Feeding behavior	0.00819009	6	102	*cfap20,prlh,atp8a2,rmi1,th,galr2*
Striated muscle tissue development	0.00819009	11	385	*cyp26b1,eya2,kcnk2,smyd1,fhl2,cenpf,twist1,med1,aldh1a2,fhod3,pdlim5*
Neurogenesis	0.00819009	26	1663	*map1b,atp8a2,tcf12,gpm6a,nr4a2,brinp3,tnc,ptprs,mag,foxo3,twist1,med1,rnf6,aldh1a2,gnat2,pdlim5,trim46,nfasc,washc5,zhx2,th,ext1,galr2,anks1a,chrna7,dok6*
Response to lipid	0.00819009	19	997	*rnf6,brinp3,ptger4,card8,med1,cyp26b1,tnc,pde4d,xrn1,foxo3,trim25,gpr83,aldh1a2,ncoa2,irf8,nr4a2,hnf4g,th,fhl2*
Eating behavior	0.00819009	4	33	*prlh,atp8a2,rmi1,th*
Camera-type eye development	0.00819009	10	317	*med1,tbc1d20,aldh1a2,atp8a2,gnat2,gpm6a,zhx2,th,tfap2a,twist1*
Developmental growth	0.00819009	15	651	*tnc,prlh,kcnk2,ptprs,mag,pde4d,foxo3,med1,rnf6,map1b,atp8a2,dysf,pdlim5,rmi1,trim46*
Eye morphogenesis	0.0084973	7	152	*tbc1d20,atp8a2,gnat2,zhx2,th,tfap2a,twist1*
Embryonic camera-type eye development	0.01187832	4	39	*aldh1a2,th,twist1,tfap2a*

Regulation of phospholipid translocation	0.01187832	2	3	*atp8a1,atp8a2*
Positive regulation of phospholipid translocation	0.01187832	2	3	*atp8a1,atp8a2*
Negative regulation of axon extension	0.01370935	4	41	*ptprs,mag,rnf6,trim46*
Eye development	0.01408643	10	365	*med1,tbc1d20,aldh1a2,atp8a2,gnat2,gpm6a,zhx2,th,tfap2a,twist1*
Growth	0.01408643	18	1018	*sertad2,st7l,tnc,prlh,kcnk2,ptprs,mag,pde4d,foxo3,med1,rnf6,map1b,atp8a2,dysf,irf8,pdlim5,rmi1,trim46*
Cellular response to lipid	0.01408643	14	671	*rnf6,brinp3,ptger4,card8,med1,cyp26b1,tnc,pde4d,foxo3,aldh1a2,irf8,nr4a2,hnf4g,fhl2*
Visual system development	0.01408643	10	366	*med1,tbc1d20,aldh1a2,atp8a2,gnat2,gpm6a,zhx2,th,tfap2a,twist1*
Anatomical structure morphogenesis	0.01669332	34	2702	*map1b,tfap2a,cyp26b1,tnc,esrp2,ptprs,rasip1,mag,fhl2,foxo3,twist1,med1,tbc1d20,rnf6,aldh1a2,atp8a2,gnat2,fhod3,dysf,gpm6a,nr4a2,itga5,pdlim5,trim46,nfasc,tiparp,zhx2,th,ext1,crispld1,chrna7,bcor,eya2,dok6*
Neuron development	0.01669332	19	1140	*map1b,atp8a2,gpm6a,tnc,ptprs,mag,rnf6,gnat2,nr4a2,pdlim5,trim46,nfasc,washc5,th,ext1,galr2,anks1a,chrna7,dok6*
Sensory system development	0.01669332	10	377	*med1,tbc1d20,aldh1a2,atp8a2,gnat2,gpm6a,zhx2,th,tfap2a,twist1*
Cell differentiation	0.01725075	48	4372	*tnc,klf1,map1b,atp8a2,tcf12,gpm6a,nr4a2,brinp3,smyd1,foxo3,glipr2,med1,tfap2a,cyp26b1,prlh,ptprs,rasip1,mag,fhl2,cenpf,twist1,tbc1d20,rnf6,steap4,aldh1a2,gnat2,fhod3,dysf,irf8,tdrd5,pdlim5,trim46,nfasc,tiparp,washc5,nxn,ptger4,zhx2,th,ext1,galr2,itga5,anks1a,trps1,pde4d,chrna7,eya2,dok6*
Behavior	0.01791936	13	619	*cfap20,prlh,kcnk2,atp8a1,atp8a2,ncoa2,nr4a2,slc16a1,itga5,rmi1,th,chrna7,galr2*
Intracellular receptor signaling pathway	0.02008492	9	323	*rnf6,med1,cyp26b1,twist1,aldh1a2,nr4a2,hnf4g,fhl2,map2k6*
Reduction of food intake in response to dietary excess	0.02011061	2	5	*prlh,rmi1*
Nervous system development	0.02011061	31	2439	*cox6b1,map1b,atp8a2,tcf12,gpm6a,nr4a2,brinp3,tnc,prlh,ptprs,mag,foxo3,twist1,med1,rnf6,aldh1a2,gnat2,pdlim5,trim46,nfasc,washc5,fut9,zhx2,th,ext1,galr2,cenpf,anks1a,tfap2a,chrna7,dok6*
Sensory organ development	0.02011061	12	561	*cyp26b1,kcnk2,med1,tbc1d20,aldh1a2,atp8a2,gnat2,gpm6a,zhx2,th,tfap2a,twist1*
Regulation of axon extension	0.02011061	5	94	*ptprs,mag,rnf6,map1b,trim46*
Response to vitamin	0.02011061	5	92	*cyp26b1,tnc,trim25,med1,aldh1a2*
Cellular hormone metabolic process	0.02011061	6	142	*cyp26b1,aldh1a2,tiparp,dgat1,med1,cyp21a2*

Negative regulation of growth	0.02011061	8	267	*sertad2,st7l,kcnk2,ptprs,mag,rnf6,irf8,trim46*
Retina morphogenesis in camera-type eye	0.02011061	4	53	*atp8a2,gnat2,zhx2,tfap2a*
Sensory organ morphogenesis	0.02011061	8	267	*cyp26b1,tbc1d20,atp8a2,gnat2,zhx2,th,tfap2a,twist1*
Negative regulation of chromosome organization	0.02019114	6	147	*atad2,xrn1,twist1,znf451,bcor,cenpf*
Regulation of neuron differentiation	0.02113374	13	656	*tcf12,brinp3,ptprs,mag,foxo3,med1,rnf6,map1b,atp8a2,pdlim5,washc5,zhx2,trim46*
Retina development in camera-type eye	0.02113374	6	149	*med1,atp8a2,gnat2,gpm6a,zhx2,tfap2a*
Neuron projection morphogenesis	0.02244972	13	662	*map1b,ptprs,mag,rnf6,atp8a2,gpm6a,nr4a2,pdlim5,trim46,nfasc,ext1,chrna7,dok6*
Response to hormone	0.02411051	17	1031	*foxo3,med1,rnf6,ncoa2,nr4a2,ptger4,chrna7,tnc,prlh,xrn1,gpr83,aldh1a2,hnf4g,th,trarg1,fhl2,gnaq*
Negative regulation of developmental growth	0.02447961	5	105	*kcnk2,ptprs,mag,rnf6,trim46*
Cell morphogenesis involved in neuron differentiation	0.02447961	12	591	*map1b,ptprs,mag,rnf6,atp8a2,nr4a2,pdlim5,trim46,nfasc,ext1,chrna7,dok6*
Cell projection morphogenesis	0.02447961	13	678	*map1b,ptprs,mag,rnf6,atp8a2,gpm6a,nr4a2,pdlim5,trim46,nfasc,ext1,chrna7,dok6*
Axon development	0.02447961	11	510	*map1b,tnc,ptprs,mag,rnf6,atp8a2,nr4a2,trim46,nfasc,ext1,dok6*
Plasma membrane bounded cell projection morphogenesis	0.02447961	13	676	*map1b,ptprs,mag,rnf6,atp8a2,gpm6a,nr4a2,pdlim5,trim46,nfasc,ext1,chrna7,dok6*
Response to organic cyclic compound	0.02545138	16	962	*rnf6,med1,tiparp,tnc,pde4d,xrn1,foxo3,trim25,gpr83,aldh1a2,ncoa2,nr4a2,slc16a1,hnf4g,th,fhl2*
Negative regulation of neuron differentiation	0.02545138	7	224	*ptprs,mag,foxo3,med1,rnf6,zhx2,trim46*
Embryonic camera-type eye morphogenesis	0.02545138	3	28	*th,twist1,tfap2a*
Regulation of extent of cell growth	0.02545138	5	109	*ptprs,mag,rnf6,map1b,trim46*
Protein K48-linked ubiquitination	0.02545138	4	62	*ube2k,march6,trim44,rnf6*

Negative regulation of chromatin organization	0.02545138	4	63	*atad2,twist1,znf451,bcor*
Cellular developmental process	0.02579863	48	4587	*tnc,klf1,map1b,atp8a2,tcf12,gpm6a,nr4a2,brinp3,smyd1,foxo3,glipr2,med1,tfap2a,cyp26b1,prlh,ptprs,rasip1,mag,fhl2,cenpf,twist1,tbc1d20,rnf6,steap4,aldh1a2,gnat2,fhod3,dysf,irf8,tdrd5,pdlim5,trim46,nfasc,tiparp,washc5,nxn,ptger4,zhx2,th,ext1,galr2,itga5,anks1a,trps1,pde4d,chrna7,eya2,dok6*
Circulatory system development	0.02618802	17	1064	*th,kcnk2,rasip1,smyd1,fhl2,twist1,med1,aldh1a2,fhod3,dysf,itga5,pdlim5,tiparp,nxn,rbm20,chrna7,bcor*
Cell part morphogenesis	0.0264455	13	697	*map1b,ptprs,mag,rnf6,atp8a2,gpm6a,nr4a2,pdlim5,trim46,nfasc,ext1,chrna7,dok6*
Anatomical structure maturation	0.0264455	6	167	*foxo3,aldh1a2,nr4a2,nfasc,washc5,anks1a*
Response to extracellular stimulus	0.02777357	11	532	*nr4a2,cyp26b1,tnc,prlh,foxo3,trim25,med1,aldh1a2,slc16a1,rmi1,th*
Response to oxygen-containing compound	0.0281392	23	1689	*foxo3,nr4a2,brinp3,ptger4,th,card8,chrna7,cyp26b1,tnc,prlh,klf1,dnm1,map2k6,pde4d,xrn1,trim25,med1,aldh1a2,ncoa2,irf8,rmi1,trarg1,gnaq*
Cellular response to oxygen-containing compound	0.02824704	18	1178	*foxo3,nr4a2,brinp3,ptger4,card8,cyp26b1,tnc,klf1,map2k6,pde4d,xrn1,med1,aldh1a2,irf8,th,trarg1,gnaq,chrna7*
Response to axon injury	0.02862969	4	69	*tnc,kcnk2,ptprs,mag*
Negative regulation of axonogenesis	0.02862969	4	69	*ptprs,mag,rnf6,trim46*
Developmental growth involved in morphogenesis	0.02862969	7	237	*tnc,ptprs,mag,med1,rnf6,map1b,trim46*
Negative regulation of protein polyubiquitination	0.02862969	2	8	*trim44,dysf*
Regulation of phospholipid transport	0.02862969	2	8	*atp8a1,atp8a2*
Positive regulation of phospholipid transport	0.02862969	2	8	*atp8a1,atp8a2*
Neuron projection development	0.02913429	16	997	*map1b,gpm6a,tnc,ptprs,mag,rnf6,atp8a2,nr4a2,pdlim5,trim46,nfasc,washc5,ext1,galr2,chrna7,dok6*
Cell maturation	0.03039891	6	178	*foxo3,nr4a2,tdrd5,nfasc,washc5,anks1a*
Axon extension	0.03039891	5	120	*ptprs,mag,rnf6,map1b,trim46*
Heart development	0.03089855	11	552	*th,kcnk2,smyd1,fhl2,twist1,med1,aldh1a2,fhod3,pdlim5,rbm20,bcor*

Cellular response to chemical stimulus	0.03089855	38	3443	*foxo3,med1,rnf6,ncoa2,nr4a2,brinp3,ptger4,shisa2,cyp26b1,card8,tfap2a,irf8,tiparp,trim44,tnc,kcnk2,klf1,map2k6,pde4d,xrn1,trim25,twist1,aldh1a2,dysf,slc16a1,hnf4g,nxn,th,trarg1,ube2k,znf451,gnaq,chrna7,fhl2,esrp2,itga5,cmbl,nat1*
Axonogenesis	0.0310125	10	471	*map1b,ptprs,mag,rnf6,atp8a2,nr4a2,trim46,nfasc,ext1,dok6*
Embryonic forelimb morphogenesis	0.03241747	3	34	*twist1,aldh1a2,tfap2a*
Cellular response to retinoic acid	0.03315736	4	74	*brinp3,cyp26b1,tnc,aldh1a2*
Homeostatic process	0.03339051	25	1962	*klf1,foxo3,abhd8,ptger4,gpr20,xrn1,ube2k,cyp26b1,crocc,prlh,map2k6,pde4d,med1,steap4,gnat2,slc16a1,tsc22d3,nxn,rmi1,th,galr2,dgat1,tbc1d20,chrna7,rfc4*
Negative regulation of cellular component organization	0.03339051	13	739	*atad2,xrn1,ptger4,ptprs,mag,twist1,rnf6,fhod3,dysf,znf451,bcor,trim46,cenpf*
Response to vitamin D	0.03347122	3	35	*tnc,trim25,med1*
Animal organ morphogenesis	0.03351451	16	1027	*tfap2a,cyp26b1,tnc,esrp2,fhl2,foxo3,twist1,med1,tbc1d20,aldh1a2,atp8a2,gnat2,tiparp,zhx2,th,bcor*
System development	0.03351451	50	4976	*cox6b1,klf1,map1b,atp8a2,tcf12,gpm6a,nr4a2,brinp3,th,foxo3,glipr2,tfap2a,cyp26b1,tnc,prlh,kcnk2,esrp2,ptprs,rasip1,mag,smyd1,fhl2,cenpf,twist1,med1,tbc1d20,rnf6,aldh1a2,gnat2,fhod3,dysf,irf8,itga5,pdlim5,trim46,nfasc,tiparp,washc5,nxn,ptger4,fut9,zhx2,ext1,galr2,rbm20,chrna7,bcor,anks1a,trps1,dok6*
Embryonic eye morphogenesis	0.03498708	3	36	*th,twist1,tfap2a*
Cell morphogenesis involved in differentiation	0.03535026	13	751	*map1b,ptprs,mag,tbc1d20,rnf6,atp8a2,nr4a2,pdlim5,trim46,nfasc,ext1,chrna7,dok6*
Negative regulation of cell growth	0.03535026	6	191	*sertad2,st7l,ptprs,mag,rnf6,trim46*
Embryonic limb morphogenesis	0.03535026	5	130	*cyp26b1,twist1,med1,aldh1a2,tfap2a*
Embryonic appendage morphogenesis	0.03535026	5	130	*cyp26b1,twist1,med1,aldh1a2,tfap2a*
Protein localization to axon	0.03535026	2	10	*trim46,nfasc*
Regulation of developmental growth	0.03607979	8	333	*prlh,kcnk2,ptprs,mag,rnf6,map1b,atp8a2,trim46*
Cellular response to organic cyclic compound	0.03631117	11	579	*rnf6,med1,tiparp,tnc,pde4d,xrn1,foxo3,nr4a2,slc16a1,hnf4g,fhl2*
Response to nutrient levels	0.03921368	10	500	*cyp26b1,tnc,prlh,foxo3,trim25,med1,aldh1a2,slc16a1,rmi1,th*

Response to steroid hormone	0.03921368	9	418	*rnf6,med1,foxo3,gpr83,ncoa2,nr4a2,hnf4g,th,fhl2*
Regulation of tooth mineralization	0.04037623	2	11	*tfap2a,bcor*
Oxidation-reduction process	0.04038443	16	1061	*cyp26b1,steap4,coq7,prlh,tsta3,pycr3,mtrr,cox6b1,aldh1a2,ppp1r3a,nxn,th,cyp21a2,twist1,tbrg4,tstd1*
Response to endogenous stimulus	0.04173373	22	1692	*foxo3,med1,rnf6,ncoa2,nr4a2,ptger4,shisa2,chrna7,tnc,prlh,klf1,pde4d,xrn1,gpr83,aldh1a2,hnf4g,th,trarg1,znf451,fhl2,gnaq,esrp2*
Vitamin metabolic process	0.04365266	5	140	*cyp26b1,mtrr,aldh1a2,slc2a3,aasdhppt*
Positive regulation of transcription, DNA-templated	0.04365266	21	1593	*zfhx4,klf1,foxo3,tcf12,ncoa2,atad2,coq7,twist1,med1,tfap2a,irf8,hnf4g,trim44,galr2,zbed1,ppp3r1,rnf6,nr4a2,sertad2,fhl2,cdk8*
Response to ketone	0.04397175	6	204	*ptger4,tnc,xrn1,foxo3,ncoa2,th*
Negative regulation of transcription by RNA polymerase II	0.04451995	14	896	*zfhx4,foxo3,coq7,zhx2,trps1,fhl2,tfap2a,irf8,twist1,med1,ncoa2,bcor,znf451,nr4a2*
Protein polyubiquitination	0.04451995	7	277	*ubox5,ube2k,rnf6,march6,trim44,dysf,fbxl7*
Response to external stimulus	0.04451995	29	2525	*card8,rps15a,nr4a2,trim44,ptger4,cyp26b1,tnc,prlh,kcnk2,ptprs,mag,pde4d,foxo3,trim25,med1,aldh1a2,atp8a2,gnat2,dysf,ifi44,irf8,gpm6a,slc16a1,nfasc,rmi1,th,ext1,gnaq,dok6*
Response to organic substance	0.04451995	37	3461	*foxo3,med1,rnf6,ncoa2,march6,nr4a2,brinp3,ptger4,th,shisa2,card8,aldh1a2,irf8,tiparp,trim44,chrna7,cyp26b1,tnc,prlh,klf1,dnm1,map2k6,pde4d,xrn1,trim25,twist1,gpr83,slc16a1,hnf4g,rmi1,trarg1,ube2k,znf451,fhl2,gnaq,esrp2,itga5*
Negative regulation of macromolecule metabolic process	0.04451995	32	2872	*serpinb1,zfhx4,foxo3,atad2,coq7,zhx2,xrn1,trps1,card8,fhl2,cenpf,twist1,tfap2a,irf8,trim44,bcor,kcnk2,pde4d,smyd1,med1,dysf,ncoa2,nxn,c1d,chrna7,rasip1,znf451,tbrg4,nr4a2,gnaq,tiparp,rps15a*
Positive regulation of gene expression	0.04451995	25	2046	*zfhx4,klf1,foxo3,tcf12,ncoa2,atad2,coq7,twist1,med1,tfap2a,irf8,hnf4g,trim44,galr2,zbed1,ppp3r1,cyp26b1,tnc,rnf6,aldh1a2,nr4a2,sertad2,rbm20,fhl2,cdk8*
Negative regulation of gene expression	0.04451995	24	1952	*zfhx4,foxo3,atad2,coq7,zhx2,trps1,card8,fhl2,cenpf,twist1,tfap2a,irf8,bcor,xrn1,smyd1,med1,dysf,ncoa2,c1d,znf451,tbrg4,nr4a2,tiparp,rps15a*
Developmental maturation	0.04451995	7	282	*foxo3,aldh1a2,nr4a2,tdrd5,nfasc,washc5,anks1a*
Negative regulation of histone modification	0.04451995	3	44	*twist1,znf451,bcor*
Protein modification by small protein conjugation	0.04451995	14	891	*dcun1d2,ubox5,ube2k,znf451,rnf6,march6,trim44,bcor,trim25,med1,dysf,nxn,fbxl7,zbed1*
Regulation of integrin activation	0.04451995	2	13	*ptger4,rasip1*

Forelimb morphogenesis	0.04451995	3	42	*twist1,aldh1a2,tfap2a*
Dopamine biosynthetic process	0.04451995	2	12	*th,nr4a2*
Negative regulation of transcription, DNA-templated	0.04451995	18	1298	*zfhx4,foxo3,atad2,coq7,zhx2,trps1,fhl2,cenpf,twist1,tfap2a,irf8,bcor,smyd1,med1,ncoa2,c1d,znf451,nr4a2*
Embryonic camera-type eye formation	0.04451995	2	12	*twist1,tfap2a*
Eyelid development in camera-type eye	0.04451995	2	13	*twist1,tfap2a*
Cellular response to organic substance	0.04451995	32	2872	*foxo3,med1,rnf6,ncoa2,nr4a2,brinp3,ptger4,shisa2,card8,irf8,tiparp,trim44,cyp26b1,tnc,klf1,map2k6,pde4d,xrn1,trim25,twist1,aldh1a2,slc16a1,hnf4g,th,trarg1,ube2k,znf451,gnaq,chrna7,fhl2,esrp2,itga5*
Cellular response to alcohol	0.04451995	4	90	*ptger4,tnc,xrn1,foxo3*
Response to amyloid-beta	0.04451995	3	43	*dnm1,foxo3,chrna7*
Negative regulation of cellular macromolecule biosynthetic process	0.04451995	20	1509	*zfhx4,foxo3,atad2,coq7,zhx2,xrn1,trps1,fhl2,cenpf,twist1,tfap2a,irf8,bcor,kcnk2,smyd1,med1,ncoa2,c1d,znf451,nr4a2*
Cardiac muscle tissue development	0.04461977	6	213	*kcnk2,fhl2,med1,aldh1a2,fhod3,pdlim5*
Axon regeneration	0.04525881	3	45	*tnc,ptprs,mag*
Neuron maturation	0.04525881	3	45	*nr4a2,nfasc,anks1a*
Regulation of nucleobase-containing compound metabolic process	0.04595578	44	4374	*eya2,zfhx4,klf1,foxo3,tfap2a,tcf12,ncoa2,atad2,coq7,zhx2,xrn1,esrp2,trps1,fhl2,cenpf,twist1,med1,irf8,rfc4,hnf4g,trim44,galr2,bcor,zbed1,ppp3r1,kcnk2,smyd1,znf45,rnf6,znf214,nr4a2,tsc22d3,znf362,sertad2,c1d,znf628,zfp2,rbm20,vgll3,card8,znf451,trim25,tbrg4,cdk8*
Tissue development	0.04604795	25	2079	*glipr2,tfap2a,cyp26b1,tnc,eya2,kcnk2,esrp2,ptprs,rasip1,smyd1,fhl2,cenpf,twist1,med1,tbc1d20,aldh1a2,fhod3,dysf,pdlim5,tiparp,ext1,itga5,bcor,trps1,pde4d*
DNA-templated transcription, initiation	0.04769373	7	293	*twist1,med1,znf451,znf45,cdk8,nr4a2,hnf4g*
Transcription initiation from RNA polymerase II promoter	0.04769373	6	221	*med1,znf451,znf45,cdk8,nr4a2,hnf4g*
Response to xenobiotic stimulus	0.04769373	7	292	*cyp26b1,foxo3,nr4a2,tiparp,th,cmbl,nat1*
Appendage morphogenesis	0.04769373	5	154	*cyp26b1,twist1,med1,aldh1a2,tfap2a*

Limb morphogenesis	0.04769373	5	154	*cyp26b1,twist1,med1,aldh1a2,tfap2a*
Positive regulation of nucleobase-containing compound metabolic process	0.04769373	24	1978	*eya2,zfhx4,klf1,foxo3,tcf12,ncoa2,atad2,coq7,twist1,med1,tfap2a,irf8,rfc4,hnf4g,trim44,galr2,zbed1,ppp3r1,rnf6,nr4a2,sertad2,rbm20,fhl2,cdk8*
Negative regulation of neurogenesis	0.04769373	7	292	*ptprs,mag,foxo3,med1,rnf6,zhx2,trim46*
Negative regulation of nitrogen compound metabolic process	0.04769373	29	2551	*serpinb1,zfhx4,foxo3,atad2,coq7,zhx2,xrn1,trps1,card8,fhl2,cenpf,twist1,tfap2a,irf8,trim44,bcor,kcnk2,pde4d,smyd1,med1,dysf,ncoa2,nxn,c1d,chrna7,rasip1,znf451,nr4a2,gnaq*
Roof of mouth development	0.04769373	4	94	*twist1,tiparp,tfap2a,bcor*
Cellular response to endogenous stimulus	0.04769373	19	1431	*foxo3,med1,rnf6,ncoa2,nr4a2,ptger4,shisa2,tnc,klf1,pde4d,xrn1,hnf4g,th,trarg1,znf451,gnaq,chrna7,fhl2,esrp2*
Response to nutrient	0.04807838	6	222	*cyp26b1,tnc,trim25,med1,aldh1a2,slc16a1*
Regulation of gene expression	0.04807838	47	4798	*zfhx4,klf1,znf451,foxo3,tfap2a,tcf12,ncoa2,atad2,coq7,zhx2,esrp2,trps1,card8,fhl2,cenpf,twist1,med1,irf8,hnf4g,trim44,galr2,bcor,zbed1,ppp3r1,cyp26b1,tnc,xrn1,smyd1,znf45,rnf6,aldh1a2,dysf,znf214,nr4a2,tsc22d3,znf362,sertad2,c1d,znf628,zfp2,rbm20,vgll3,trim25,tbrg4,tiparp,cdk8,rps15a*
Developmental cell growth	0.04807838	6	223	*ptprs,mag,rnf6,map1b,pdlim5,trim46*
Oocyte development	0.04807838	3	48	*foxo3,tdrd5,washc5*
Regulation of neurogenesis	0.04807838	13	824	*tcf12,brinp3,ptprs,mag,foxo3,med1,rnf6,map1b,atp8a2,pdlim5,washc5,zhx2,trim46*

Table S6. Scale-eater adaptive alleles used for assessing stages of adaptation.

We estimated ages for all adaptive alleles that were in or near (within 20-kb) of a gene associated with a GO term for behavior or craniofacial traits on the Ensemble 96 annotation database and were significantly enriched in our GO enrichment analysis (Table S5). Sweep ages, stage category assignment, any additional annotations we found for genes and their references are provided. Also included is a partial list of other significantly enriched GO terms for each gene. For visual clarity in the table, the broader GO terms (terms that > 1000 genes listed in database) are not included. See Table S5 for full list. Sweep ages are listed as the 95% HPD range (X indicates missing age estimates because estimates across starTMRCA runs did not converge for that sweep).

Gene	Sweep Age	Stages Category	GO enrichment annotations	GWAS annotations	Other annotations	References for other annotations	Other GO enrichment annotations (Partial list)
galr2	696-1008	craniofacial	behavior; feeding behavior	oral jaw size	bone tissue development	(*42*, *43*, *69*)	Behavior, Feeding behavior
cfap20	974-1215	feeding behavior	behavior; feeding behavior	--	--	(*70*)	Behavior, Feeding behavior
atp8a1	118-1419	behavior	behavior	--	--	(*71*)	Regulation of phospholipid transport, Positive regulation of phospholipid transport, Regulation of phospholipid translocation, Positive regulation of phospholipid translocation
rmi1	652-952	feeding behavior	behavior; feeding behavior	--	--	(*72*)	Developmental growth, Response to extracellular stimulus, Response to nutrient levels, Eating behavior, Reduction of food intake in response to dietary excess
th	746-958	feeding behavior/ craniofacial	eye development; behavior; feeding	--	--	(*73*, *74*)	Camera-type eye development, Response to xenobiotic stimulus, Sensory organ morphogenesis, Response to ketone, Eye

			behavior				morphogenesis, Camera-type eye morphogenesis, Embryonic camera-type eye development, Embryonic eye morphogenesis, Eating behavior, Embryonic camera-type eye morphogenesis, Dopamine biosynthetic process
ncoa2	622-902	behavior	behavior	--	--	--	Response to steroid hormone, Response to ketone
nr4a2	762-942	behavior	behavior	--	--		Cell morphogenesis involved in neuron differentiation, Cellular response to organic cyclic compound, Response to extracellular stimulus, Axon development, Axonogenesis, Response to steroid hormone, Intracellular receptor signaling pathway, DNA-templated transcription,Response to xenobiotic stimulus, Developmental maturation, Transcription initiation from RNA polymerase II promoter, Cell maturation, Anatomical structure maturation, Neuron maturation, Dopamine biosynthetic process
kcnk2	452-618	craniofacial	Muscle tissue development; behavior	oral jaw size	--		Developmental growth, Behavior, Sensory organ development, Heart development, Striated muscle tissue development, Regulation of developmental growth, Negative regulation of growth, Cardiac muscle tissue development, Negative regulation of developmental growth, Response to axon injury
slc16a1	459-661	behavior	Behavior	--	feeding behavior	(*75*)	Response to organic cyclic compound,Cellular response to organic cyclic compound, Response to extracellular stimulus, Response to nutrient levels, Response to nutrient
itga5	639-932	craniofacial	behavior	--	eye development; pharengeal arch development	(*76*, *77*)	Anatomical structure morphogenesis, Tissue development, Circulatory system development

chrna7	864-1111	behavior	behavior	--		--	Neuron projection development, Cell morphogenesis involved in differentiation, Cell part morphogenesis, Cell projection morphogenesis, Plasma membrane bounded cell projection morphogenesis, Neuron projection morphogenesis , Cell morphogenesis involved in neuron differentiation, Response to amyloid-beta
med1	X	craniofacial	eye development; muscle tissue development	--		--	Intracellular receptor signaling pathway, Camera-type eye development, "DNA-templated transcription,Negative regulation of neurogenesis, Developmental growth involved in morphogenesis, Negative regulation of neuron differentiation, Response to nutrient, Transcription initiation from RNA polymerase II promoter, Cardiac muscle tissue development, Appendage morphogenesis, Limb morphogenesis, Retina development in camera-type eye, Cellular hormone metabolic process, Embryonic limb morphogenesis, Embryonic appendage morphogenesis, Response to vitamin, Response to vitamin D
gnat2	X	craniofacial	eye development	--		--	Camera-type eye development, Sensory organ morphogenesis, Eye morphogenesis, Retina development in camera-type eye, Camera-type eye morphogenesis, Neural retina development, Retina morphogenesis in camera-type eye
eya2	962-1295	muscle	muscle tissue development	--	--	--	Striated muscle tissue development
tfap2a	292-431	craniofacial	eye devolopment;		pigmentation; embryonic cranial	(*78–80*)	Camera-type eye development, Sensory organ morphogenesis, Appendage morphogenesis, Limb morphogenesis,

			mouth development		skeleton morphogenesis		Eye morphogenesis, Retina development in camera-type eye, Embryonic limb morphogenesis, Embryonic appendage morphogenesis, Camera-type eye morphogenesis, Roof of mouth development, Neural retina development, Retina morphogenesis in camera-type eye, Forelimb morphogenesis, Embryonic camera-type eye development, Embryonic eye morphogenesis, Embryonic forelimb morphogenesis, Embryonic camera-type eye morphogenesis, Eyelid development in camera-type eye, Embryonic camera-type eye formation, Regulation of tooth mineralization
tbc1d20	854-1103	craniofacial	eye development	--	--	--	Cell morphogenesis involved in differentiation, Sensory organ development, Sensory system development, Visual system development, Eye development, Camera-type eye development, Sensory organ morphogenesis, Eye morphogenesis, Camera-type eye morphogenesis
smyd1	662-934	muscle	muscle tissue development	--	--	--	Circulatory system development, Heart development, Striated muscle tissue development
cenpf	452-618	muscle	muscle tissue development	oral jaw size	--	--	Negative regulation of cellular component organization, Striated muscle tissue development, Negative regulation of chromosome organization
pdlim5	550-736	muscle	muscle tissue development	oral jaw size	behavior	(*81*)	Neuron projection development, Regulation of neurogenesis, Cell morphogenesis involved in differentiation, Cell part morphogenesis, Cell projection morphogenesis, Plasma membrane bounded cell projection morphogenesis, Neuron projection morphogenesis,

							Regulation of neuron differentiation, Developmental growth, Cell morphogenesis involved in neuron differentiation, Heart development, Striated muscle tissue development, Developmental cell growth, Cardiac muscle tissue development
bcor	505-727	craniofacial	mouth development	--	retina development	(*82*)	Negative regulation of transcription by RNA polymerase II, Protein modification by small protein conjugation, Negative regulation of cellular component organization, Heart development, Negative regulation of chromosome organization, Negative regulation of chromatin organization, Negative regulation of histone modification, Regulation of tooth mineralization
fhod3	767-999	muscle	muscle tissue development	--	ear development	IMPC: https://www.mousephenotype.org/data/genes/MGI:1925847#phenotypesTab	Circulatory system development, Negative regulation of cellular component organization, Heart development, Striated muscle tissue development, Cardiac muscle tissue development
twist1	300-434	craniofacial	muscle tissue development;eye development	oral jaw size	mandibular arch skeleton	(*83*, *84*)	Camera-type eye development, DNA-templated transcription,Sensory organ morphogenesis, Appendage morphogenesis, Limb morphogenesis, Eye morphogenesis, Negative regulation of chromosome organization, Embryonic limb morphogenesis, Embryonic appendage morphogenesis, Camera-type eye morphogenesis, , Negative regulation of chromatin organization, Negative regulation of histone modification, Forelimb morphogenesis, Embryonic camera-type eye development, Embryonic eye morphogenesis, Embryonic forelimb

							morphogenesis, Embryonic camera-type eye morphogenesis, Eyelid development in camera-type eye, Embryonic camera-type eye formation
zhx2	X	craniofacial	eye development	--	--	--	Camera-type eye development, Negative regulation of neurogenesis, Sensory organ morphogenesis, Negative regulation of neuron differentiation, Eye morphogenesis, Retina development in camera-type eye, Camera-type eye morphogenesis, Neural retina development, Retina morphogenesis in camera-type eye
fhl2	890-1169	craniofacial	muscle tissue development	--	--	--	Response to lipid, Response to organic cyclic compound, Negative regulation of transcription by RNA polymerase II, Cellular response to lipid, Cellular response to organic cyclic compound, Heart development, Response to steroid hormone, Striated muscle tissue development, Intracellular receptor signaling pathway, Cardiac muscle tissue development
prlh	1123-1466	feeding behavior	behavior; feeding behavior	--	--	(*85*)	Developmental growth, Response to extracellular stimulus, Response to nutrient levels, Regulation of developmental growth, Eating behavior, Reduction of food intake in response to dietary excess
ald1ha2	878-1279	craniofacial	muscle tissue development, eye development	--	limb morphogenesis	(*86*)	Camera-type eye development, Developmental maturation, Response to nutrient, Cardiac muscle tissue development, Anatomical structure maturation, Appendage morphogenesis, Limb morphogenesis, Cellular hormone metabolic process, Vitamin metabolic process, Embryonic limb morphogenesis, Embryonic appendage morphogenesis, Response to vitamin, Cellular response to retinoic acid,

			Forelimb morphogenesis, Embryonic camera-type eye development, Embryonic forelimb morphogenesis

Table S7. Molluscivore adaptive alleles used for assessing stages of adaptation. We estimated ages for all adaptive alleles that were in or near (within 20-kb) of a gene associated with a GO term for behavior or craniofacial traits on the Ensemble 96 annotation database and were significantly enriched in our GO enrichment analysis (Table S5). Sweep ages, stage category assignment, any additional annotations we found for genes and their references are provided. Also included is a partial list of other significantly enriched GO terms for each gene. For visual clarity in the table, the broader GO terms (terms that > 1000 genes listed in database) are not included. See Table S5 for full list. Sweep ages are listed as the 95% HPD range (X indicates missing age estimates because estimates across starTMRCA runs did not converge for that sweep).

Gene	Sweep Age	Stages Category	GO enrichment annotations	GWAS annotations	Other researched relevant annotations	References for other annotations	Other GO enrichment annotations
cyp26b1	214-582	craniofacial	muscle tissue development	--	craniofacial development	(*87*, *88*)	Striated muscle tissue development, Intracellular receptor signaling pathway, Response to xenobiotic stimulus, Sensory organ morphogenesis, Response to nutrient, Appendage morphogenesis, Limb morphogenesis, Cellular hormone metabolic process, Vitamin metabolic process, Embryonic limb morphogenesis, Embryonic appendage morphogenesis, Response to vitamin, Cellular response to retinoic acid
ext1	405-687	craniofacial	cranial skeletal system development	nose height	--	(*89*)	Neuron projection development, Cell morphogenesis involved in differentiation,Cell part morphogenesis,Cell projection morphogenesis, Plasma membrane bounded cell projection morphogenesis, Neuron projection morphogenesis, Cell morphogenesis involved in neuron differentiation, Axon development, Axonogenesis

gnaq	180-737	craniofacial	skeletal system development	--	pigmentation; jaw size	(*90*, *91*)	Regulation of biological quality, Response to organic substance, Cellular response to chemical stimulus, Negative regulation of macromolecule metabolic process, Cellular response to organic substance, Negative regulation of nitrogen compound metabolic process, Response to external stimulus, Response to endogenous stimulus, Response to oxygen-containing compound, Cellular response to endogenous stimulus, Cellular response to oxygen-containing compound, Response to hormone
zhx2	1147-1793	craniofacial	eye development	--	--		Regulation of neurogenesis, Regulation of neuron differentiation, Sensory organ development, Sensory system development, Visual system development, Eye development, Camera-type eye development, Negative regulation of neurogenesis, Sensory organ morphogenesis, Negative regulation of neuron differentiation, Eye morphogenesis, Retina development in camera-type eye, Camera-type eye morphogenesis, Neural retina development, Retina morphogenesis in camera-type eye
tiparp	x	craniofacial	mouth development; muscle tissue development	--		--	Response to organic cyclic compound, Cellular response to organic cyclic compound , Response to xenobiotic stimulus, Cellular hormone metabolic process, Roof of mouth development
atp8a2	x	feeding behavior	behavior; feeding behavior	--		(*92*)	Developmental growth, Response to extracellular stimulus, Response to nutrient levels, Eating behavior, Reduction of food intake in response to dietary excess

Table S8. Top 5 BLAST hits for LG15 QTL. Bolded values indicate the top hit that was used to determine the region the significant oral jaw size QTL aligned to an 18-Mb region on scaffold c_bro_v1_0_scaf8 (8840660-27314762**)** in the *C. brontotheroides* reference genome that contained 3 genes (*map2k6*, *galr2*, and *grid2ip*).

LG15 marker	Scaffold	% identity	Length (bp)	Mismatch	Start	End	E-value	Bitscore
10999	**c_bro_v1_0_scaf8**	**97.917**	**96**	**2**	**8840660**	**8840755**	**1.95E-42**	**174**
10999	c_bro_v1_0_scaf8	100	17	0	17544438	17544422	4.6	34.2
10999	c_bro_v1_0_scaf36	100	20	0	201747	201728	0.074	40.1
10999	c_bro_v1_0_scaf7	100	19	0	13795738	13795756	0.29	38.2
10999	c_bro_v1_0_scaf52	100	18	0	23185857	23185840	1.2	36.2
10999	c_bro_v1_0_scaf38	100	18	0	1880370	1880387	1.2	36.2
33382	**c_bro_v1_0_scaf8**	**100**	**93**	**0**	**27314670**	**27314762**	**1.97E-45**	**184**
33382	c_bro_v1_0_scaf8	93.617	47	3	26627380	26627426	8.05E-11	69.9
33382	c_bro_v1_0_scaf8	93.617	47	3	27916662	27916616	8.05E-11	69.9
33382	c_bro_v1_0_scaf8	95.238	42	2	1464518	1464477	3.18E-10	67.9
33382	c_bro_v1_0_scaf8	95.238	42	2	11224060	11224019	3.18E-10	67.9

Table S9. Per generation mutation rate estimation from high coverage sequencing of parents and F1 from two crosses of San Salvador Island (SSI) species. Details about the average coverage of genome sequences in three offspring across two crosses, the number of de novo variants at steps in the filtering pipeline, and the specific filter thresholds used for each individual to filter down to high quality de novo variants in each (shared alleles).

Cross	***C. variegatus x C. brontotheroides***		***C. variegatus x C. desquamator***
Offspring	F1.A	F1.B	F1.A
Avg. coverage	67.5X	45.1X	32.7X
Known heterozygous sites genotype quality (GQ)	X>99	X>99	X>99
Known heterozygous sites base quality rank sum (BaseQRankSum)	1.4<x<2.6	1.4<x<2.6	1.4<x<2.7
Known heterozygous sites mapping quality (MQ)	x>54	x>54	x>54
Known heterozygous sites mapping quality rank sum (MQRankSum)	1.6<x<1.9	1.6<x<1.9	1.4<x<2
Known heterozygous sites quality by depth (QD)	24<x<36	24<x<36	24<x<36
Known heterozygous sites depth (DP)	27 <x<77	15 < x< 54	12< x < 39
Known heterozygous sites allele depth (AD)	10<x<42	5<x<30	4< x < 21
Known heterozygous sites read position rank sum (ReadPosRankSum)	-1.8<x<2.3	1.8<x<2.3	1.4<x<2.34
Known heterozygous sites StrandOddsRatio (SOR)	0.17<x<1.4	0.14<x<1.4	0.19<x<1.3
Known heterozygous sites FisherStrand (FS)	4.6<x<7.5	4.6<x<7.3	45<x<7.5
GATK new mutation sites (bp)	9114	8936	331
mpileup new mutation sites (bp)	14772	14182	7206
Shared alleles (bp)	20	37	9
Accessible genome (bp)	698887016	712364816	695995433
Mutation rate estimate	1.43×10^{-8}	2.59×10^{-8}	6.46×10^{-9}

Table S10. Parameters for selective sweep analyses in SweeD.

The average coverage, composite likelihood ratio threshold based on neutral simulations, and the population size change parameters and individual used for each species.

Species	Average Coverage	CLR threshold	SweeD Commands
SSI generalist	28.87X	4.89	-folded -strictPolymorphic -G 0.4068 -eN 5.45 181.8 -s 64
SSI molluscivore	17.37X	4.47	-folded -strictPolymorphic -G 0.389 -eN 5.88 196 -s 88
SSI scale-eater	18.21X	5.28	-folded -strictPolymorphic -G 0.218 -eN 8.11 270 -s 52
RC	21.04X	4.41	-folded -strictPolymorphic -G 0.23 -eN 11.15 269.1 -s 34
NP	22.67X	2.28	-folded -strictPolymorphic -G 0.198 -eN 13.35 445.07 -s 30
DR	NA	5.37	-folded -strictPolymorphic -G 0.236 -eN 10.83 362.8 -s 20
NCC	27.62X	5.09	-folded -strictPolymorphic -G 0.29 -eN 8.01 374.4 -s 24
VEN	17.21X	18.05	-folded -strictPolymorphic -G 8.87 -eN 0.086 0.345 -eN 1.077 38.78 -s 22

Table S11. The number of introgression regions in the SSI specialists. We determined introgressed regions of the genome as a region with a f_d statistic (ranges from 0 to 1) value above the threshold found in neutral simulations with no gene flow. These introgressed regions from each donor population were then overlapped with regions of the genome with strong genetic divergence (alleles with $F_{st} \geq 0.95$) and signatures of a hard selective sweep (above demographic simulation based thresholds SweeD CLR > 5.28; OmegaPlus ω > 3.31 for scale-eaters and SweeD CLR > 4.47; OmegaPlus ω > 4.23 for molluscivores) to determine the number of adaptive introgression regions. These adaptive introgression regions range in size from 50-kb to 110-kb in length. For each introgression test, *C. artifrons* was used as the outgroup population (e.g. O) while the other specialist was used as the sister species (e.g. P1).

Donor population (P3)	f_d threshold	Number of candidate introgression regions	Number of candidate adaptive introgression regions
Introgression with Molluscivore			
Rum Cay	0.81	536	5
New Providence	0.72	660	7
Dominican Republic	0.81	375	8
North Carolina	0.69	138	0
Venezuela	0.69	54	0
Introgression with Scale-eater			
Rum Cay	0.81	385	5
New Providence	0.72	645	9
Dominican Republic	0.81	426	11
North Carolina	0.71	163	3
Venezuela	0.69	15	0

Table S12. Caribbean pupfish populations used to detect signatures of introgression in San Salvador Island (SSI) specialists and generalist lineages on other islands. The f_d statistic was used to detect introgression between combinations of P2 and P3 populations, given the tree (((P1,P2),P3),O). For this series of tests we used *C. artifrons* as the outgroup in which limited gene flow is expected to have occurred with the others.

-	Sister group (P1)	Introgression into (P2)	Introgression from (P3)	Adaptive introgression regions
Focal introgression regions in scale-eater				
A.	*C. brontotheroides*	*C. desquamator*	*C. laciniatus* NP	11
	C. brontotheroides	*C. desquamator*	*C. higuey* DR	8
	C. brontotheroides	*C. desquamator*	*C. variegatus* NC	4
	C. brontotheroides	*C. desquamator*	*C. dearborni* VZ	0
B.	*C. variegatus* SSI	*C. higuey* DR	*C. laciniatus* NP	2
	C. variegatus SSI	*C. higuey* DR	*C. variegatus* NC	3
	C. variegatus RC	*C. higuey* DR	*C. laciniatus* NP	0
	C. variegatus RC	*C. higuey* DR	*C. variegatus* NC	0
	C. variegatus SSI	*C. laciniatus* NP	*C. variegatus* NC	4
	C. variegatus RC	*C. laciniatus* NP	*C. variegatus* NC	1
	C. variegatus RC	*C. laciniatus* NP	*C. variegatus* NC	2
	C. variegatus SSI	*C. variegatus* RC	*C. higuey* DR	3
	C. variegatus SSI	*C. variegatus* RC	*C. laciniatus* NP	4
	C. variegatus SSI	*C. variegatus* RC	*C. variegatus* NC	4
Focal introgression regions in molluscivore				
C.	*C. desquamator*	*C. brontotheroides*	*C. laciniatus* NP	5
	C. desquamator	*C. brontotheroides*	*C. higuey* DR	6
	C. desquamator	*C. brontotheroides*	*C. variegatus* NC	2
	C. desquamator	*C. brontotheroides*	*C. dearborni VZ*	0
D.	*C. variegatus* SSI	*C. higuey* DR	*C. laciniatus* NP	0
	C. variegatus SSI	*C. higuey* DR	*C. variegatus* NC	1
	C. variegatus RC	*C. higuey* DR	*C. laciniatus* NP	0
	C. variegatus RC	*C. higuey* DR	*C. variegatus* NC	0
	C. variegatus SSI	*C. laciniatus* NP	*C. variegatus* NC	1
	C. variegatus RC	*C. laciniatus* NP	*C. variegatus* NC	0
	C. variegatus RC	*C. laciniatus* NP	*C. variegatus* NC	0
	C. variegatus SSI	*C. variegatus* RC	*C. higuey* DR	2

	C. variegatus SSI	*C. variegatus* RC	*C. laciniatus* NP	1
	C. variegatus SSI	*C. variegatus* RC	*C. variegatus* NC	3

1436
1437

Table S13. Candidate adaptive introgression regions from Rum Cay generalists (*C. variegatus*) and San Salvador Island (SSI) specialists. We determined introgressed regions of the genome as regions with a f_d statistic (ranges from 0 to 1) value above the threshold found in neutral simulations with no gene flow. These introgressed regions from Rum Cay were then overlapped with regions of the genome with strong genetic divergence (alleles with $F_{st} \geq 0.95$) and signatures of a hard selective sweep (above demographic simulation-based thresholds SweeD CLR > 5.28; OmegaPlus ω > 3.31 for scale-eaters and SweeD CLR > 4.47; OmegaPlus ω > 4.23 for molluscivores) to determine the number of adaptive introgression regions. For each introgression test, *C. artifrons* was used as the outgroup population (e.g. O) while the other specialist was used as the sister species (e.g. P1).

Scaffold	Variant Position	Start	End	Gene
Introgression with Molluscivore				
c_bro_v1_0_scaf11	12962909	12965001	13010000	*shisa2, atp8a2*
c_bro_v1_0_scaf16	35813565	35765001	35875000	*rfc4*
c_bro_v1_0_scaf18	18167642	18150001	18215000	*anks1a*
c_bro_v1_0_scaf18	18177499	18150001	18225000	*sarg*
c_bro_v1_0_scaf52	19358574	19345001	19395000	*fn1*
Introgression with Scale-eater				
c_bro_v1_0_scaf1	15017907	14995001	15065000	*rbm20*
c_bro_v1_0_scaf5	28411973	28365001	28455000	*gse1*
c_bro_v1_0_scaf37	3586373	3585001	3650000	*chrna7*
c_bro_v1_0_scaf43	30358142	30355001	30405000	*c1d*
c_bro_v1_0_scaf53	11080970	11080001	11130000	*zhx2*

Table S14. Candidate adaptive introgression regions from Dominican Republic generalists (*C. higuey*) and San Salvador Island (SSI) specialists. We determined introgressed regions of the genome as regions with a f_d statistic (ranges from 0 to 1) value above the threshold found in neutral simulations with no gene flow. These introgressed regions from Dominican Republic population were then overlapped with regions of the genome with strong genetic divergence (alleles with $F_{st} \geq 0.95$) and signatures of a hard selective sweep (above demographic simulation based thresholds SweeD CLR > 5.28;OmegaPlus ω > 3.31 for scale-eaters and SweeD CLR > 4.47; OmegaPlus ω > 4.23 for molluscivores) to determine the number of adaptive introgression regions. For each introgression test, *C. artifrons* was used as the outgroup population (e.g. O) while the other specialist was used as the sister species (e.g. P1).

Scaffold	Variant Position	Start	End	Gene
Introgression with Molluscivore				
c_bro_v1_0_scaf1	28938769	28935001	28985000	*rps15a*
c_bro_v1_0_scaf1	28962108	28935001	28995000	*notum2*
c_bro_v1_0_scaf1	28969771	28935001	28995000	*coq7*
c_bro_v1_0_scaf7	12326193	12305001	12375000	*smek1*
c_bro_v1_0_scaf7	12606143	12605001	12685000	*otof*
c_bro_v1_0_scaf11	11256440	11210001	11295000	*ube2w*
c_bro_v1_0_scaf18	18167642	18135001	18225000	*anks1a,sarg*
c_bro_v1_0_scaf19	6430544	6410001	6465000	*trim44*
Introgression with Scale-eater				
c_bro_v1_0_scaf5	28411973	28385001	28450000	*gse1*
c_bro_v1_0_scaf8	19759133	19735001	19790000	*map2k6*
c_bro_v1_0_scaf18	28961523	28915001	29010000	*itga5*
c_bro_v1_0_scaf19	7822448	7815001	7870000	*nap1l4*
c_bro_v1_0_scaf34	25414453	25400001	25460000	*cadps*
c_bro_v1_0_scaf34	26069290	26020001	26115000	*srgap3*
c_bro_v1_0_scaf37	3700741	3685001	3750000	*trim46*
c_bro_v1_0_scaf44	12541185	12540001	12620000	*kcnk2, cenpf*
c_bro_v1_0_scaf44	24564920	24540001	24620000	*gpm6a*

c_bro_v1_0_scaf53	18998120	18990001	19045000	*hdac9b*
c_bro_v1_0_scaf53	20294941	20245001	20330000	*steap4*

1464
1465

Table S15. Candidate adaptive introgression regions from New Providence Island generalists (*C. laciniatus*) and San Salvador Island (SSI) specialists. We determined introgressed regions of the genome as regions with a f_d statistic (ranges from 0 to 1) value above the threshold found in neutral simulations with no gene flow. These introgressed regions from New Providence Island population were then overlapped with regions of the genome with strong genetic divergence (alleles with $F_{st} \geq 0.95$) and signatures of a hard selective sweep (above demographic simulation based thresholds SweeD CLR > 5.28;OmegaPlus ω> 3.31 for scale-eaters and SweeD CLR > 4.47; OmegaPlus ω > 4.23 for molluscivores) to determine the number of adaptive introgression regions. For each introgression test, *C. artifrons* was used as the outgroup population (e.g. O) while the other specialist was used as the sister species (e.g. P1).

Scaffold	Variant Position	Start	End	Gene
Introgression with Molluscivore				
c_bro_v1_0_scaf1	29209555	29160001	29250000	*gga1*
c_bro_v1_0_scaf1	29241942	29195001	29250000	*klf1*
c_bro_v1_0_scaf7	12326193	12300001	12375000	*smek1*
c_bro_v1_0_scaf7	12628199	12610001	12670000	*otof*
c_bro_v1_0_scaf24	20486354	20470001	20540000	*cyp26b1*
c_bro_v1_0_scaf33	12634285	12590001	12655000	*bri3bp, wdr31*
c_bro_v1_0_scaf47	16145704	16110001	16195000	*ttc33*
Introgression with Scale-eater				
c_bro_v1_0_scaf5	27882801	27845001	27900000	*tcf12*
c_bro_v1_0_scaf7	12604722	12555001	12620000	*otof*
c_bro_v1_0_scaf11	9503186	9500001	9550000	*prlh*
c_bro_v1_0_scaf11	11975348	11930001	12010000	*ncoa2*
c_bro_v1_0_scaf16	32982520	32950001	33030000	*crocc*
c_bro_v1_0_scaf18	28961523	28915001	28970000	*itga5*
c_bro_v1_0_scaf37	8265887	8220001	8315000	*mylipa*
c_bro_v1_0_scaf43	30297117	30250001	30325000	*ppp3r1*
c_bro_v1_0_scaf53	20832687	20830001	20880000	*galnt1*

Table S16. Candidate adaptive introgression regions from North Carolina Coast generalists (*C. variegatus*) and San Salvador Island (SSI) specialists.

We determined introgressed regions of the genome as regions with a f_d statistic (ranges from 0 to 1) value above the threshold found in neutral simulations with no gene flow. These introgressed regions from North Carolina population were then overlapped with regions of the genome with strong genetic divergence (alleles with $F_{st} \geq 0.95$) and signatures of a hard selective sweep (above demographic simulation based thresholds SweeD CLR > 5.28; OmegaPlus ω> 3.31 for scale-eaters and SweeD CLR > 4.47; OmegaPlus ω> 4.23 for molluscivores) to determine the number of adaptive introgression regions. For each introgression test, *C. artifrons* was used as the outgroup population (e.g. O) while the other specialist was used as the sister species (e.g. P1).

Scaffold	Variant Position	Start	End	Gene
Introgression with Scale-eater				
c_bro_v1_0_scaf1	28962108	28945001	28995000	*notum2,coq7*
c_bro_v1_0_scaf1	38350857	38330001	38400000	*gpr83*
c_bro_v1_0_scaf34	32388612	32380001	32440000	eya2

Table S17. Selective sweep ages on San Salvador Island using coalescent-based starTMRCA approach. The 95% high posterior density region of the posterior distribution of sweep ages for all denovo and introgressed adaptive alleles in scale-eater estimated using starTMRCA. A selection of standing variants that were calculated for the stages of adaptation analyses (GO terms related to behavior and craniofacial morphology) included as well. Introgressed adaptive alleles are labeled by the population introgressed from: New Providence Island (INTRO.NP), Dominican Republic (INTRO.DR), and North Carolina (INTRO.NC).

Gene	Spatial Distribution	Scaffold	Position	Mean Age	95 % HPD Lower	95% HPD Upper
scaf34.NA	INTRO.NC	c_bro_v1_0_scaf34	17475008	2583	2277	2871
card8	SGV	c_bro_v1_0_scaf46	1311093	2095	1728	2488
scaf46.NA	SGV	c_bro_v1_0_scaf46	13200234	1867	1637	2088
scaf11.NA	de novo	c_bro_v1_0_scaf11	21634014	1585	1388	1799
scaf52.NA	INTRO.NC	c_bro_v1_0_scaf52	4987013	1463	1219	1709
cmbl	de novo	c_bro_v1_0_scaf11	9924142	1375	1199	1566
galnt1	INTRO.NP	c_bro_v1_0_scaf53	20864827	1365	1227	1513
prlh	INTRO.NP	c_bro_v1_0_scaf11	9496004	1289	1124	1466
scaf37.NA	INTRO.NC	c_bro_v1_0_scaf37	14881950	1284	1099	1492
atp8a1	SGV	c_bro_v1_0_scaf44	14973114	1277	1119	1419
trim46	INTRO.DR	c_bro_v1_0_scaf37	3700741	1268	1098	1423
scaf44.NA	INTRO.NC	c_bro_v1_0_scaf44	28137436	1268	1147	1393
scaf6.NA	de novo	c_bro_v1_0_scaf6	923414	1259	1070	1462
scaf53.NA	SGV	c_bro_v1_0_scaf53	4776006	1222	1082	1380
gpr83	INTRO.NC	c_bro_v1_0_scaf1	38363517	1203	1079	1337
scaf8.NA	INTRO	c_bro_v1_0_scaf8	16314185	1193	978	1425
scaf43.NA	INTRO.NC	c_bro_v1_0_scaf43	27190362	1185	1070	1295
scaf6.NA	INTRO	c_bro_v1_0_scaf6	955941	1174	1045	1318
scaf24.NA	DENOVO	c_bro_v1_0_scaf24	20383519	1159	956	1361
eya2	SGV	c_bro_v1_0_scaf34	32255078	1131	962	1296
scaf53.NA.NC	INTRO.NC	c_bro_v1_0_scaf53	10409675	1096	926	1318
cfap20	SGV	c_bro_v1_0_scaf37	5095975	1093	974	1216
aldh1a2	SGV	c_bro_v1_0_scaf5	27704112	1063	878	1279
aasdhppt	SGV	c_bro_v1_0_scaf21	26917283	1046	916	1175
fhl2	SGV	c_bro_v1_0_scaf9	25305758	1020	891	1170

cadps	INTRO.DR	c_bro_v1_0_scaf34	25417185	1012	917	1115
grid2ip	SGV	c_bro_v1_0_scaf8	21601776	998	877	1127
chrna7	SGV	c_bro_v1_0_scaf37	3593615	986	864	1111
scaf34.NA.DR	INTRO.DR	c_bro_v1_0_scaf34	22649365	984	773	1171
st7l	de novo	c_bro_v1_0_scaf34	31258254	940	757	1163
scaf43.NA	INTRO.NC	c_bro_v1_0_scaf43	18320970	936	805	1079
fhod3	SGV	c_bro_v1_0_scaf53	18640776	888	768	999
crocc	INTRO.NP	c_bro_v1_0_scaf16	32982520	888	740	1060
galr2	de novo	c_bro_v1_0_scaf8	19961303	861	696	1008
nr4a2	SGV	c_bro_v1_0_scaf52	13841760	853	762	942
ppp3r1	INTRO.NP	c_bro_v1_0_scaf26	30297160	851	725	968
pde4d	DENOVO	c_bro_v1_0_scaf21	32304491	847	747	958
th/nap1l4	SGV	c_bro_v1_0_scaf19	7822448	847	747	958
dysf	SGV	c_bro_v1_0_scaf24	20221166	830	683	978
gse1	INTRO.DR	c_bro_v1_0_scaf5	28411973	829	700	947
mag	SGV	c_bro_v1_0_scaf53	17420175	824	615	1042
scaf53.NA.NP	INTRO.NP	c_bro_v1_0_scaf53	12368389	821	700	940
smyd1	SGV	c_bro_v1_0_scaf39	1662237	802	662	935
itga5	SGV	c_bro_v1_0_scaf18	28962001	792	639	932
rmi1	SGV	c_bro_v1_0_scaf39	4281152	789	652	952
ptprs	de novo	c_bro_v1_0_scaf16	8251751	789	555	1043
scaf44.NA	de novo	c_bro_v1_0_scaf44	10558794	782	676	898
chpf	de novo	c_bro_v1_0_scaf52	21897888	776	659	897
scaff44.NA.2	de novo	c_bro_v1_0_scaf44	16942340	763	626	890
ncoa2	INTRO.NP	c_bro_v1_0_scaf11	11975827	760	622	903
scaf19.NA	INTRO.NP	c_bro_v1_0_scaf19	6605756	756	641	862
tcf12	INTRO.NP	c_bro_v1_0_scaf5	27887771	729	606	862
abhd8	SGV	c_bro_v1_0_scaf16	13454820	729	624	821
serpinb1	SGV	c_bro_v1_0_scaf16	10637011	729	624	821
tdrd5	SGV	c_bro_v1_0_scaf16	12833025	720	618	822
zfhx4	de novo	c_bro_v1_0_scaf11	8072317	694	595	809
scaf53.NA.4	INTRO.DR	c_bro_v1_0_scaf53	32457769	675	573	783
scaf5.NA	INTRO.NP	c_bro_v1_0_scaf5	28307404	675	558	798
pdlim5	SGV	c_bro_v1_0_scaf47	24141970	645	550	737
bcor	SGV	c_bro_v1_0_scaf52	5558993	613	506	727
slc16a1	SGV	c_bro_v1_0_scaf18	29613954	556	460	662
tmem26	de novo	c_bro_v1_0_scaf43	26585181	546	473	617
cenpf/kcnk2	INTRO.DR	c_bro_v1_0_scaf44	12538313	533	452	619
hdac9b	INTRO.DR	c_bro_v1_0_scaf53	18998120	445	367	538
scaf52.NA.2	INTRO.DR	c_bro_v1_0_scaf52	13758756	424	333	521

mindy3	SGV	c_bro_v1_0_scaf53	20112997	420	334	501
znf628	SGV	c_bro_v1_0_scaf53	24744443	420	334	501
olfm1	de novo	c_bro_v1_0_scaf47	14782939	398	294	507
otof	INTRO.NP	c_bro_v1_0_scaf7	12603683	371	227	525
twist1	de novo	c_bro_v1_0_scaf53	18968932	367	300	435
tfap2a	SGV	c_bro_v1_0_scaf34	32255078	359	293	431
mylipa	INTRO.NP	c_bro_v1_0_scaf37	8265887	206	95	326

Table S18. .Selective sweep ages on San Salvador Island using coalescent-based starTMRCA approach. The 95% high posterior density region of the posterior distribution of sweep ages for all introgressed candidate alelles in molluscivore estimated using starTMRCA. A selection of standing variants (SGV) that were calculated for the stages of adaptation analyses (GO terms related to behavior and craniofacial morphology) included as well. Introgressed adaptive alleles are labeled by the population introgressed from: New Providence Island (INTRO.NP), Dominican Republic (INTRO.DR), and North Carolina (INTRO.NC).

Gene	Spatial Distribution	Scaffold	Position	Mean Age	95 HPD Lower	95 HPD Upper
abhd8	SGV	c_bro_v1_0_scaf16	13455352	471	294	649
cox6b1	SGV	c_bro_v1_0_scaf53	24790621	402	236	577
cyp26b1	INTRO.NP	c_bro_v1_0_scaf24	20486531	396	215	582
ext1	SGV	c_bro_v1_0_scaf26	264812	546	405	687
gga1	SGV	c_bro_v1_0_scaf1	29209563	914	831	997
gnaq	SGV	c_bro_v1_0_scaf33	12883992	439	181	737
zhx2	SGV	c_bro_v1_0_scaf53	11080970	1490	1148	1793
znf628	SGV	c_bro_v1_0_scaf53	24744443	325	169	486
18.NA	INTRO.NP	c_bro_v1_0_scaf18	2258923	763	550	965
19.NA	INTRO.NC	c_bro_v1_0_scaf19	7642081	3560	3021	4080
4.NA	INTRO.NP	c_bro_v1_0_scaf4	16217615	369	227	532
43.NA.NCC	INTRO.NC	c_bro_v1_0_scaf43	27435224	408	249	576
5.NA	INTRO.DR	c_bro_v1_0_scaf5	27117941	726	469	997
52.NA	INTRO.DR	c_bro_v1_0_scaf52	4982714	820	599	1032
53.NA	INTRO.DR	c_bro_v1_0_scaf53	10434469	903	569	1339
53.NA.NCC	INTRO.NC	c_bro_v1_0_scaf53	10904586	3131	2428	3604
bri3bp.wdr31	INTRO.NP	c_bro_v1_0_scaf33	12644789	376	162	594
klf1	INTRO.DR	c_bro_v1_0_scaf1	29253566	1603	1504	1694
otof	INTRO.DR	c_bro_v1_0_scaf7	12606143	444	367	510
trim44	INTRO.DR	c_bro_v1_0_scaf19	6441342	15922	14639	17127
ttc33	INTRO.NP	c_bro_v1_0_scaf47	16146578	262	127	393
ube2w	INTRO.DR	c_bro_v1_0_scaf11	11268935	1022	903	1144

Table S19. Selective sweep ages on San Salvador Island (SSI) using coalescent-based McSwan approach. 95% high posterior density region of the posterior distribution of sweep ages of adaptive alleles in scale-eater and molluscivore genomes estimated using McSwan (*64*).

Gene	Trait	Scaffold	Position Start	Position Stop	Region Size	95% HPD Lower	95% HPD Upper
			Scale-eater				
cfap20	habitat preference	c_bro_v1_0_scaf37	5000841	5017240	16399	6747.04	8490.23
prlh	habitat preference	c_bro_v1_0_scaf11	9200146	9276987	76841	6594.56	9210.36
card8	pigmentation	c_bro_v1_0_scaf46	1451011	1663431	212420	973.64	5097.36
kcnk2, cenpf	trophic morphology	c_bro_v1_0_scaf44	12227155	12305895	78740	2936.44	3966.91
smyd1	trophic morphology	c_bro_v1_0_scaf39	1643098	1647708	4610	3054.91	6030.54
tcf12	trophic morphology	c_bro_v1_0_scaf5	27975725	28016276	40551	1607.22	5119.88
twist1	trophic morphology	c_bro_v1_0_scaf53	18953132	19092361	139229	1636.34	3413.14
itga5	trophic morphology	c_bro_v1_0_scaf18	28040450	28049258	8808	1697.39	2357.06
			Molluscivore				
ext1	trophic morphology	c_bro_v1_0_scaf26	162903	230930	68027	814.01	1060.49
tiparp	trophic morphology	c_bro_v1_0_scaf21	33602383	33606685	4302	3353.84	5003.16
cyp26b1	trophic morphology	c_bro_v1_0_scaf24	20527588	20602663	75075	1447.58	4567.30

Data S1.

***Cyprinodon* pupfish sampling information.** The pond/lake names, localities, island, country, and species names, and individual codes of the pupfish individuals used in this study.

Data S2.

San Salvador Island scale-eater candidate adaptive alleles. The scale-eater adaptive alleles that were nearly-fixed ($F_{st} \geq 0.95$) and in a region with a signature of a hard selective sweep (SweeD CLR> 5.28;OmegaPlus > 3.31) and the genes within 20-kb of those alleles.

Data S3.

San Salvador Island molluscivore candidate adaptive alleles. The candidate molluscivore alleles that were nearly-fixed ($F_{st} \geq 0.95$) and in a region with a signature of a hard selective sweep (SweeD CLR> 4.47;OmegaPlus > 4.27) and the genes within 20-kb of those alleles.

Data S4.

Differentially expressed genes between specialists at 2 dpf. The gene names and *P*-values of genes that were found to be significantly differential expressed (FDR> 0.05) between scale-eaters and mollsucivores at the 2 days post-fertilization larval stage in a previous study (*48*).

Data S5.

Differentially expressed genes between specialists at 8 dpf. The gene names and *P*-values of genes that were found to be significantly differential expressed (FDR> 0.05) between scale-eaters and mollsucivores at the 8 days post-fertilization larval stage in a previous study (*48*).

Data S6.

San Salvador Island GWAS trait measurements. Trait values of standard length, lower oral jaw size, nasal protrusion distance, and caudal fin pigmentation measured across the three species of SSI radiation to include in a GWAS for alleles underlying these traits.

Data S7

Top genomic regions associated with lower oral jaw size in a GWAS of San Salvador Island species. Regions in which all the alleles within a 20-kb windows had a summed PIP score that was in the 99th percentile of all summed PIP scores for association with lower oral jaw size across 10 independent runs of Bayesian linear mixed model implemented in GEMMA (*45*).

Data S8.

Top genomic regions associated with lower caudal fin pigmentation in a GWAS of San Salvador Island species. Regions in which all the alleles within a 20-kb windows had a summed PIP score that was in the 99th percentile of all summed PIP scores for association with caudal fin pigmentation across 10 independent runs of Bayesian linear mixed model implemented in GEMMA (*45*).

Data S9.

Top genomic regions associated with lower maxillary nasal protrusion in a GWAS of San Salvador Island species. Regions in which all the alleles within a 20-kb windows had a summed PIP score that was in the 99th percentile of all summed PIP scores for association with maxillary nasal protrusion across 10 independent runs of Bayesian linear mixed model implemented in GEMMA.